Arborescent Polystyrene-*graft*-Polyisoprene Copolymers as Polymer Processing Additives

By
Wai Yau Lin

A thesis
presented to the University of Waterloo
in fulfillment of the
thesis requirement for the degree of
Master of Science
in
Chemistry

Waterloo, Ontario, Canada, 2009

I hereby declare that I am the sole author of this thesis. This is a true copy of the thesis, including any required final revisions, as accepted by my examiners.

I understand that my thesis may be made electronically available to the public.

Abstract

Some commodity polymers such as linear low density polyethylene (LLDPE) suffer from melt defects including sharkskin, cyclic melt fracture, and gross melt fracture during processing. The occurrence of these defects sets an upper limit to the rate at which these polymers can be processed, thus increasing production costs. One method to eliminate or delay the formation of melt defects is through the addition of polymer processing additives (PPA). These PPA migrate to the surface of the polymer melt and form a layer inducing slippage on the metallic surfaces of processing equipment such as extruder screws and extrusion dies. This reduces energy consumption and increases processing throughput. Effective PPA are generally phase-separated from the host polymer and migrate to the die wall. Arborescent polymers (AP) are a class of dendritic branched polymers with characteristics, including a compact structure and a rigid sphere-like topology, making them potentially useful as PPA.

A series of linear polyisoprene (PIP) and arborescent polystyrene-*graft*-polyisoprene copolymer samples was synthesized for the current investigation. The branched copolymers were derived from polystyrene (PS) substrates of different architectures (linear and branched), functionalized with acetyl or chloromethyl groups, and coupled with PIP macroanions. The copolymers thus obtained were modified by hydrosilylation with a perfluorohydrosilane (PHS), namely (tridecafluoro-1,1,2,2-tetrahydrooctyl)dimethylsilane, on 17 to 50 % of the isoprene units. The linear PIP samples were also modified by hydrosilylation for comparison. The additives were blended with LLDPE at concentrations of 0.1 %*w/w* and 0.5 %*w/w* to evaluate their performance as PPA by extrusion at different shear

(deformation) rates. A coadditive [poly(ethylene glycol), $\overline{M_w}$ ≈ 4,000, PEG4K] was also blended with three of the PPA samples for comparison. Furthermore, the size of the PPA droplets within the LLDPE matrix was monitored by optical microscopy.

All the samples led to some degree of improvement in the extrusion of LLDPE, but the lower molecular weight PPA appeared to perform better than those with a high molecular weight. Interestingly, several PPA samples caused the early onset of CMF but glossy, defect-free surfaces were obtained at higher shear rates. This suggests that a minimum shear rate is required for these additives to coat the extrusion die. The incorporation of coadditive improved the performance of the PPA at 0.5 %*w/w* PPA concentration, but little or no effect was observed at 0.1 %*w/w*. The size of the PPA droplets dispersed in LLDPE ranged from 1.0-1.5 μm, increasing to 1.4-2.1 μm with the coadditive.

Acknowledgements

I would like to take this opportunity to express my gratitude and appreciation to my supervisor, Professor Mario Gauthier, for his guidance and support over the course of this study.

I would like to express my thanks to my Supervisory Committee Members, Professors Jean Duhamel and Costas Tzoganakis, for their valuable time and helpful suggestions.

I would like to thank Professor Neil McManus, in the Department of Chemical Engineering at the University of Waterloo, for allowing the use of his GPC equipment. Also, I would like to thank Dr. Shuihan Zhu and Ms. Michelle Zhou, in the Department of Chemical Engineering at the University of Waterloo, for their guidance in using the rheometer and the GPC, respectively.

I would like to thank all my co-workers at the University of Waterloo for their assistance and friendship over the course of this research, but particularly Dr. Steven J. Teertstra, Dr. Firmin Moingeon, Dr. Abdul Munam, Jason Dockendorff, Olivier Nguon, Gregory Whitton, and Shahla Aliakbari.

My special thanks go to my wife and my son for their love, understanding, and support.

The financial support of Imperial Oil Limited for the work is gratefully acknowledged.

I dedicate this work to all my family, in particular my mother Man Ying Lin, my son Jason and my wife Wendy for their indefatigable patience, support, and encouragements.

Table of Contents

List of Figures

List of Tables

List of Equations and Schemes

List of Abbreviations and Symbols

$\overline{M_w}$	Weight-average molecular weight
$\overline{M_n}$	Number-average molecular weight
2VP	2-Vinylpyridine
A_2	Second virial coefficient
AP	Arborescent polymer
ATRP	Atom transfer radical polymerization
BN	Boron nitride
C_e	Coupling efficiency
CMF	Cyclic melt fracture
csc	Critical self-assembly concentration
D_h	Hydrodynamic diameter
DLS	Dynamic light scattering
DPE	1,1-Diphenylethylene
D_z	Diffusion coefficient
f_w	Branching functionality
G’	Storage modulus
G”	Loss modulus
GMF	Gross melt fracture
GPC	Gel permeation chromatography
L/D	Length/Diameter ratio
LALS	Low angle light scattering
LLDPE	Linear low density polyethylene
MALLS	Multi angle laser light scattering
MWD	Molecular weight distribution
n-BuLi	*n*-Butyllithium
PDDF	Real space pair distance distribution function
PDI	Polydispersity index = $\overline{M_w}/\overline{M_n}$

PDMS	Polydimethylsiloxane
PEG4K	Poly(ethylene glycol), $\overline{M_w} \approx 4{,}000$
PEG	Poly(ethylene glycol)
PEO	Poly(ethylene oxide)
PEOX	Poly(2-ethyl-2-oxazoline)
PHS	Perfluorinated hydrosilane / (tridecafluoro-1,1,2,2-tetrahydrooctyl)dimethylsilane
PIP	Polyisoprene
PPA	Polymer processing additive
PS	Polystyrene
P2VP	Poly(2-vinylpyridine)
PTFE	Polytetrafluoroethylene
RALS	Right Angle Light Scattering
R_g	Radius of gyration
R_h	Hydrodynamic radius
SANS	Small-angle neutron scattering
sec-BuLi	*sec*-Butyllithium
SEM	Scanning electron microscopy
SFM	Scanning force microscopy
SFRP	Stable free radical polymerization
SS	Sharkskin
TEM	Transmission electron microscopy
T_g	Glass transition temperature
THF	Tetrahydrofuran
TMEDA	N,N,N',N'-Tetramethylethylenediamine
TTS	Time-temperature superposition
ΔG^o	Standard Gibbs free energy
ΔH^o	Standard enthalpy
ΔS^o	Standard entropy
η_o	Zero-shear viscosity

Chapter 1 – Introduction

1.1 Opening remarks

Dendritic polymers with a randomly branched architecture can be divided into two groups, namely hyperbranched and dendrigraft macromolecules.[1,2] Hyperbranched polymers are typically synthesized in a one-pot method by the self-condensation of polyfunctional AB_n monomers. The resulting structure is imperfect, since polymer branches of variable length are produced and the polydispersity index (PDI, $\overline{M_w}/\overline{M_n}$) of the product is usually greater than two.

On the other hand, arborescent polymers (AP) are synthesized through multi-step reactions using polymeric building blocks. This leads to improved control over the length of the branches and thus a more uniform structure. The PDI of AP is correspondingly lower (<1.1) than for hyperbranched polymers. By varying their characteristics, AP could be tailored to optimize their performance in different applications. The number of studies on applications of these materials has been very limited so far, however.

The processing of thermoplastics requires additives, among others to improve their surface appearance and increase the throughput. In the absence of these additives the achievable throughput is much lower, due to melt defects occurring at high shear (deformation) rates, leading to increased production costs. Hyperbranched polymers have been investigated as PPA by Hong et al.[3,4] yielding interesting results. As such, it is reasonable to extend the PPA studies to include AP additives. Variations in the characteristics of the arborescent PPA (size and number of branches, fluorine content) would be interesting.

1.2 Outline

Chapter 2 includes a review on melt defects in polymers, dendritic polymers, polymer processing additives, and the use of branched polymers as processing additives. The objectives of the current investigation are set out in Chapter 3. Experimental procedures for the synthesis, blending, testing, and characterization of the polymers are outlined in Chapter 4. The Results and Discussion section – Chapter 5 – provides a summary of the results obtained and a discussion of the data collected. In Chapter 6, the conclusions drawn from the results and suggestions for future work are presented.

Chapter 2 – Background

2.1 Processing of commodity polymers

A broad range of commercial polymers must be processed on a daily basis. This includes commodity polymers such as polyolefins, polymethacrylates, polystyrene (PS), and poly(vinyl chloride), which are produced with a wide range of molecular weights and PDI values. The ease of processing of these materials varies widely, but polymers with a narrow molecular weight distribution (MWD) are generally more difficult to process than those with a broad MWD.[5] This is partly due to the fact that low molecular weight polymers have a lower zero shear viscosity than high molecular weight polymers.[6] These low molecular weight components effectively dilute or separate the high molecular weight chains, reducing the overall zero shear viscosity of a broad MWD polymer. In other words, the low molecular weight components of the polymer act as lubricants for the higher molecular weight material.[5,6]

2.1.1 Melt defects in polymers

Polymers for different uses are produced in millions of tons every year and processed by different methods including film blowing, injection molding, and melt extrusion. From PS to polyethylene to polyelectrolyte membranes, production limitations drive the cost of these polymers toward new summits. These limitations occur even at low shear rates, causing surface imperfections such as sharkskin (SS), cyclic melt fracture (CMF) and gross melt fracture (GMF). For example, when molten polymers are extruded through a die under pressure (shear stress) to form a monofilament by extrusion, they undergo four appearance changes as the shear rate increases. These changes are depicted in Figure 2-1 as a function of processing rate (shear or deformation rate). As the shear rate increases, the extrudate changes from a glossy smooth surface to a ridged (SS) surface after crossing the first critical shear

stress (change in slope).[7,8] At even higher shear rates, the extrudate crosses a second critical shear rate leading to alternating smooth and ridged surfaces (CMF). Beyond CMF the extrudate may suffer from GMF, where the excessive throughput leads to a completely distorted filament.[7,8] That being said, SS is most problematic because it appears first and even at very low processing rates – within the usual range of polymer processing rates.[9,10] SS is therefore the surface defect that has the highest impact on manufacturing.

A number of researchers have looked into the causes of SS formation; however contradictory evidence arose from these studies. Some investigators proposed that SS is induced by slippage of the extrudate at the die wall, while others suggested that SS is due to sticking on the die wall.[7,8,11-13] The exact SS formation mechanism is still elusive, but it is widely accepted that SS is formed when the extrudate exits the die.[12,14]

2.2 Commercial processing additives

Additives of various chemical compositions are commonly used to minimize melt defect formation and reduce the load (or indirectly the shear stress) in polymer processing. This includes stearates, boron nitride, and polymer-based additives.[9] All these additives have led to increased processing rates for different commodity products, but the most widely used additives are polymer-based. These products, known as polymer processing additives (PPA), include Viton® FreeFlow™ and Dynamar™ FX9613. These fluoropolymers, incorporated at low concentrations (typically less than 0.1 %w/w or 1000 ppm), increase the processability of molten polymers. The use of fluoropolymers as PPA was accidentally discovered in the 1960s,[15,16] and they have been further investigated for that purpose over the years. The major

additives used to improve the processability of molten polymers will be discussed briefly below.

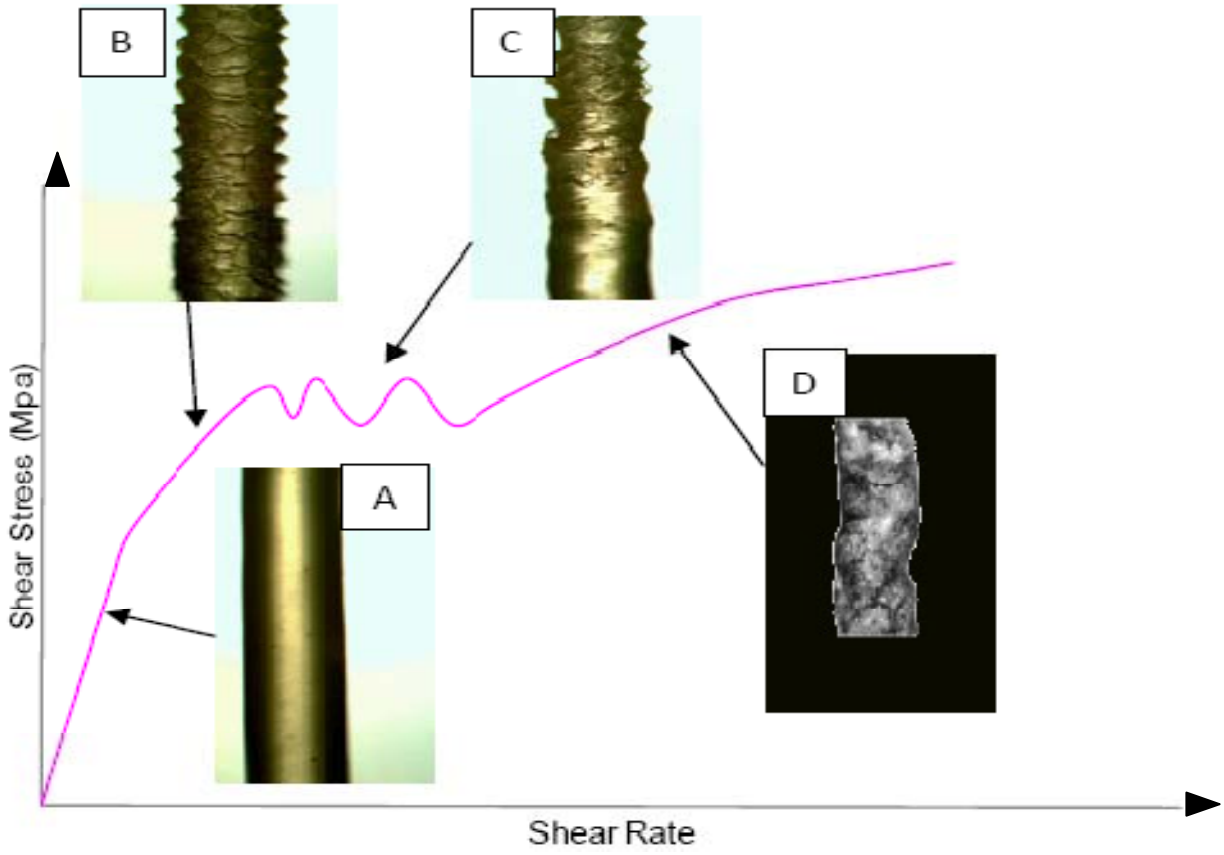

Figure 2-1: Typical flow curve for linear low density polyethylene (LLDPE).

The diagram shows (A) a smooth extrudate, (B) sharkskin, (C) cyclic melt fracture, and (D) gross melt fracture.[9] The abscissa represents the shear rate and the ordinate represents the applied pressure (load). A change in slope indicates the crossing of a critical point leading to a change in extrudate appearance.

2.2.1 Boron nitride

Boron nitride (BN) was found to eliminate SS and CMF, and to delay the onset of GMF under certain conditions depending on the die, the temperature, and the loading level

used.[9] Rosenbaum et al. suggested that BN acts as lubricant within the bulk of the polymer, which prevents the formation of SS and GMF.[17] In capillary rheometry experiments using a circular die, the incorporation of 0.05-0.1 %*w/w* BN in LLDPE eliminated SS formation, but the onset of CMF and GMF were unaffected.[17] It was also noticed that the addition of BN had essentially no effect on the flow curve, as the curve obtained for virgin (pure) LLDPE overlapped with the one containing BN. Significant improvement in processability was observed when a die for wire coating was used, however. At the same concentrations as above, SS and CMF were completely eliminated and GMF was delayed to a shear rate of ca. 920 s^{-1}, well above that of the virgin LLDPE resin (ca. 500 s^{-1}) (Figure 2-2).[9] Virgin LLDPE displayed SS and GMF formation at 80 s^{-1} and 800 s^{-1}, respectively. Even at a concentration of 0.01 %*w/w* BN, the surface of the extrudate remained glossy at shear rates up to 800 s^{-1}.

The influence of temperature was also investigated.[17] At 163 ^{0}C, optimal performance was observed for BN concentrations between 500 and 1000 ppm. At the same temperature with 5000 ppm BN, melt fracture was however not eliminated. For an increase in temperature from 163 to 204 ^{0}C, the best performance was observed for blends with 5000 ppm BN, the surface remaining glossy at higher shear rates. The influence of temperature on the optimal loading was attributed to a temperature-dependent critical dispersion concentration above which the BN formed aggregates, thus impeding the performance of the additive.

Boron nitride blended with Teflon® further increased the range of allowable shear rates from 1300 s^{-1} to 2400 s^{-1} (with 0.05 %*w/w* BN) and 1800 s^{-1} (with 0.05 %*w/w* Teflon®), due to enhanced mixing of the additive with the polymer in the barrel of the capillary rheometer.[17]

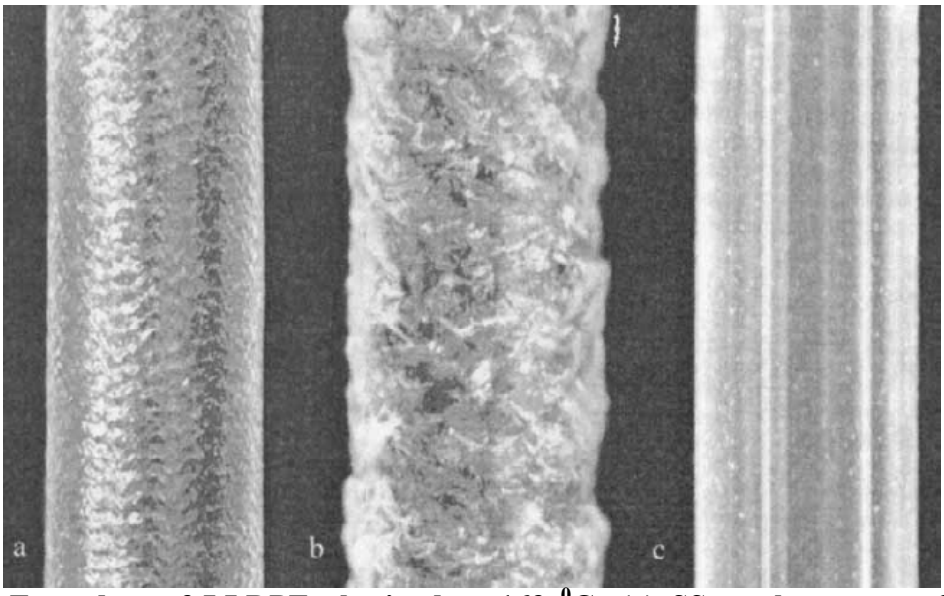

Figure 2-2: Extrudate of LLDPE obtained at 163 ^{0}C: (a) SS at shear rate of 80 s^{-1} without BN, (b) GMF at 800 s^{-1} without BN, and (c) glossy extrudate at 800 s^{-1} with 0.01 %*w/w* BN.
From Achilleos et al.[9]

2.2.2 Stearates

Stearates are the metal salts of stearic acid (e.g. calcium stearate, zinc stearate).[9] It has been shown that stearates, when blended with metallocene polyolefins (with a narrow MWD), produce die conditioning phenomena similar to those observed for Teflon®. These stearates form a stagnant layer allowing the host polymer to slip during extrusion. Metallocene blends with ca. 1000 ppm stearates display an initial load rise when extruded in capillary rheometry experiments, which drops after several consecutive runs through reloading of the rheometer barrel. The load eventually attains a steady state value, indicating that full conditioning (coating) of the die is achieved.[18] The authors also showed that in the presence of long chain branching in the polymer, the die conditioning time increased.

2.2.3 Polydimethylsiloxane oils and derivatives

Polydimethylsiloxane (PDMS) oils and their derivatives have been used as PPA since the 1970s. Silicone oil serves as a lubricant and a release agent in the injection molding of polyolefins.[19] Due to the incompatibility of silicone oil and polyolefins, the silicone oil tends to migrate to the surface, which relieves the frictional properties of the polyolefins. However, the use of silicone oil must be avoided when the polyolefins need to be printed, painted, or come in contact with food products: The residues on the surface hinder the adhesion of paint and are relatively toxic.

Ultra high molecular weight PDMS, marketed by Dow Corning, also works as a processing additive for polyethylene and polypropylene. Due to their high molecular weight, these PDMS residues remain solid after processing of the host polymer. Consequently, they do not affect paint adhesion on the surface of the processed polymer.[19] Reductions in LLDPE surface roughness have also been reported for this additive.[20]

2.2.4 Polymer processing additives

PPA are widely used to improve the processability of commercial polymers and eliminate surface defects. Typical PPA have a high fluorine content, to promote their separation from the host polymer, and thus become dispersed as small droplets within the host polymer. During melt processing, these droplets migrate from the polymer matrix to the die wall and form a stagnant layer of additive acting as a lubricant (Figure 2-3).[15,21] An effective PPA is generally immiscible with the host polymer, as miscibility diminishes the ability of a PPA to migrate to the wall.[10,22]

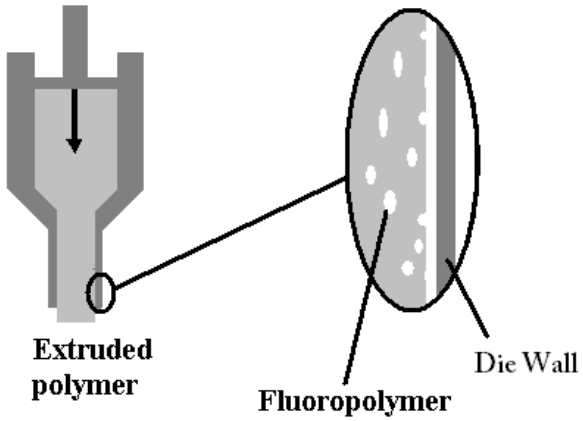

Figure 2-3: Cross section of extrusion equipment for polymer processing.
As the polymer (grey) is extruded, the PPA (white) migrates to the die wall and forms a layer at the polymer-die interface.

A PPA is typically used at a concentration between 500 ppm (0.05 %*w/w*) and 1000 ppm (0.1 %*w/w*).[9] No detrimental effects have been observed on the appearance and the mechanical properties of the extrudate at these concentrations.[23,24] The effectiveness of a PPA at 1000 ppm on the processing of LLDPE can be seen in Figure 2-4.[25] For pure LLDPE, SS formation starts at 200 s^{-1} but in the presence of the PPA, SS is completely eliminated and CMF is delayed to shear rates above 800 s^{-1}.

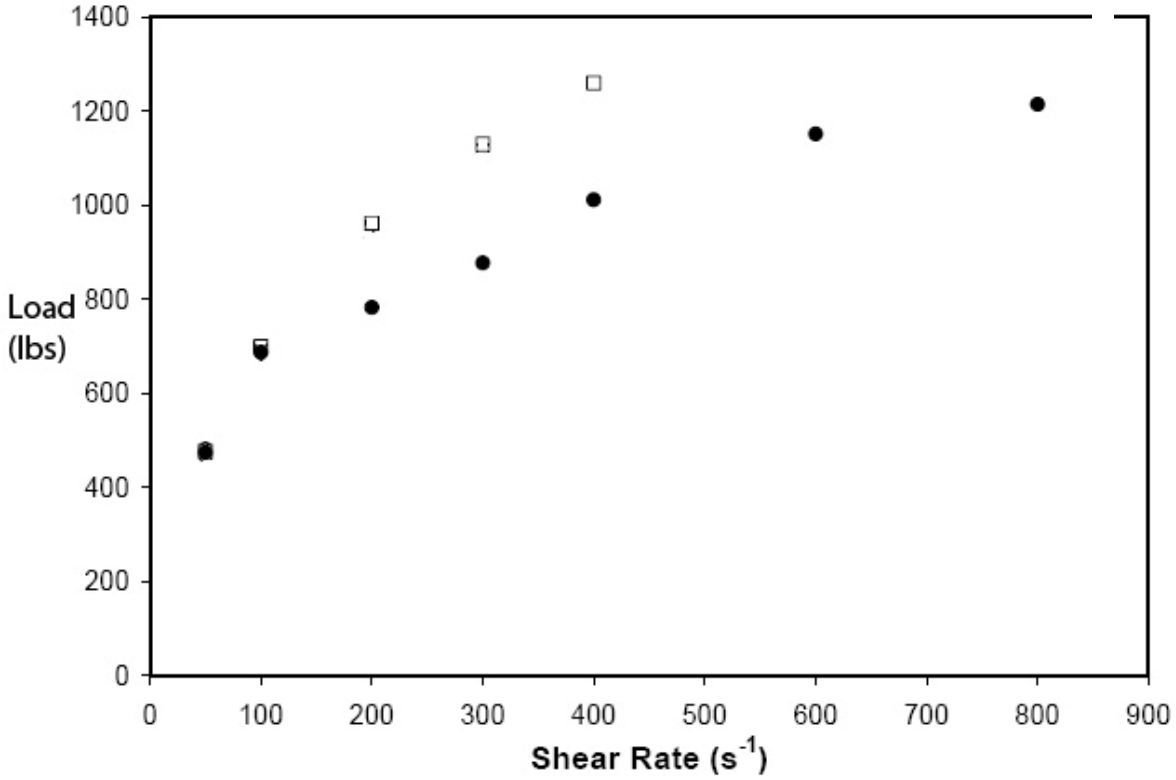

Figure 2-4: Comparison of linear low density polyethylene (LLDPE) processing with (•) and without (□) PPA.
Sharkskin formation starts at 200 s^{-1} for virgin LLDPE and cyclic melt fracture (CMF) after 300 s^{-1}. For LLDPE with 0.1 %*w/w* PPA, SS formation is completely eliminated and CMF is delayed to above 800 s^{-1}. From Teertstra.[25]

As mentioned before, these PPA are dispersed as small droplets within the polymer matrix. Some studies have demonstrated that the formation of the PPA coating is affected by the average droplet size, which should be around 0.2 µm for optimal results,[9] while others have shown that a droplet size between 2 µm and 10 µm could also be very effective.[10,26] It was determined that the thickness of the coating formed by larger droplets fluctuated more as compared to smaller droplets, however.[10] The variation in coating thickness with the droplet size is described in Figure 2-5A. Furthermore, the droplet size and the amount of polymer

blend that must be passed through the extrusion die to form a stable coating vary in an opposite fashion: as the droplet size decreases, an increased amount of polymer is required to build up a stable coating. In Figure 2-5B, the percent melt fracture – defined as the portion of the extrudate surface covered with SS – decreases as more polymer passes through the die. By comparing both figures, it can be seen that the effective coating thickness for melt fracture elimination is between 150 and 200 nm.[10] Larger droplets lead to shorter coating times and thicker coatings, but thicker coatings are unnecessary as SS is eliminated even with very thin coatings.

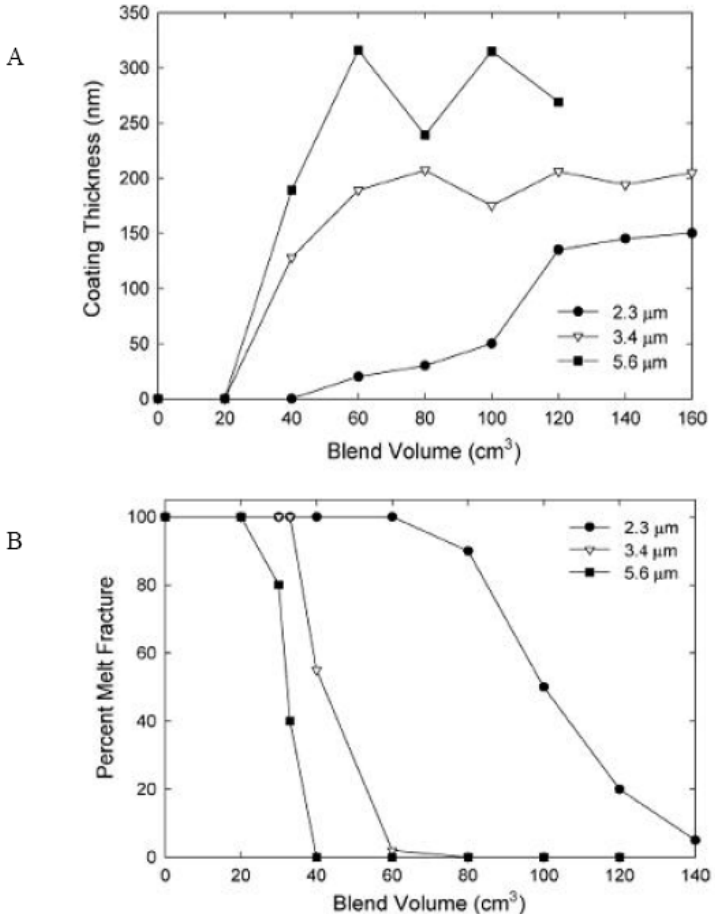

Figure 2-5: Dependence of (A) coating thickness and (B) percent melt fracture on the volume of polymer extruded and the PPA droplet size.
A PPA concentration of 0.1 %*w/w* (1000 ppm) was used in all cases. From Bigio et al.[10]

2.2.5 Coadditives

Coadditives are typically low molecular weight polymers that are commonly used in conjunction with processing additives to enhance their performance. Poly(oxyalkylene)s such as poly(ethylene glycol) (PEG)[25,27-29] and poly(ε-caprolactone),[26] when used in combination with a PPA, have been shown to provide enhanced performance over the pure PPA or the coadditive alone, demonstrating that the additive-coadditive combination leads to a synergistic effect.[25] It has been suggested that PEG acts as a partitioning agent between the host polymer and the PPA, which reduces the stress encountered by the PPA during processing and prevents the breakup of the PPA droplets.[25-27,29] This means that PEG coats the PPA droplets and prevents their breakup.

2.3 Dendritic polymers

Macromolecules with a dendritic (multi-level) well-defined branched architecture were first described by Buhleier et al.[30] These macromolecules can be divided into three classes of dendritic polymers: hyperbranched polymers, dendrimers, and dendrigraft polymers. A high branching functionality can be achieved for all three dendritic polymer families, but they can be distinguished by their architecture. Hyperbranched polymers are synthesized mainly according to one-pot condensation schemes using multifunctional monomers of the AB_2 or AB_3 type (Figure 2-6).[1,2] This leads to multiple structural imperfections such as missing branches, and variations in the length of the linear chain segments.[3] Dendrimers are obtained through a series of protection-condensation-deprotection reaction cycles allowing precise control over the architecture and providing a very narrow MWD.[2] Unfortunately, the molecular weight increases very slowly by this approach due to the fact that small molecules serve as building blocks.

Much faster increases in molecular weight could be achieved using polymeric building blocks and a large number of coupling sites on the substrate. This is the approach used in the synthesis of arborescent polymers (AP), the type of dendrigraft polymer used in the current investigation. The molecular weight of AP increases geometrically for successive generations, yielding very high molecular weights and branching functionalities in a few cycles. Very narrow MWD (PDI < 1.1) can be achieved for the AP as compared to hyperbranched polymers (PDI > 2).[2]

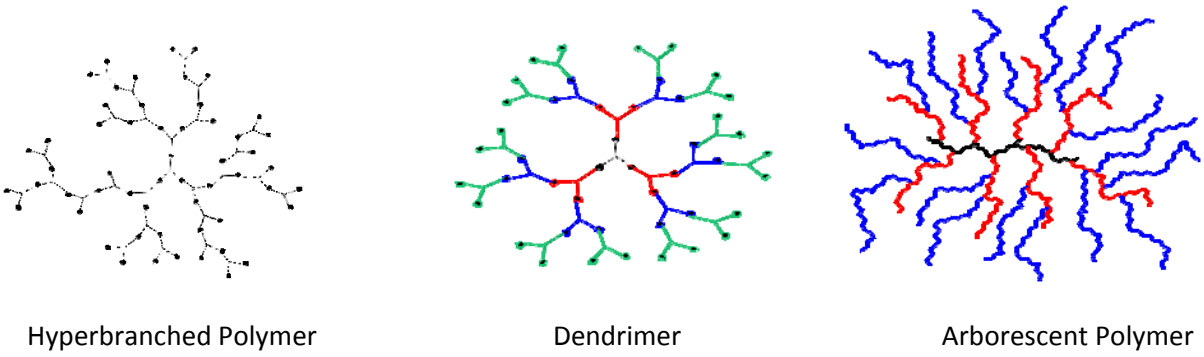

Figure 2-6: Comparison of the architecture of hyperbranched polymers, dendrimers, and arborescent polymers.

2.3.1 Synthetic processes for dendrigraft polymers

The synthesis of dendrigraft polymers can be achieved by two different processes, namely divergent and convergent methods. In the divergent method, growth of the molecules takes place from the core outwards, by grafting side chains in successive reaction cycles. Convergent methods utilize the reversed process, whereby side chains are grown and combined into larger fragments by successive coupling reactions of a single reactive site located at the core (focal point) of the fragments. The current discussion will be limited to the

synthesis and the properties of dendrigraft (including arborescent) polymers obtained by divergent methods, since this is the type of polymers used in the current investigation. Inconsistent naming systems have been proposed by different groups, but for simplicity and convenience, a unique naming system will be used throughout this thesis. Molecules consisting in a linear polymer substrate grafted only once with side chains, also known as a comb-branched structure, will be called generation 0 or G0 (Scheme 2-1). The G0 polymers, when further grafted with side chains, are identified as generation 1 or G1 (the first generation with a dendritic or multi-level branched architecture), and so on.

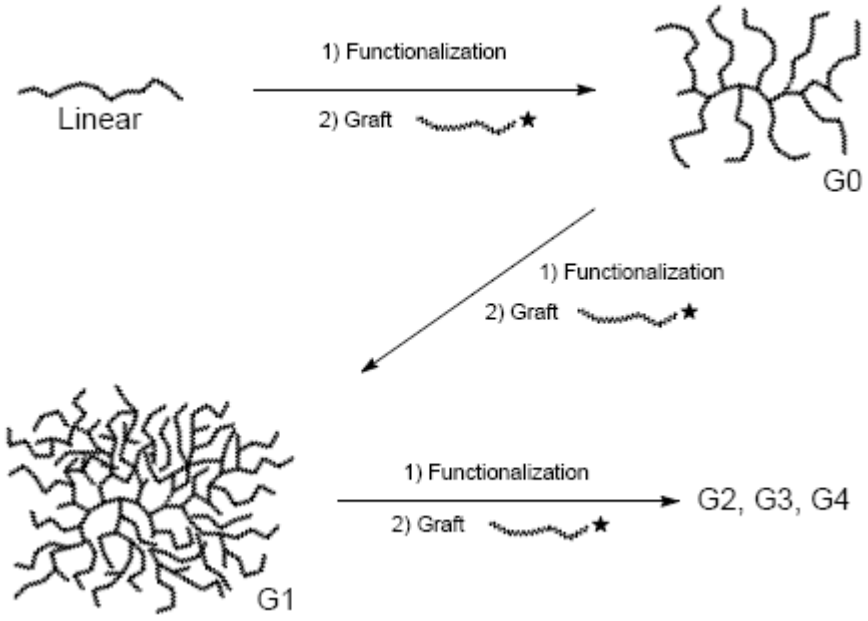

Scheme 2-1: Generic "grafting onto" scheme for the synthesis of dendrigraft polymers.

The divergent synthetic process can be divided into two sub-categories as "grafting onto" and "grafting from" techniques. The "grafting onto" path starts from a linear polymer that is randomly functionalized with coupling sites and reacted with living polymer chains to yield a G0 structure (Scheme 2-1). The G0 polymer can be further functionalized with

coupling sites and grafted to obtain a G1 polymer. Higher generation (G2, G3…) polymers result from repetition of the functionalization and grafting procedures. In the "grafting from" technique, the substrate is functionalized with reactive sites serving as initiator for the polymerization of a monomer. The side chains are thus grown from the substrate in this approach. It should be pointed out that the "grafting onto" techniques are much more widespread in practice, possibly due to the fact that in most cases, the "grafting from" method does not allow the detailed characterization of the side chains (molecular weight and PDI) nor the exact number of chains added. Another problem is that the polyfunctional initiator substrates, being highly charged, are often insoluble in common polymerization solvents.[31]

2.3.1.1 "Grafting onto" methods

Comb-burst ® polymers

Comb-burst® polyethylenimine was first reported by Tomalia et al.[32] The synthetic scheme relies on the coupling of "living" cationic poly(2-ethyl-2-oxazoline) (PEOX) chains with polyethylenimine substrates (Scheme 2-2). PEOX chains with a narrow MWD are obtained by cationic polymerization of 2-ethyl-2-oxazoline. The polymer is then deacylated to yield secondary amine groups, acting as coupling sites for the living PEOX chains. Repetition of the deacylation and grafting cycles yields upper generation polymers. This reaction provides polyethylenimine-*graft*-poly(2-ethyl-2-oxazoline) copolymers, or polyethylenimine homopolymers if the poly(2-ethyl-2-oxazoline) copolymer is deacylated in the final step.

Polymers of generations up to G3 have been characterized by Yin et al.[33] (Table 2-1) and are characterized by a geometric increase in molecular weight over successive generations and a relatively narrow MWD (PDI = 1.2 – 1.5). The grafting yield, defined as the fraction of living polymer chains generated that was coupled with the substrate, ranged from 65 to 80 %. An increase in either the length of side chains or the generation number of the polymers led to a decrease in grafting yield.

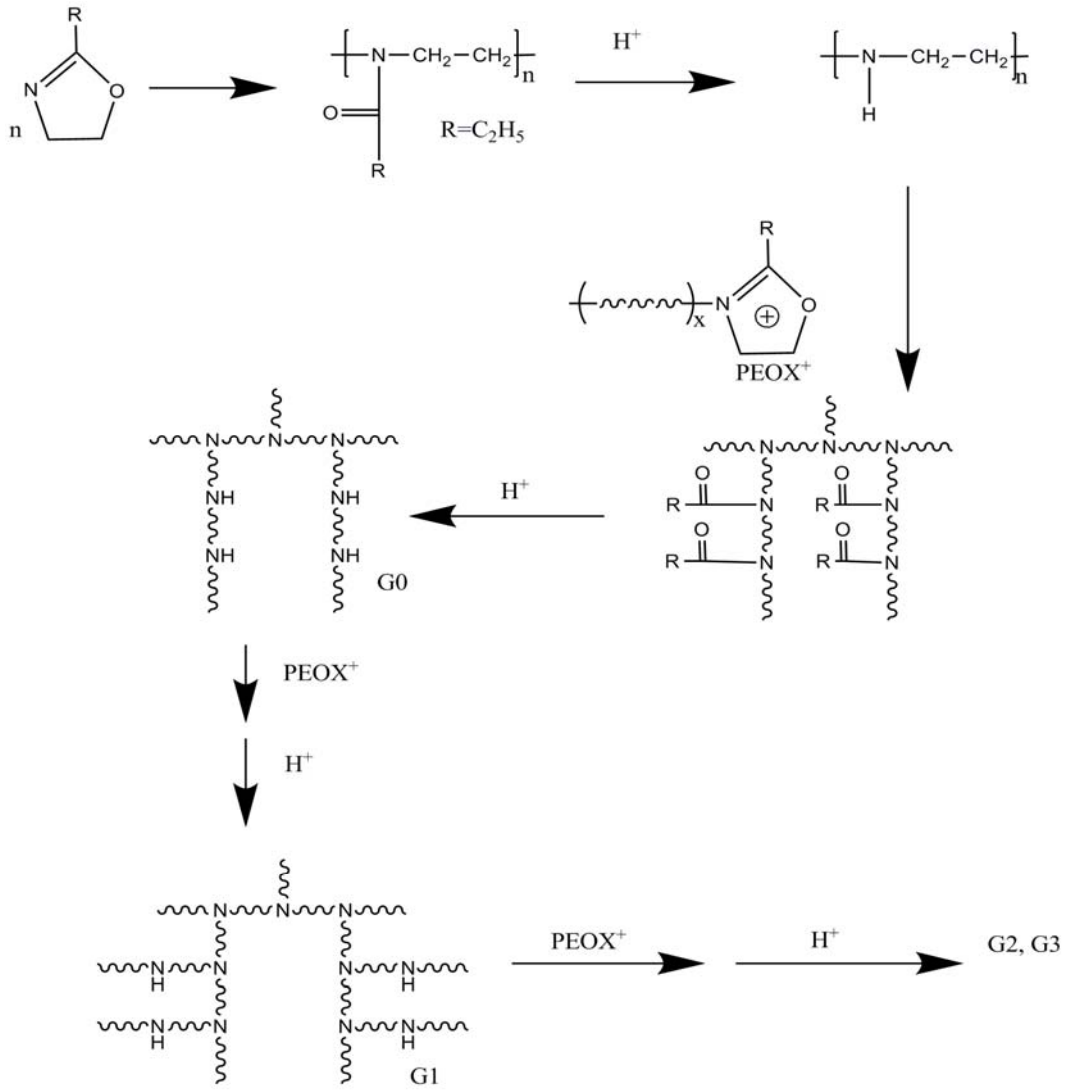

Scheme 2-2: Comb-burst® polyethylenimine synthesis.
From Teertstra.[25]

Table 2-1: Characterization data for Comb-burst® polyethylenimines
Adapted from Yin et al.[33]

	$\overline{M_w}$ (RI)[a]	$\overline{M_w}$ (LS)	PDI(LS)	f_w[b]
Linear polyethylenimine	3000	1000	1.05	--
G0	4900	2500	1.22	5
G1	8000	139,000	1.34	26
G2	87,000	1,080,000	1.47	176
G3	274,000	10,400,000	1.20	745

[a] Apparent weight-average molecular weight from GPC analysis calibrated with PEG
[b] Number of side chains added per generation based on $\overline{M_w}$ (LS) and the number of coupling sites

The intrinsic viscosity of these polymers was investigated as a function of generation number and found to increase nonlinearly up to G2, before decreasing slightly for G3 due to a denser, more rigid structure.[34] This behavior is consistent with that observed for other dendritic polymer systems such as the dendrimers.[35,36]

Arborescent polystyrene

Arborescent PS was synthesized by a method similar to Comb-burst® polymers, but by grafting "living" PS *macroanions* onto a substrate. Another important distinction between the two approaches is that the coupling sites in the AP syntheses are not inherent to the monomer but rather introduced randomly on the substrate by chemical functionalization. For PS substrates, both chloromethyl[37] and acetyl groups[38] have been investigated as coupling sites.

For example, a linear PS substrate was synthesized by anionic polymerization using *sec*-butyllithium (*sec*-BuLi) and chloromethylated under dilute solution conditions, to minimize the occurrence of intermolecular cross-linking. In a different reaction, living PS anions serving as side chains were capped with one unit of 1,1-diphenylethylene (DPE)

before they were reacted with the chloromethylated substrate (Scheme 2-3). Capping of the macroanions with one DPE unit increased the grafting yield from 50 to 96 %, due to the suppression of metal-halogen exchange reactions. Narrow MWD and controllable molecular weights were attained in these reactions (*vide infra*).

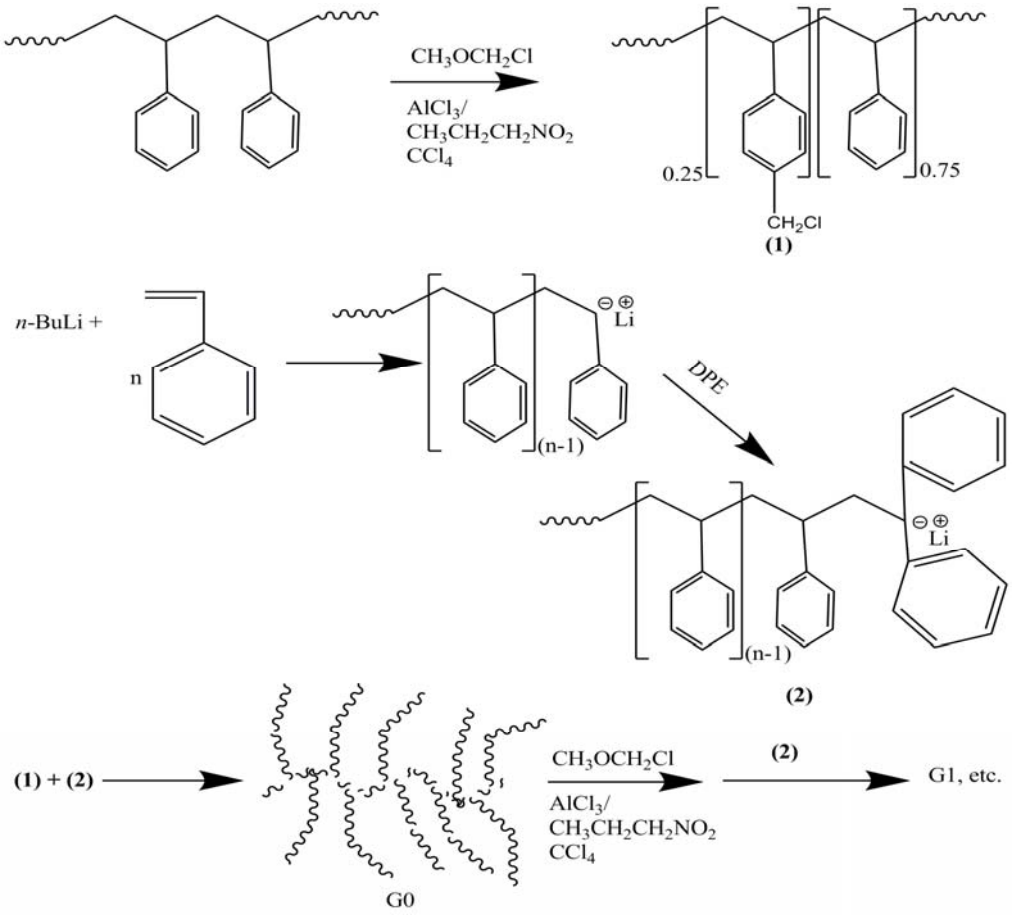

Scheme 2-3: Synthesis of arborescent polystyrene by anionic polymerization and grafting onto chloromethylated substrate.
From Teertstra. [25]

Acetyl coupling sites were also investigated by Li et al. for the preparation of arborescent PS.[38] By this method, the highly toxic chloromethyl methyl ether and carbon tetrachloride used in the functionalization step could be eliminated. Acetyl functionalities were introduced through Friedel-Crafts acylation (Scheme 2-4). Living polystyryllithium,

when capped with a few units of 2-vinylpyridine (2VP) or isoprene in the presence of LiCl, providing the G0PS in up to 95 % yield. Chain capping and the addition of salt were necessary to decrease the reactivity of the macroanions and avoid the competing proton abstraction reaction from the acetyl functionality; the grafting yield was decreased to 65 % in the absence of these modifications.

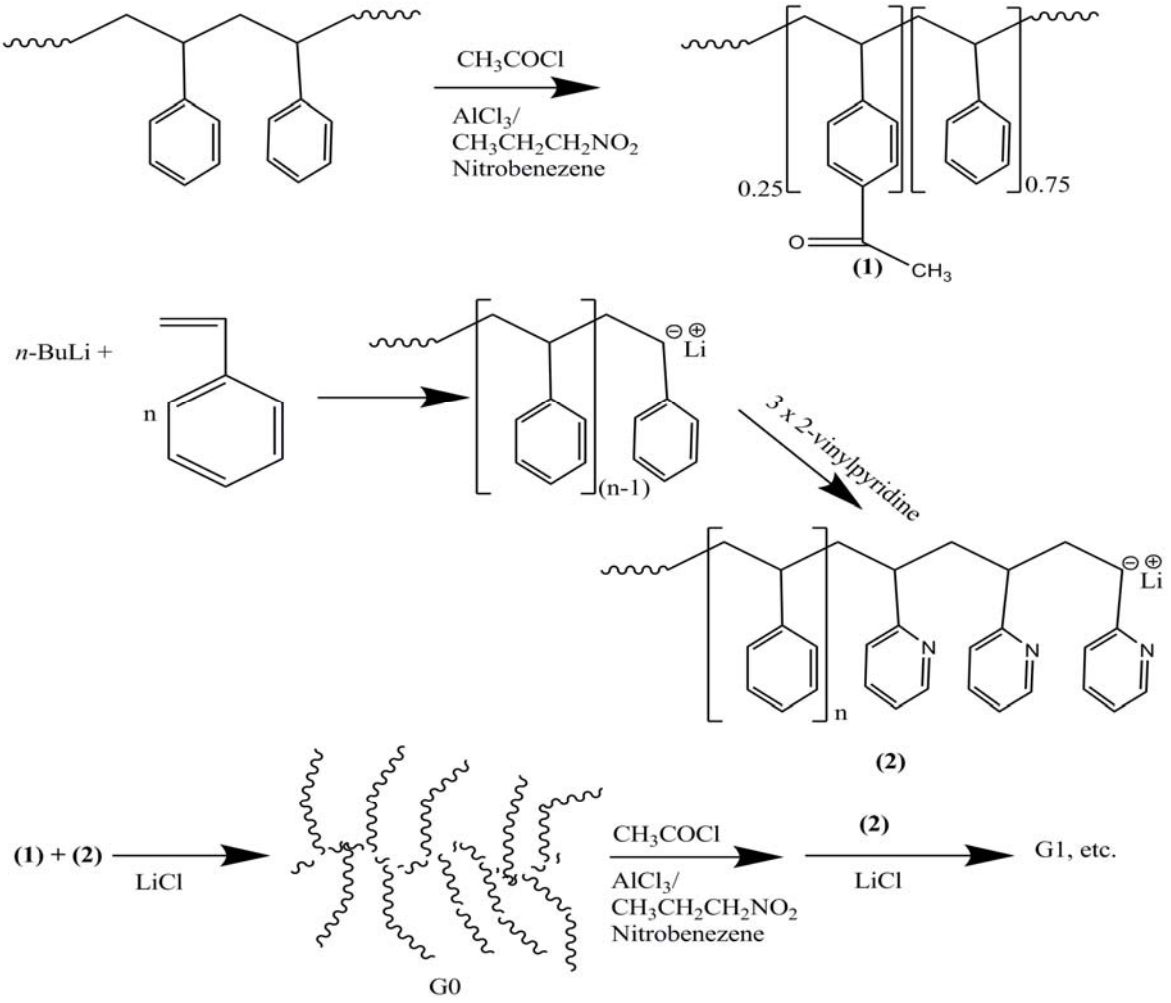

Scheme 2-4: Synthesis of arborescent polystyrene by grafting onto acetylated polystyrene substrate.
Adapted from Teertstra.[25]

Regardless of the synthetic path selected (chloromethyl or acetyl coupling sites), the molecular weight, branching functionality, and polydispersity obtained for the products over successive generations were very similar.[31] Characterization results for two series of arborescent PS of generations up to G4, synthesized by the chloromethylation path, with a side chain molecular weight of either 5,000 or 30,000, are reported in Table 2-2.[39] The nomenclature adopted specifies the overall generation number of the polymers and the molecular weight of the side chains. For example, G0PS5 corresponds to a linear PS substrate grafted with $\overline{M_w}$ ≈ 5,000 PS side chains (G0 overall). Arborescent PS samples with weight-average molecular weights $\overline{M_w}$ (LS) ≈ 6 x 10^4 - 5 x 10^8 (from light scattering measurements) and branching functionalities f_w = 14 - 22,000 were thus obtained. A low polydispersity (1.07-1.22) was maintained for all generations of arborescent PS. A geometric increase in molecular weight was observed up to G2, but the increase was more modest for the G3 and G4 polymers. This was attributed to increased steric hindrance for higher generations, leading to a decrease in grafting yield. The decreased grafting yield for the upper generations could also be partly due to difficulties in eliminating protic impurities from the larger grafting substrates. The molecular weight determined by gel permeation chromatography (GPC) analysis was strongly underestimated when compared with the absolute molecular weight from light scattering measurements, obviously due to the compact structure of the arborescent molecules.

The procedures described above for the synthesis of arborescent PS, while successful, are typically applied on a small (10- to 20-g) scale. The large scale (100 g) synthesis of these materials was recently investigated by Munam and Gauthier to allow the generation of large amounts of material necessary for some of the physical characterization work.[40] The grafting

yield (fraction of side chain precursor grafted on the substrate) for the small-scale procedure originally described by Li et al., when applied on a 100-g scale, decreased from 95 to 75 %. It was noticed that after capping the living polystyryllithium side chain precursor with only 3 equivalents of 2VP prior to grafting, as it was done for the small-scale reactions, the GPC traces for the polymer became bimodal (Figure 2-7b). The fact that the leftmost peak in the elution curve for the capped chains had a molecular weight twice as large as the primary chains hinted at dimerization due to a side reaction. This problem was attributed to the very

Table 2-2: Characterization data for arborescent polystyrene synthesized from chloromethyl coupling sites

Adapted from Gauthier et al.[39]

Sample[a]	Side chain		Arborescent polystyrene			
	$\overline{M_w}$ (BR)[b] (x 10^3)	PDI (BR)[b]	$\overline{M_w}$ (RI) (x 10^3)	PDI (RI)	$\overline{M_w}$ (LS) (x 10^3)	f_w[c]
G0PS5	4.3	1.03	130	1.07	67	14
G1PS5	4.6	1.03	300	1.2	870	170
G2PS5	4.2	1.04	450	1.15	13,000	2900
G3PS5	4.4	1.05	--	--	90,000	17,500
G4PS5	4.9	1.08	--	--	200,000	22,000
G0PS30	28	1.15	210	1.12	510	18
G1PS30	27	1.09	590	1.22	9,000	310
G2PS30	27	1.09	--	--	100,000	3400
G3PS30	28	1.09	--	--	500,000	14,300

[a] Series prepared from linear polystyrene core with $\overline{M_w} \approx 4800$, PDI = 1.08

[b] Absolute value determined by GPC calibrated with linear polystyrene standards

[c] Number of branches added for each generation, calculated from $\overline{M_w}$ (LS) increase and $\overline{M_w}$ (BR)

fast polymerization rate of 2VP in tetrahydrofuran (THF), leading to incomplete capping of the living polystyryllithium chains under the poor stirring conditions encountered in a large reactor. Consequently, some noncapped chains that were still present in the mixture attacked

the pyridine ring of another chain in the position α- to the nitrogen atom, causing dimerization.[40] The problem could be avoided in the large-scale reactions by DPE capping of polystyryllithium prior to the addition of 3 to 6 equiv of 2VP, to ensure capping of all the chains by 2VP units.

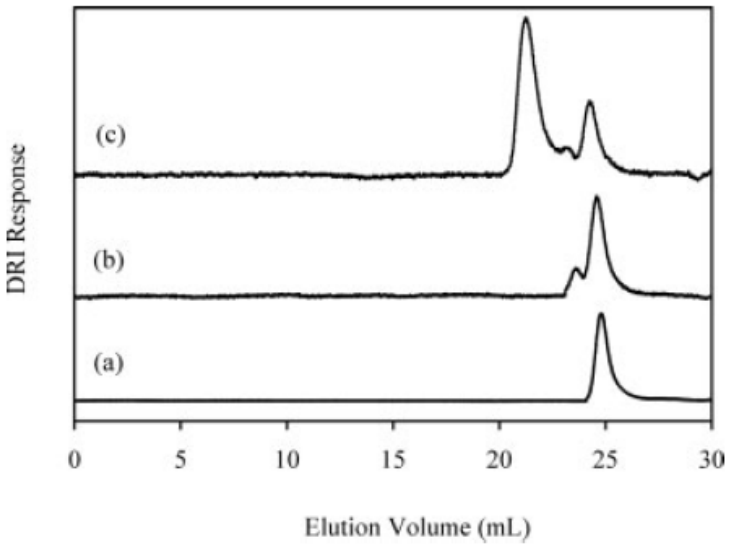

Figure 2-7: GPC elution curves for the large scale synthesis of arborescent polystyrene. (a) Polystyrene side chains before capping, (b) after capping with 3 equiv of 2VP, and (c) after coupling with a linear acetylated substrate. From Munam and Gauthier.[40]

The physical properties of arborescent PS were investigated by different techniques in solution and in the molten state, to obtain information on the morphology of the molecules and to establish structure-property correlations.

Dilute solutions of arborescent PS were thus investigated in light scattering experiments to determine the scaling behavior of their second virial coefficient (A_2), radius of gyration (R_g) and diffusion coefficient (D_z). The scaling exponents obtained in double logarithmic plots of each parameter vs. molecular weight (Table 2-3) show that AP are best described as having a rigid sphere-like morphology in dilute solutions.[41]

Table 2-3: Scaling parameters for the second virial coefficient (A_2), radius of gyration (R_g), and diffusion coefficient (D_z) for linear coils, arborescent polymers, and hard spheres

Adapted from Gauthier et al.[41]

Parameter	Linear coils	Hard spheres	Arborescent polymers
D_z	-0.6	-0.33	-0.34
A_2	0.6	0.33	0.2
R_g	-0.2	-1	-0.9

The behavior of AP was also investigated in semi-dilute solutions in terms of the so-called osmotic modulus, defined as the ratio of the absolute $\overline{M_w}$ (at infinite dilution) to the apparent $\overline{M_w}$ (at finite polymer concentrations) determined as a function of a scaling parameter X proportional to concentration c.[31,41] The osmotic modulus, which measures intermolecular repulsions, was compared for AP of generations G0 to G2, linear polymer coils, and hard spheres (Figure 2-8). It is clear that the modulus rises much more rapidly with concentration for AP than for linear coils. An increase is observed from G0 to G1, whereas no further increase is seen for G2. Hence structural stiffening occurs from G0 to G1, but residual interpenetrability is still present for higher generation polymers. This result is consistent with a morphology corresponding to a hard core surrounded by a soft shell.

Solution studies of arborescent PS were also conducted using small-angle neutron scattering (SANS) measurements to gain insight into the morphology of the molecules.[42] It was observed that by changing the solvent type used in the measurements from deuterated toluene (a good solvent) to deuterated cyclohexane (a poor or θ-solvent), the R_g of the molecules decreased for G2 and G3 PS, but not for the lower generation molecules. The scaling exponents (ν) for $R_g \sim M^{\nu}$ were determined to be 0.25 and 0.32 in deuterated cyclohexane and in deuterated toluene, respectively.[42] The fact that the scaling exponent in

cyclohexane was lower than the value expected for rigid spheres of uniform density (ν = 0.33) was attributed to a non-uniform density of chain segments within the molecules. A power law model for the radial density function [ρ(r)] corresponding to Equation 2-1, where r is the distance of the chain segments from the center of the molecules and R_{max} is the hydrodynamic radius, was proposed to fit the SANS scattering profiles obtained.

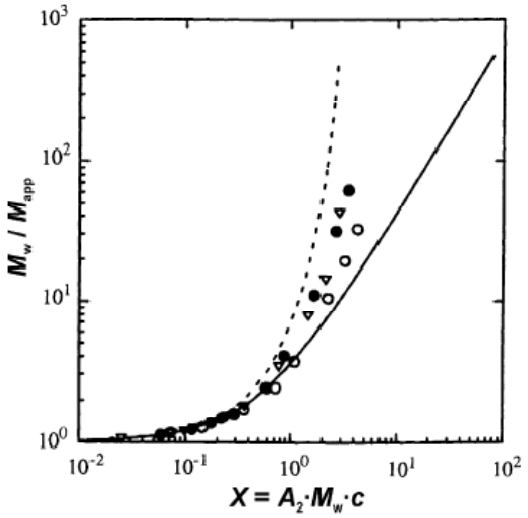

Figure 2-8: Osmotic modulus as a measure of the structural rigidity of arborescent polymers.
(o) G0PS5; (•)G1PS5; (Δ)G2PS5; (--)hard spheres; (—)random coils. From Gauthier et al.[41]

$$\rho(r) = 1 - \left(\frac{r}{R_{max}}\right)^{\propto} \qquad \textbf{Equation 2-1}$$

The power law model with α = 4, found to fit the experimental data, is characterized by a high, constant segmental density in the inner (core) portion of the molecules and a diffuse layer on the outside (Figure 2-9). As the exponent, α, approaches infinity, Equation 2-1 becomes identical with the hard sphere model.

The extent of interpenetration of the PS "layers" added in successive grafting reactions was examined for arborescent PS substrates grafted with deuterated PS chains by the SANS contrast matching method.[43] The principle behind the contrast matching method is illustrated in Figure 2-10. In a shell-matching solvent the shell becomes invisible and the R_g can be determined for the core portion of the molecules, and vice versa. It was noted that swelling of the molecules was more significant for the shell than for the core, due to the increased mobility of the shell chains only attached at one end, in contrast to the more rigid core chains attached at multiple branching points.

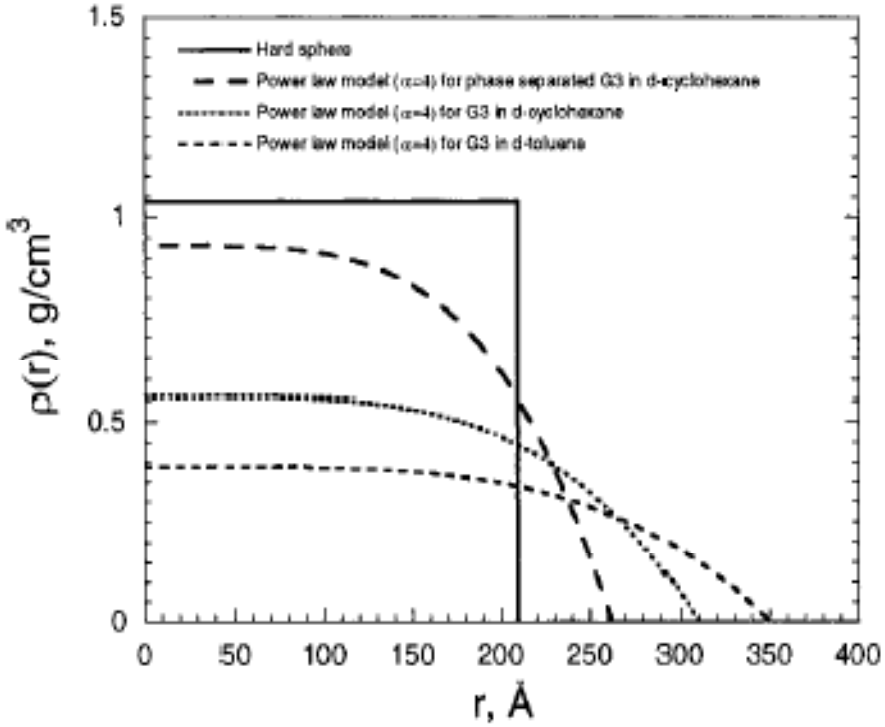

Figure 2-9: Radial density profile for power law model and hard sphere model.
From Choi et al.[42]

The scattering intensity profile was related to the so-called real space pair distance distribution function (PDDF), which enables the determination of the overall shape and size

of objects.[43] The PDDF obtained for G3 and G4 PS molecules, compared in Figure 2-11b, have the shape expected for a core-shell morphology. Significantly, the G4PS sample displays two clear maxima whereas G3PS displays only one. This indicates that the G4PS molecules have better phase separation between the core and the shell than the G3 polymers. In Figure 2-11c, it can also be seen that the curve crosses from a negative sign to a positive sign, corresponding to the scattering contrast between the PS core and the deuterated PS shell.

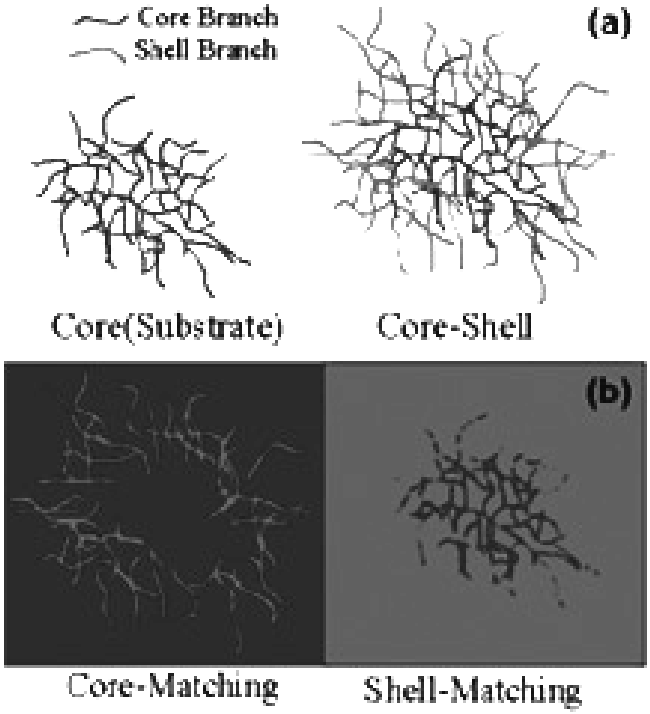

Figure 2-10: (a) Arborescent polystyrene molecules, (b) appearance in core-matching and shell-matching solvents.
From Yun et al.[43]

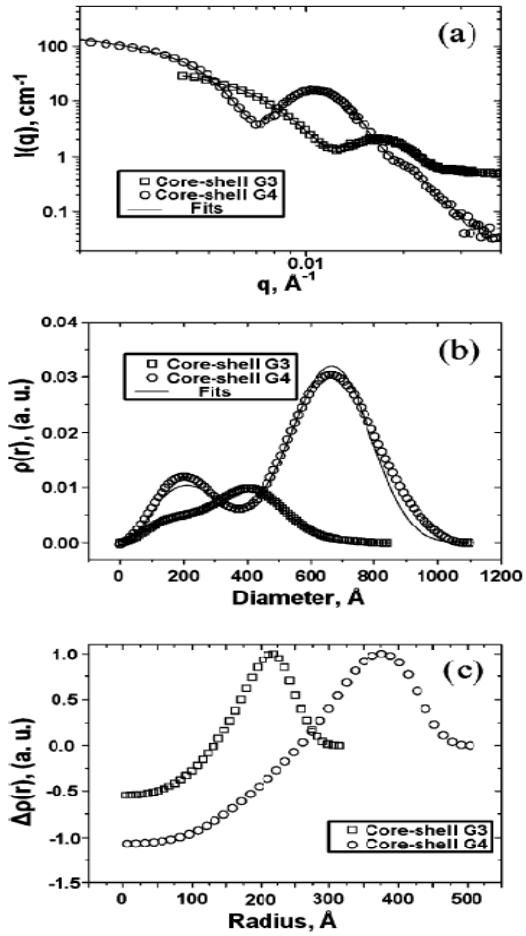

Figure 2-11: (a) Experimental SANS data fitted by the Indirect Fourier Transform method in deuterated toluene, (b) corresponding PDDF and (c) contrast profile.

From Yun et al.[43]

Another technique used to probe the morphology of arborescent molecules is fluorescence quenching measurements in dilute solutions.[44] Linear and arborescent PS were labeled with pyrene derivatives and characterized in quenching experiments with either nitrobenzene or nitrated linear PS. It was noted that the branched polymers behaved like two-phase systems, corresponding to a shell of flexible polymer surrounding a less penetrable, highly hindered core. A decrease in the fraction of accessible pyrene labels was also

observed for higher generation polymers. This result was consistent with a gradual increase in stiffening of the core for successive generations.

Beyond the dilute and semi-dilute solution studies discussed above, the behavior of arborescent PS was also investigated in the molten state, where the molecules are much more likely to interpenetrate and entangle with each other. The melt rheology of arborescent PS was investigated as a function of chain length and generation number.[45] It was noted that arborescent PS molecules have a very low zero-shear viscosity (η_o) relatively to linear PS of similar molecular weight. A scaling behavior $\eta_o \sim \overline{M_w}^1$ was also observed as compared with $\eta_o \sim \overline{M_w}^{3.4}$ for linear PS, consistent with a very low degree of entanglement for AP vs. linear polymers. Furthermore, η_o increased with the length of the side chains for both G0 and G1 PS (Figure 2-12). For the G2 and G3 molecules a change in entanglement mode was observed, the two systems displaying a decrease in η_o as the molecular weight of the side chains increased.

Finally, scanning force microscopy (SFM) was used to investigate the molecular organization of G1-G3 arborescent PS molecules in thin films.[46] A G1PS sample yielded granular films with no distinct order, but the G3PS film was characterized by a hexagonally packed array structure. Films of arborescent PS with short side chains ($\overline{M_w}$ = 5,000) had a thickness relatively close to the diameter of the molecules, whereas longer side chains ($\overline{M_w}$ = 30,000) yielded a flattened "pancake-like" appearance. Annealing of the films above their glass transition temperature (T_g) caused the short-chain films to rupture, the individual molecules regaining a perfectly spherical shape due to elastic recovery, while for longer side chains no recovery was observed during annealing.

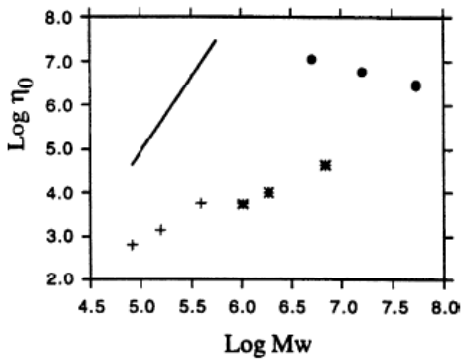

Figure 2-12: Zero shear viscosity as a function of molecular weight.
(+) G0PSx; (⁎) G1PSx; (•) G3PSx (x = 5, 10, 20); (—) Linear polystyrene. From Hempenius et al. [45]

Arborescent polybutadiene

Hempenius et al. utilized successive functionalization and grafting reactions to generate arborescent polybutadiene by anionic polymerization and grafting.[47] Butadiene was polymerized in hexane to yield ca. 6 % of 1,2-butadiene units that were subjected to hydrosilylation with chlorodimethylsilane to produce chlorosilyl coupling sites (Scheme 2-5). These sites were then coupled with polybutadienyllithium to obtain a G0 or comb-branched structure. An excess of side chains was required in these reactions, since it was impossible to monitor the grafting process by titration of the colorless polybutadienyllithium side chain precursor with the chlorosilylated substrates in analogy to what was done for arborescent PS.

Arborescent polybutadienes up to generation G2 and containing ca. 10 coupling sites per side chain with a molecular weight of approximately 10^4 were characterized. A geometric increase in molecular weight (from 190,000 to 71,000,000) and branching functionality (10 -

1160) were observed over successive generations while maintaining low PDI values (1.1-1.3).

The solution properties of G2 arborescent polybutadienes were found to be consistent with a hard sphere morphology, the ratio of R_g(LS) over R_h(viscometry) being 0.8 (for hard spheres, this ratio should be 0.775), as compared with 1.4-1.5 for linear polybutadiene.

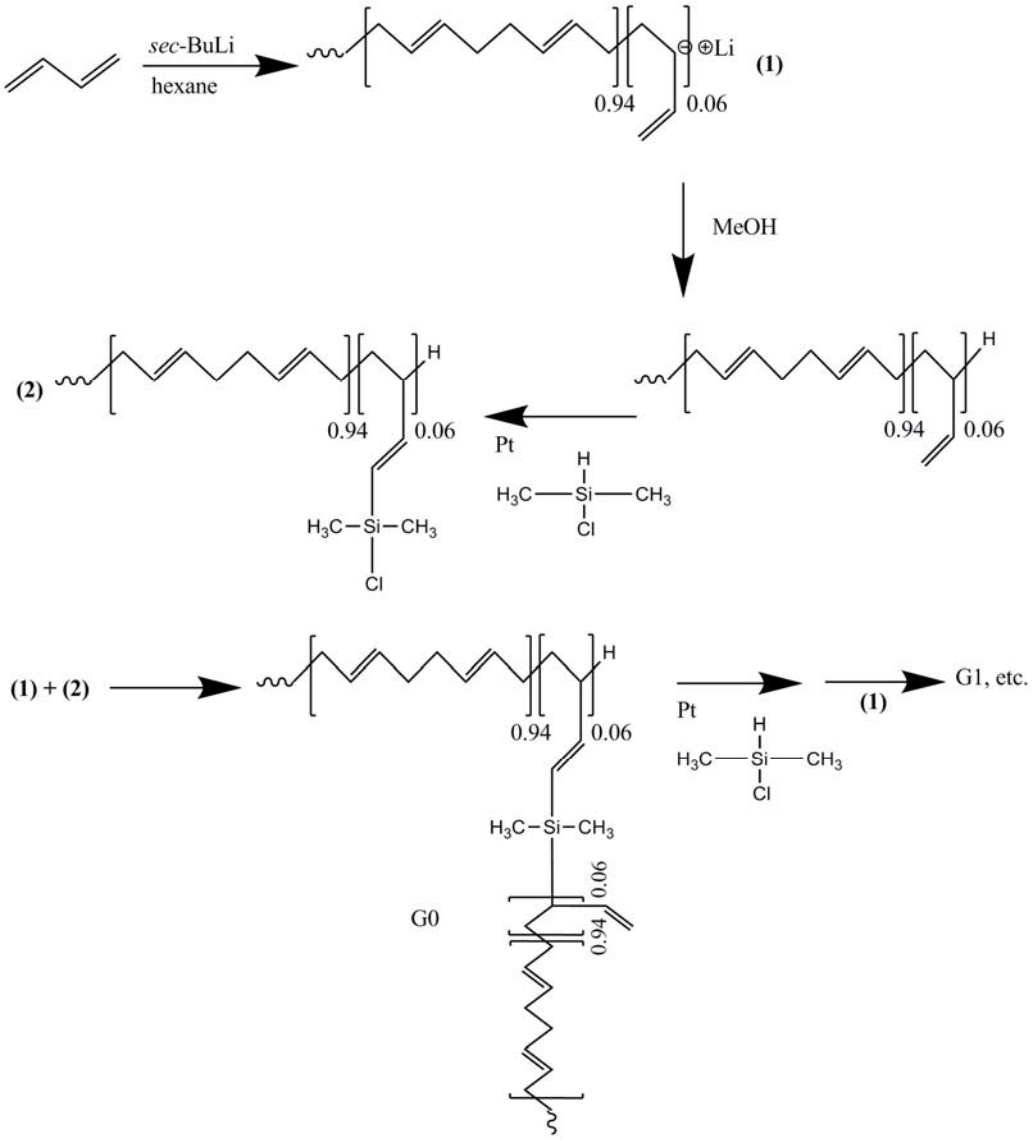

Scheme 2-5: Synthesis of arborescent polybutadiene.

From Teertstra.[25]

Arborescent polystyrene-*graft*-polyisoprene

The synthesis of polystyrene-*graft*-polyisoprene was achieved by grafting living polyisoprenyllithium chains onto PS substrates functionalized with either chloromethyl[48] or acetyl coupling sites.[38] The synthetic strategy with chloromethyl coupling sites was analogous to that provided in Scheme 2-3, but polyisoprenyllithium chains capped with DPE were used in the last grafting cycle. The grafting reaction on acetylated PS was likewise analogous to that described in Scheme 2-4 using polyisoprenyllithium chains, but the grafting yield was enhanced by the addition of LiCl. While this had no influence on the grafting yield per se, capping of the polyisoprenyllithium chains with a few 2VP units was advantageous to produce a darker-colored solution facilitating the colorimetric titration of the living polyisoprene (PIP) solution with acetylated PS, since the color gradually faded as the macroanions were consumed in the grafting reaction.

The microstructure of the PIP side chains can be controlled through the polymerization solvent polarity. Thus the polymerization of isoprene in THF yielded mixed microstructure side chains (with nearly equal proportions of 1,2-, 1,4-, and 3,4-units), whereas in cyclohexane a high *cis*-1,4-microstructure content could be achieved (>70 % *cis*-1,4 units).[48] The morphology of polystyrene-*graft*-polyisoprene copolymers was investigated by the SFM technique (Figure 2-13). For G1PS-PIP5 a distinct core-shell morphology could be observed in the phase contrast mode but for G0PSPIP5, phase separation between the two components was less distinct. Furthermore the PS core could not be detected for copolymers with long side chains ($\overline{M_w} \approx 30{,}000$), presumably due to the low PS content of these copolymers.

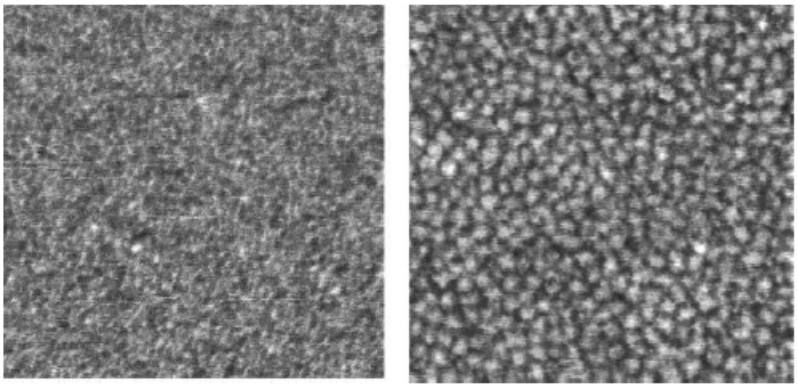

Figure 2-13: Phase contrast SFM images for (left) G0PS-PIP5 and (right) G1PS-PIP5. The width of the image is 500 nm. From Kee and Gauthier.[48]

The T_g of polystyrene-*graft*-polyisoprene and linear PIP was investigated by differential scanning calorimetry (Table 2-4).[49] For linear PIP with 30K < $\overline{M_w}$ < 340K, the T_g was virtually independent of $\overline{M_w}$ (-64.0 ^{0}C ≤ T_g ≤ -65.0 ^{0}C) and insensitive to slight changes in microstructure. The T_g for the side chain samples behaved similarly in spite of their lower molecular weight (5K < $\overline{M_w}$ < 30K). This was attributed to the fact that the linear PIP samples had a $\overline{M_w}$ above the critical molecular weight (M_c ≈ 2500) for T_g insensitivity in PIP.[50] The T_g of the copolymers were only slightly (< 2 ^{0}C) higher than the corresponding side chain T_g, possibly as a result of reduced chain end mobility due to coupling with the PS substrate at one end, or else due to limited miscibility between the core and the shell portions of the molecules. These results are consistent with the two-phase morphology observed in the AFM measurements.[48]

Dynamic mechanical measurements were utilized to investigate the viscoelastic properties of polystyrene-*graft*-polyisoprene as a function of generation, branch length, and composition (Figure 2-14). The dynamic modulus curve for PS-cPIP5 (*cis*-1,4-PIP side chains) lacked an entanglement plateau, due to the low molecular weight of the branches as

compared with the critical entanglement molecular weight for PIP ($M_e \approx 5400$) (Figure 2-14).[51] An entanglement plateau appeared as the length of side chains was increased, however. The dynamic modulus curves for polystyrene-*graft*-polyisoprene copolymers of overall generation G1 for all side chain length was nearly identical to those observed for G1 arborescent PS[45] and star-branched polybutadienes.[52]

Table 2-4: Arborescent polystyrene-*graft*-polyisoprene composition and T_g analysis

Adapted from Teertstra and Gauthier.[49]

Sample	PS content (mol %)[a]	T_g (^{0}C)[b]	
		Linear PIP/Side chain	Arborescent copolymer
cPIP30	--	-64.2	--
cPIP110	--	-64.9	--
cPIP130	--	-65.0	--
cPIP340	--	-64.7	--
cPIP1M	--	-64.6	--
PS-cPIP5	6.2	-65.7	-64.2
PS-cPIP10	3.6	-63.7	-61.6
PS-cPIP30	0.89	-64.1	-62.4
PS-cPIP40	0.89	-63.5	-62.5
G0PS-cPIP5	7.2	-65.5	-63.6
G0PS-cPIP10	3.6	-64.3	-62.3
G0PS-cPIP30	1.8	-64.9	-64.0
G0PS-cPIP40	1.8	-64.3	-63.1
G1PS-cPIP5	7.2	-66.3	-63.2
G1PS-cPIP30	4.5	-65.2	-63.5
G2PS-cPIP5	26	-66.2	-63.1
G2PS-cPIP30	20	-64.6	-63.3

[a] Volume fraction of polystyrene in molecule based on molecular weight increase and bulk densities ρ_{PS} =1030 kg/m^3 and ρ_{PIP} =913 kg/m^3 at 25 ^{0}C.
[b] Variation of ± 0.2 ^{0}C for a minimum of two measurements.

The loss modulus (G") curves for the G1 copolymers displayed two inflection points corresponding to the relaxation of the PIP side chains (at intermediate frequencies) and the

entire molecules (at low frequencies), respectively. As the side chain molecular weight increased, the inflection points shifted to lower frequencies.

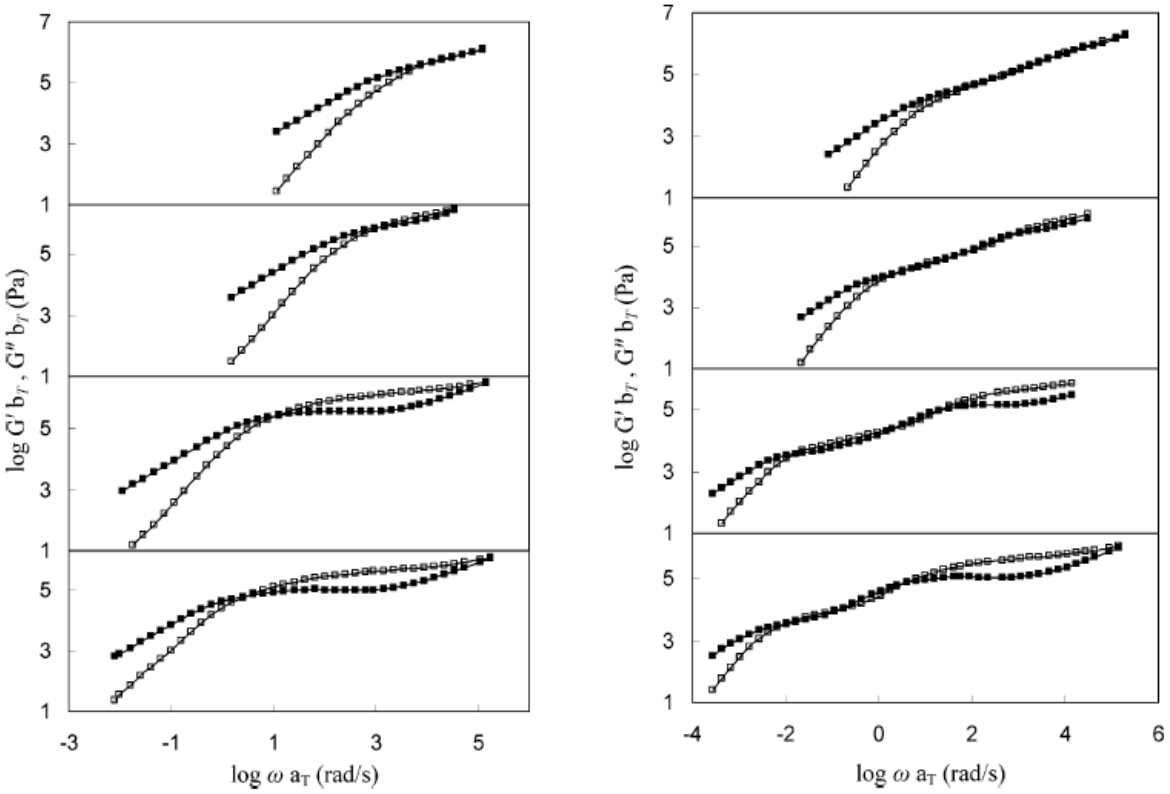

Figure 2-14: Dynamic modulus curves for (left) PS-PIPx and (right) G0PS-PIPx at 20 ^{0}C.
(▪) loss modulus, G"; (▫) storage modulus, G'. The side chain length increases from top to bottom (x = 5, 10, 30, 40). From Teertstra and Gauthier.[49]

The dynamic modulus curves for copolymers of overall generations G2 and G3 (Figure 2-15) were significantly different from the G0 and G1 copolymers. Their storage modulus (G') was larger than G", and the G' curve reached a plateau at low frequencies. Both G1PS-PIP30 and G2PS-PIP30 also displayed an inflection point (Figure 2-15) at nearly the same frequency, corresponding to the relaxation of the PIP side chains.

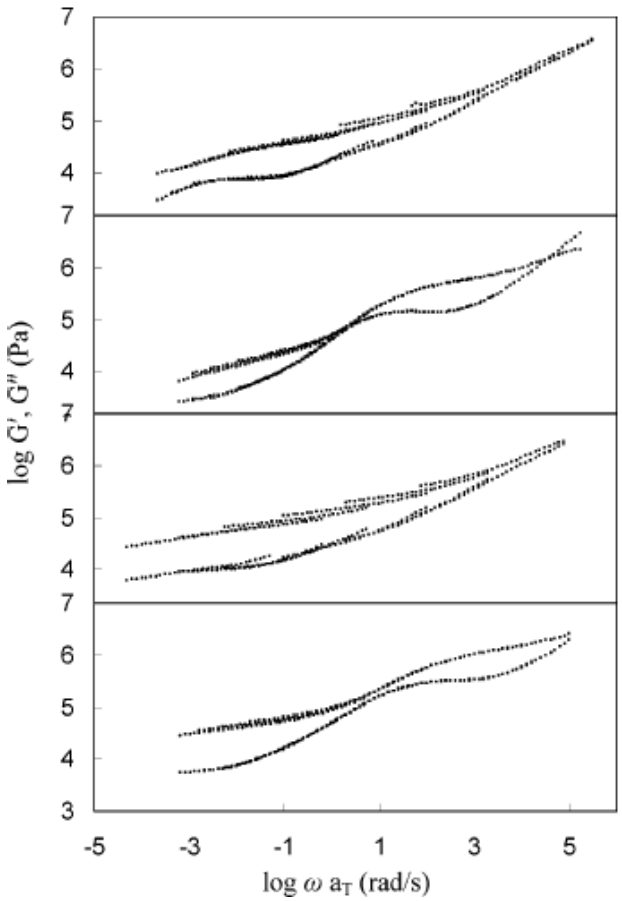

Figure 2-15: Dynamic modulus curves for overall G2 and G3 polyisoprene copolymer at 20 ^{0}C.
From top to bottom: G1PS-PIP5, G1PS-PIP30, G2PS-PIP5 and G2PS-PIP30 with G' (upper), G" (lower). From Teertstra and Gauthier.[49]

Failure of the time-temperature superposition (TTS) principle at low to intermediate frequencies was also observed for the modulus curves of G1PS-PIP5 and G2PS-PIP5, but both samples obeyed the TTS at high frequencies (corresponding to low temperatures). This effect was attributed to the biphasic nature of the copolymers, in analogy to other phase-separated systems reported in the literature.

The η_o of the G0, G1 and G2 copolymers was compared to linear PIP samples of similar molecular weights. All copolymers displayed lower η_0 values than linear PIP of identical $\overline{M_w}$ (Figure 2-16), with a slight apparent upturn observed for the higher molecular

weight G0 and G1 samples. Even though the effect was minor, it was attributed to enhanced entanglement formation for the PIP side chains, in analogy to star-branched polybutadienes[51] and hyperbranched polyisobutylenes.[53] The G2 copolymers were also characterized by a significant decrease in η_0 as their overall molecular weight increased from 13,000,000 to 23,000,000 for side chains with $\overline{M_w} \approx$ 5,000 and 30,000 respectively. The drop was attributed to the higher branching density of the copolymers with shorter side chains, G1PS-PIP5 having a 3 times higher η_0 value than G1PS-PIP30. The higher η_0 for the short side chain sample hints at a change from a rigid, dense globular structure (G1PS-PIP30) to a more flexible structure (G1PS-PIP5).

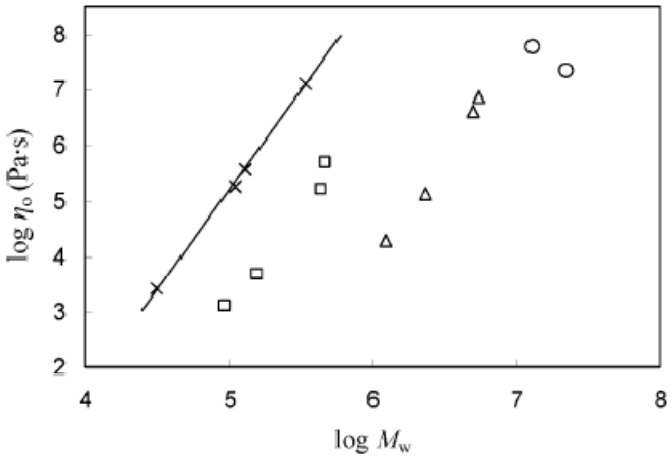

Figure 2-16: Zero-shear viscosity as a function of molecular weight at 20 ^{0}C in solution. (x) Linear polyisoprene; (▫) G0 copolymers; (Δ) G1 copolymers; (o) G2 copolymers. From Teertstra and Gauthier.[49]

Arborescent polystyrene-*graft*-poly(2-vinylpyridine)

The synthesis of polystyrene-*graft*-poly(2-vinylpyridine) has been accomplished by coupling living poly(2-vinylpyridine)lithium with both chloromethylated[54,55] and acetylated[55]

polystyrene substrates. The reaction proceeded in similar fashion to Schemes 2-3 and 2-4 except for the last grafting reaction, where living P2VP homopolymer chains were grafted onto the substrate. Due to the much lower reactivity of P2VP anions as compared to PS anions, capping of the living P2VP chains with DPE was unnecessary. In the presence of N,N,N',N'-tetramethylethylenediamine (TMEDA), to increase the reactivity of the P2VP macroanions by complexation with the lithium counterion, the grafting yield increased from 84 % to 92 % when grafting P2VP onto chloromethylated linear PS.

The thermodynamics of the self-assembly of arborescent polystyrene-*graft*-poly(2-vinylpyridine) copolymers in solution were recently investigated by Yun et al.[56] The hydrodynamic diameter of the molecules (D_h) was monitored with dynamic light scattering (DLS) measurements in methanol and in toluene as a function of temperature (Figure 2-17). For both G1PS-P2VP5 and G1PS-P2VP30 dissolved in toluene (poor solvent for the P2VP shell) an initial increase in D_h was observed as the temperature was increased, but was followed by an abrupt decrease above 26 ^{0}C for G1PS-P2VP5 and 41 ^{0}C for G1PS-P2VP30. Clearly, aggregation occurred below these critical temperatures. The persistence of the aggregates to higher temperatures for the copolymers with longer side chains suggests that their aggregation is energetically more favorable. For both copolymers dissolved in methanol, a good solvent for the P2VP shell, no aggregation was observed over the whole temperature range investigated.

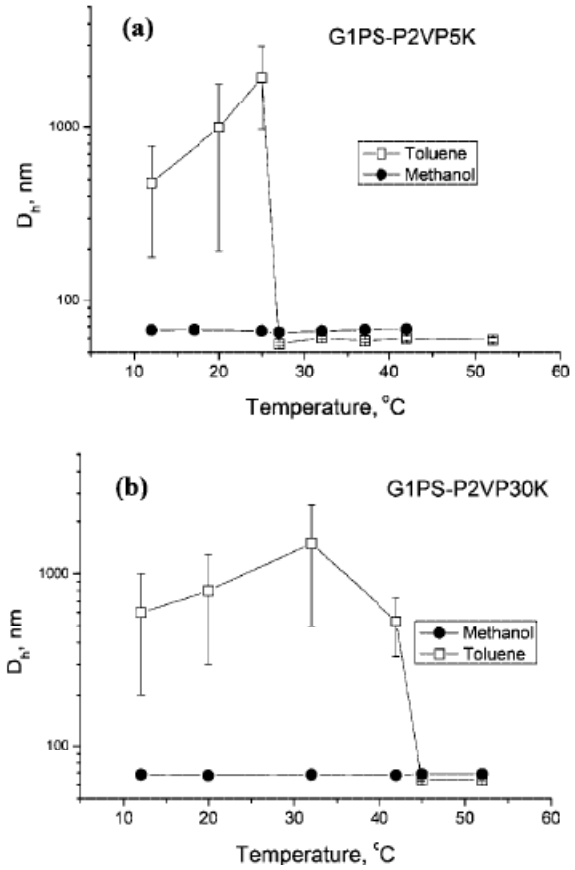

Figure 2-17: Temperature dependence of D_h in methanol and in toluene for (a) G1PS-P2VP5 and (b) G1PS-P2VP30.
From Yun et al.[56]

The critical self-assembly concentration (csc), defined as the minimum concentration required for the formation of aggregates, was determined as a function of temperature using DLS measurements (Figure 2-18a). This allowed the determination of the standard Gibbs free energy for self-assembly [$\Delta G^0 = RT\ln(csc)$] as a function of the csc and the temperature (Figure 2-18b), as well as the standard enthalpy (ΔH^0) of self assembly from the Gibbs-Helmholtz equation ($\Delta H^0 = R[d \ln(csc)/d T^{-1}]$). Finally, the standard entropy (ΔS^0) for self assembly was determined as the slope of a plot of ΔG^0 vs. T according to the relationship $\Delta G^0 = \Delta H^0 - T \Delta S^0$. It was determined that ΔG^0 for both copolymers was negative, longer side chains leading to a more negative value than shorter side chains. This indicates that the

self-assembly of the copolymer in toluene is favorable due to the solvophobic (unfavorable) interactions of the solvent with the P2VP shell segments, the more negative ΔG^0 value for the longer side chain sample confirming an energetically more favorable aggregation process. The ΔH^0 and ΔS^0 values for both copolymers were negative, indicating that self-assembly of the copolymer was enthalpically favored, but entropically disfavored due to the highly organized structure of the aggregates. They also found that the superstructures formed by arborescent copolymers were much larger than those formed by linear and star-shaped block copolymers under similar conditions.

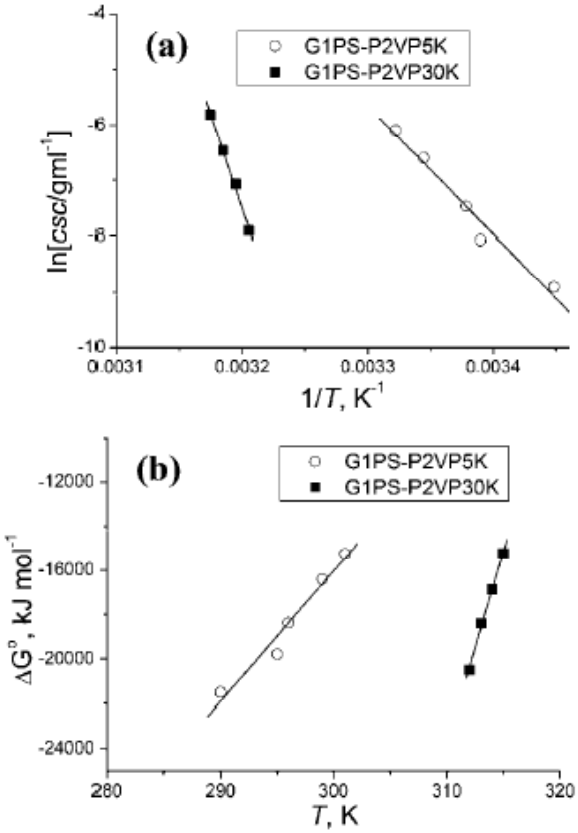

Figure 2-18: Temperature dependence of (a) the csc and (b) the Gibbs free energy for G1PS-P2VP5 and G1PS-P2VP30.
From Yun et al.[56]

The superstructures formed below the critical self-assembly temperature were investigated by scanning electron microscopy (SEM) and transmission electron microscopy (TEM) imaging (Figure 2-19). Aggregates were observed in both TEM and SEM for G1PS-P2VP5 when the solutions were evaporated at 20 ^{0}C, while none were present when the same solutions were evaporated at 30 ^{0}C. The large sphere structures tended to associate further during solvent evaporation, giving rise to even larger aggregates (Figure 2-19b) but some unassociated copolymer molecules could still be detected, even at temperatures below the critical temperature (Figure 2-19a). This behavior contrasts with that of linear and star-block copolymers, which formed only monodispersed micelles below the critical micelle temperature.

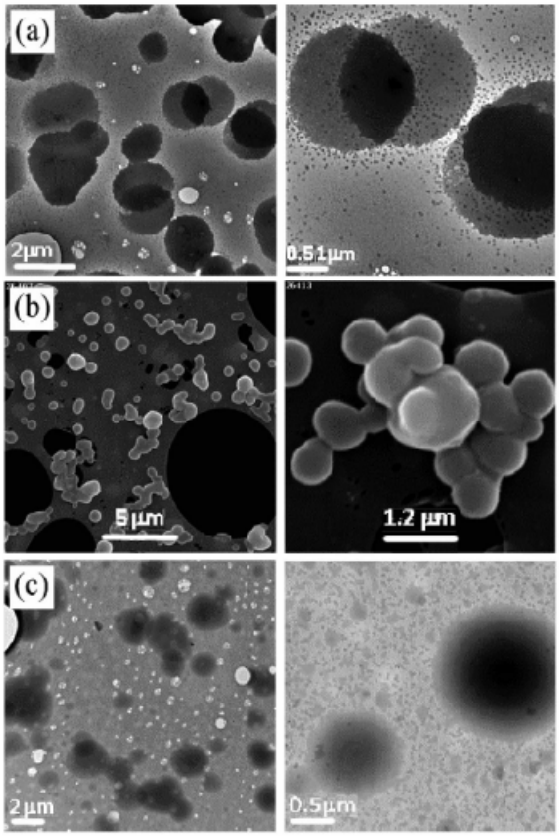

Figure 2-19: (a) TEM and (b) SEM images for G1PS-P2VP5, and (c) TEM image for G1PS-P2VP30.
Evaporation of toluene at 20 ^{0}C. From Yun et al.[56]

Arborescent polystyrene-*graft*-(poly(2-vinylpyridine)-*block*-polystyrene)

The synthesis of complex arborescent polystyrene-*graft*-(poly(2-vinylpyridine)-*block*-polystyrene) layered molecular structures, incorporating a core and a shell of PS chains surrounding an inner poly(2-vinylpyridine) layer, was recently reported by Dockendorff et al.[57] The reaction scheme used was similar to Scheme 2-4 with the exception of the last grafting cycle, where living poly(2-vinylpyridine)-*block*-polystyrene chains were grafted onto acetylated PS substrates.

The grafting yield for the G0 and G2 polystyrene-*graft*-(poly(2-vinylpyridine)-*block*-polystyrene) copolymers was 17 and 20 %, respectively, which is surprisingly low when compared with arborescent PS homopolymer (87 % and 55 %)[38] and arborescent polystyrene-*graft*-poly(2-vinylpyridine) copolymer (86 % and 34 %) syntheses with comparable characteristics (same substrate generation and side chain length).[55] The low grafting yield was attributed to the formation of micelles by the PS-b-P2VP macroanions hindering the grafting reaction.

Arborescent polystyrene-*graft*-poly(*tert*-butyl methacrylate)

The synthesis of arborescent polystyrene-*graft*-poly(*tert*-butyl methacrylate) copolymers was achieved by Kee and Gauthier,[58] starting from chloromethylated PS substrates as shown in Scheme 2-3. The chloromethylated substrates were subjected to a halogen exchange reaction with sodium bromide to convert the coupling sites to more reactive bromomethyl groups (Scheme 2-6). A living poly(*tert*-butyl methacrylate) solution was then titrated with the bromomethylated substrate to generate the copolymers. The

corresponding poly(methacrylic acid) derivatives were generated by treating the copolymers with trimethylsilyl iodide and HCl.

Two series of arborescent polystyrene-*graft*-poly(*tert*-butyl methacrylate) copolymers with a side chain molecular weight of either $\overline{M_w} \approx$ 5,000 or 30,000 were synthesized.

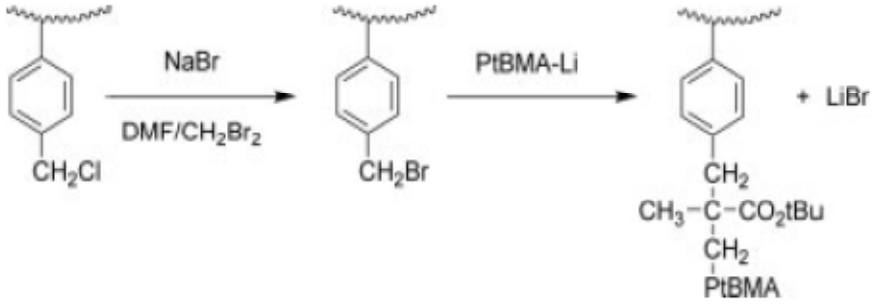

Scheme 2-6: Conversion of chloromethylated to bromomethylated substrate and coupling with poly(*tert*-butyl methacrylate).
From Kee and Gauthier.[58]

2.3.1.2 "Grafting from" methods

Dendrimer-like poly(ethylene oxide) (PEO)

The synthesis of dendritic PEO molecules with a controlled architecture analogous to dendrimers, but incorporating PEO chain segments as spacers rather than monomer units between the branching points, was reported by Six and Gnanou.[59] The method used (Scheme 2-7) is based on the anionic ring opening polymerization of ethylene oxide starting from a trifunctional initiator (the potassium salt of trimethylolpropane), and subsequently from the chain ends of the polymer substrate. Chemical modification of each terminus of the newly grown chains with a chloro, iodo or tosyl derivative of 2,2-dimethyl-5-ethyl-5-hydroxymethyl-1,3-dioxane, followed by hydrolysis, provided the dihydroxyl branching points serving as initiator for the growth of two chains in the next generation.

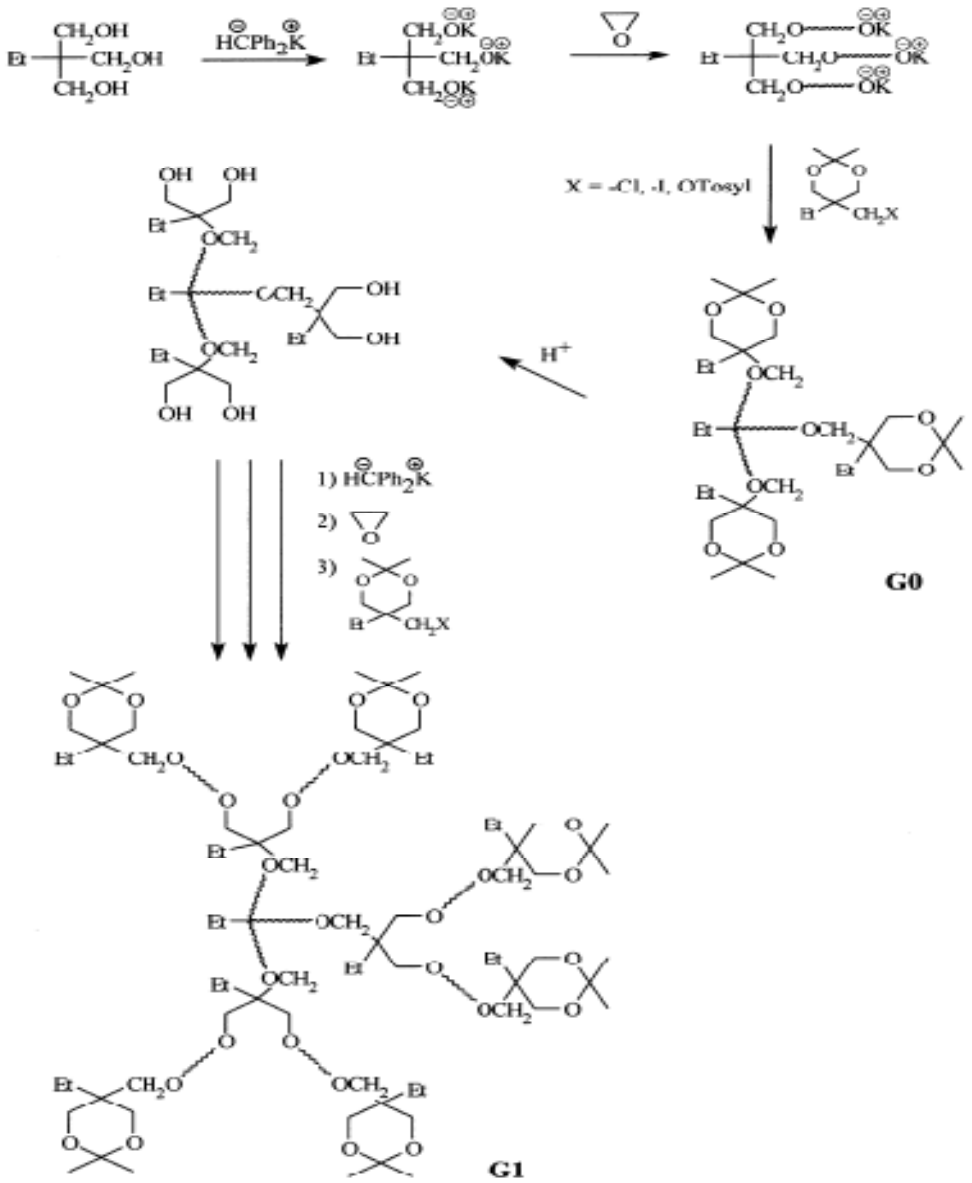

Scheme 2-7: Synthetic scheme for the preparation of dendritic PEO through a "grafting from" method.
From Teertstra.[31]

Series of G1 PEO samples derived from the same trifunctional core but incorporating side chains with different molecular weights (by using different amounts of monomer in the chain growth step) have been characterized. Due to the inherent character of the "grafting from" method the side chains could not be characterized, but the overall PDI of the polymers

remained relatively low (1.1-1.3). The molecular weight determined by GPC analysis using a linear PEO standards calibration curve was underestimated for the G1 polymers as compared to the absolute values determined from LS analysis, in analogy with other dendrigraft polymers.

Dendrimer-like polystyrene-*graft*-poly(ethylene oxide) (PS-PEO)

A variation of the procedure described in Scheme 2-7 allowed the generation of copolymers with six PS segments in the core and 12 PEO chains in the shell.[60] Hexa[4-(1-chloroethyl)phenethyl]benzene activated with $SnCl_4$ served to initiate the cationic polymerization of styrene. The six-arm star-branched PS, containing chlorine chain termini, was then reacted with allyltrimethylsilane and $SnCl_4$ to obtain allylic functionalities that were transformed into hydroxyl groups by reaction with 9-borabicyclo[3.3.1]nonane (9-BBN) and H_2O_2. Growth of the PEO chains was achieved after introducing branching points as described in Scheme 2-7, by reaction with the chloro, iodo or tosyl derivative of 2,2-dimethyl-5-ethyl-5-hydroxymethyl-1,3-dioxane and hydrolysis.

GPC analysis using a solvent selective for the PEO chains (e.g. water/acetonitrile) as the mobile phase led to a single population (peak) corresponding to unimolecular micelles. This was compared to star-branched copolymers with six outer PEO arms of similar composition yielding bimodal distributions, indicative of aggregation. The unimolecular distribution therefore indicated that the 12-arm PEO copolymer shielded the cores more effectively from each other.

The formation of micelles was also confirmed by comparing ^1H NMR analysis results in deuterated chlorinated solvents (e.g. CD_2Cl_2 and $CDCl_3$) and in deuterated methanol. In

chlorinated solvents, signals for both the PEO and PS chains could be seen, but in methanol only the PEO signal was detected.

Dendrimer-like poly(ethylene oxide)-*graft*-polystyrene (PEO-PS)

The synthesis of poly(ethylene oxide)-*graft*-polystyrene with terminal branching was achieved similarly to the synthesis of the dendritic PEO homopolymers (Scheme 2-7).[61] In this case trimethylolpropane and pentaerythritol served in the preparation of 3- and 4-arm star-branched PEO, respectively. The chain ends were modified with 2,2-bis(2-(bromomethyl)-propionato)propionyl chloride to introduce AB_2 branching points containing two 2-bromopropionate groups. These were activated with a copper bromide/2,2'-bipyridine catalyst system to grow PS segments by an atom transfer radical polymerization (ATRP) mechanism.

Arborescent polyglycidol

Walach et al.[62] reported a "grafting from" scheme for the preparation of arborescent architectures starting from the polymerization of glycidol acetal with potassium *tert*-butoxide (Scheme 2-8). Deprotection of the acetal functionalities with formic acid yielded pendent hydroxyl groups on the linear polyglycidol substrate that were titrated with potassium *tert*-butoxide (< 10 mol%) to serve as initiator in the growth of side chains. Repetition of the deprotection, titration, and side chain growth cycles yielded AP of generations up to G2.

Characterization results for some of the polyglycidol samples were reported. A geometric increase in molecular weight and a slight increase in PDI were observed for successive generations. In spite of the low degree of ionization used in the chain growth step,

to ensure the solubility of the polymers in organic solvents, between 76 % and 89 % of the polyglcidol units were identified as branching points. This was attributed to fast proton exchange occurring between the alcoholate anions and the free hydroxyl groups on the substrate. The authors suggested that partial deprotection rather than full deprotection of the acetal groups could have avoided this problem.

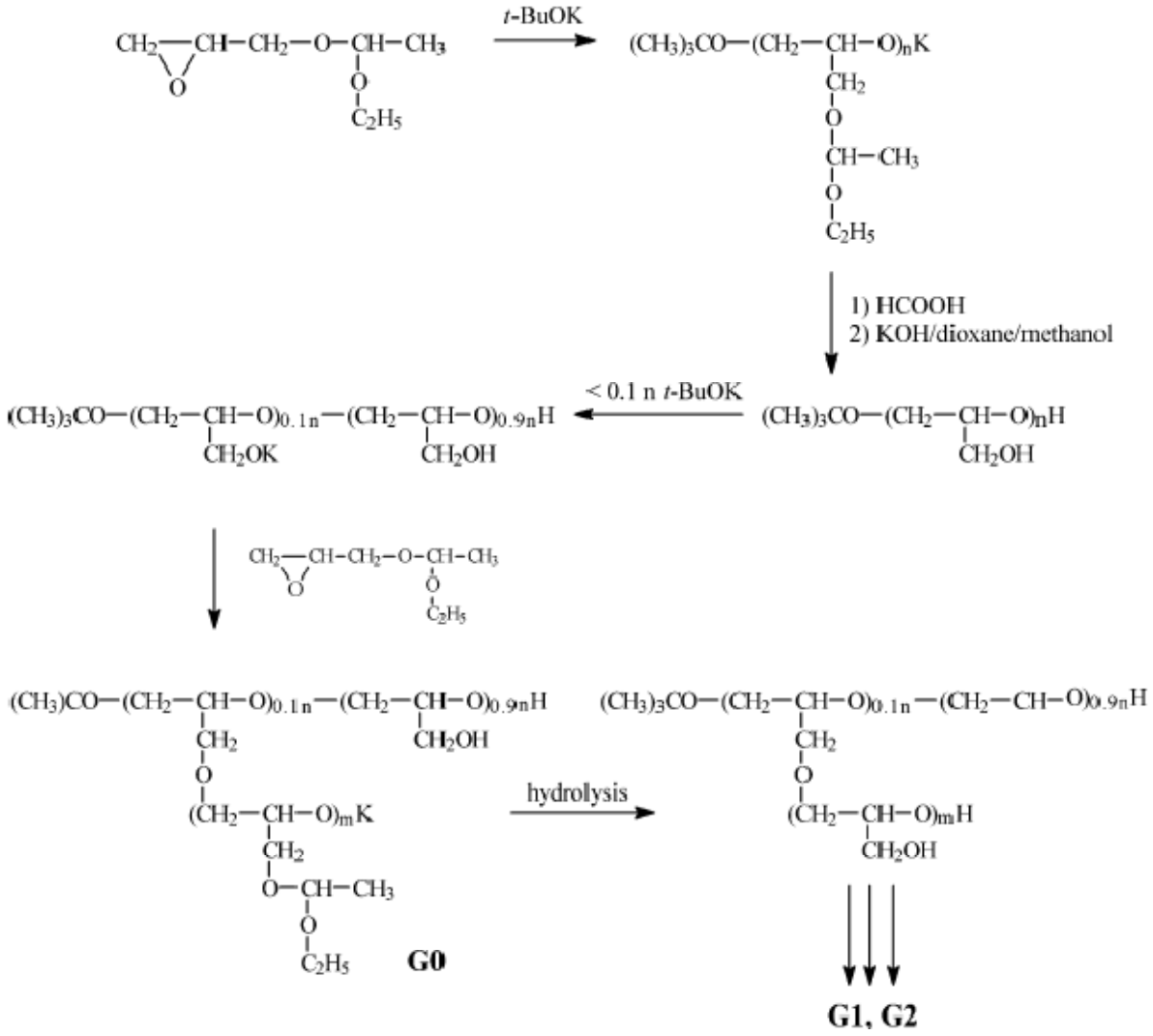

Scheme 2-8: Synthesis of dendritic polyglycidol.
From Teertstra.[31]

Dendrigraft polymers by "living" free radical polymerization

The synthesis of styrene homopolymers and styrene-methacrylate copolymers by the stable free radical polymerization (SFRP) and atom transfer radical polymerization (ATRP) techniques has been attempted with some degree of success.[63] A linear substrate was obtained by the SFRP of styrene and *p*-(4'-chloromethylbenzyloxymethyl)styrene comonomers (Scheme 2-9). The chloromethyl groups of the copolymer were then reacted with the sodium salt of hydroxyl-terminated 2,2,6,6-tetramethylpiperidine-N-oxide)styrene before a side chain growth cycle using styrene and *p*-(4'-chloromethylbenzyloxymethyl)styrene to obtain a G0 copolymer. The chloromethyl groups were then activated with CuCl and 2,2'-bipyridine to serve as initiating sites for styrene or *n*-butyl methacrylate polymerizations by ATRP.

For example, the molecular weight of a G0 substrate ($\overline{M_n}$ = 84,000, PDI = 1.24) increased significantly to $\overline{M_n}$ = 230,000 – 410,000 for the G1PS homopolymers while the PDI only increased slightly in most cases (PDI = 1.23 – 1.59). The modest increase in PDI was attributed to the large number of radical propagating centers increasing the probability of cross-linking. Cleavage of the side chains from the G0 substrate with trimethylsilyl iodide allowed the analysis of the PS side chains, which had molecular weights consistent with the expected values and PDI values < 1.3.

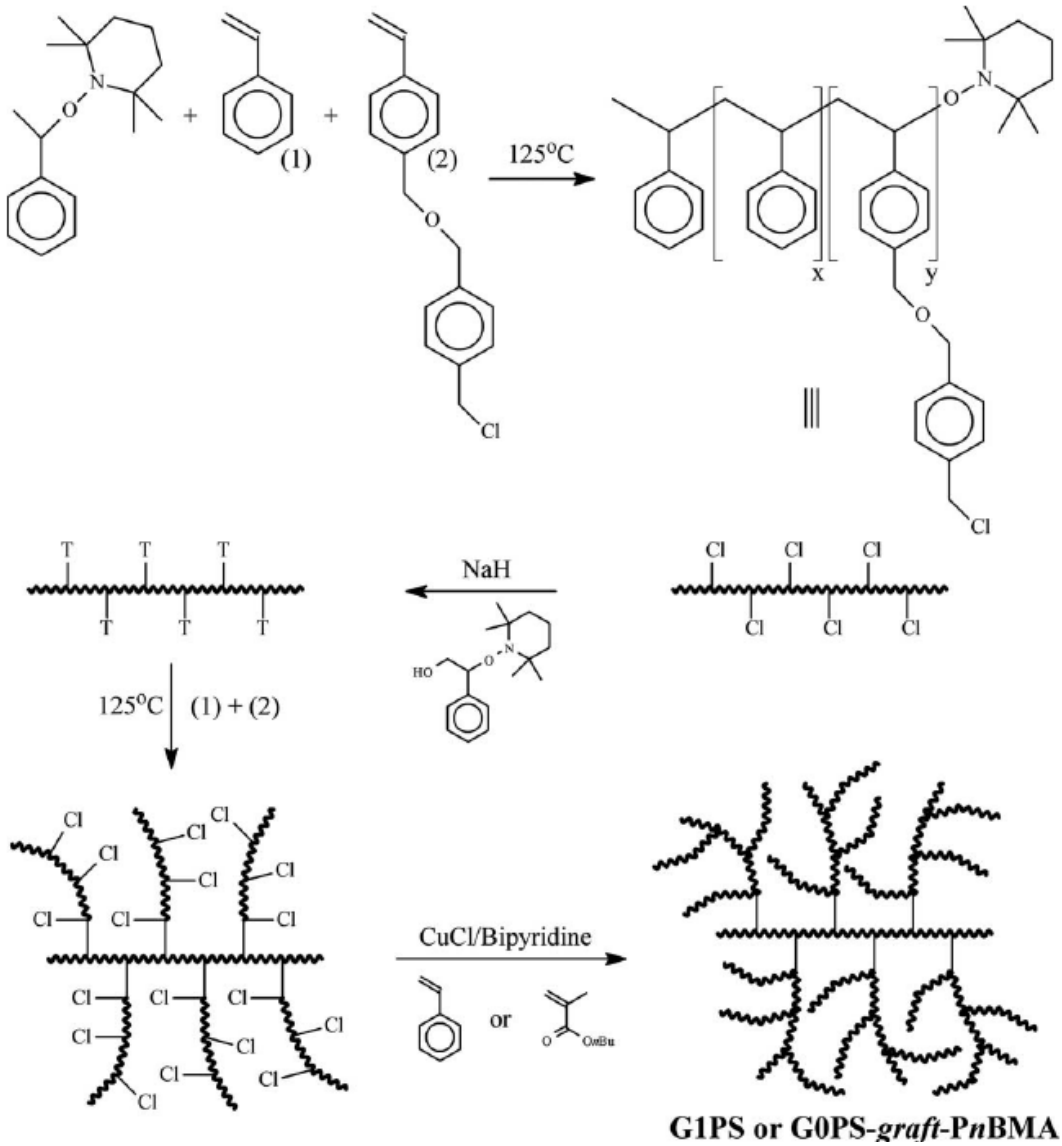

Scheme 2-9: Dendrigraft polystyrene and polystyrene-*graft*-poly(methacrylate) copolymers by SFRP and ATRP.
From Teertstra.[31]

2.3.1.3 Hybrid methodology

Arborescent polystyrene-*graft*-poly(ethylene oxide)

Only one synthetic procedure combining the "grafting onto" and the "grafting from" methodologies has been reported for the synthesis of arborescent polystyrene-*graft*-poly(ethylene oxide).[64] This approach provides highly controllable structures and low PDI

values, but inherits the limitations of the "grafting from" techniques hindering the complete characterization of the chains grown in the last reaction cycle.

Arborescent PS substrates were synthesized by a variation of the method described in Scheme 2-3 by coupling chloromethylated substrates with PS containing protected hydroxyl chain termini in the last cycle. This was achieved with a bifunctional initiator, 6-lithiohexyl acetaldehyde acetal, in the preparation of the side chains (Scheme 2-10). After grafting, the polymer was hydrolyzed to deprotect the hydroxyl groups, which were titrated with potassium napthalide to generate initiating sites for the polymerization of ethylene oxide.

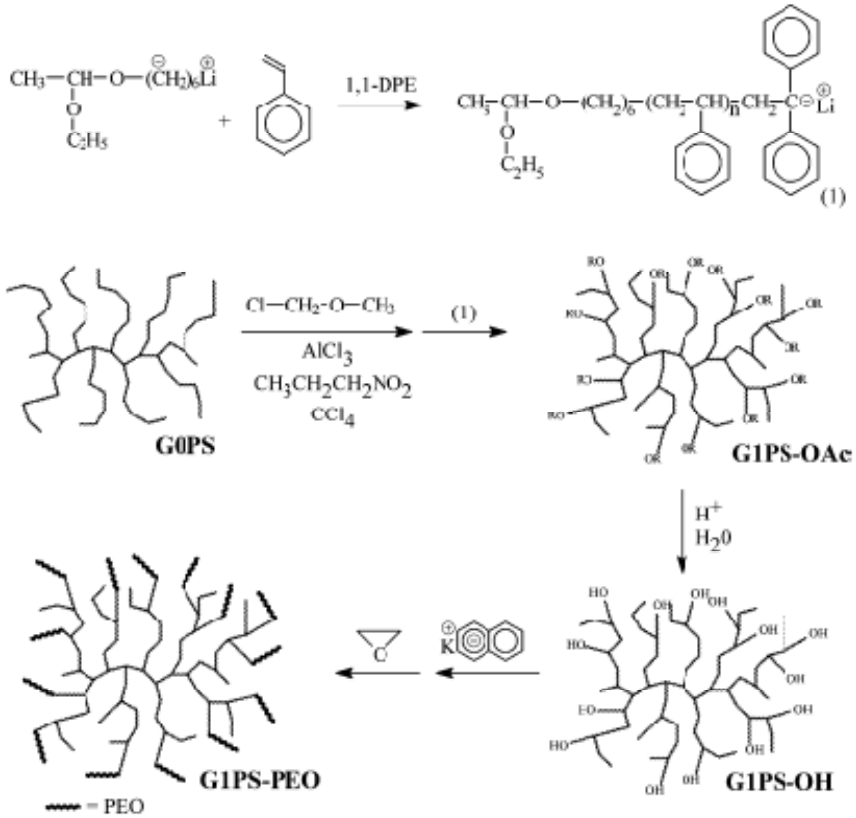

Scheme 2-10: Synthesis of arborescent polystyrene-*graft*-poly(ethylene oxide) through a hybrid method.

From Teertstra.[31]

Arborescent PS-PEO copolymers of generations up to G3 and PEO contents varying between 19 % and 66 %*w/w* were obtained, the PDI remaining low (PDI = 1.07 – 1.21) after the addition of the PEO block.

Detailed studies on the morphology and the physical characterization of these copolymers have been published recently. The self-assembly behavior of these amphiphiles was investigated as a function of branching density (generation number) and PEO content.[65] It was determined that superstructures formed spontaneously at the air-water interface upon spreading of a copolymer solution, the topology and association level of the superstructures depending on the composition and the structure of the molecules.[65] Ribbon-like superstructures were thus observed for PEO contents between 19 and 30 %*w/w*, irrespective of the arborescent copolymer architecture (Figure 2-20a). Large island-like superstructures were obtained for low PEO contents (≤ 15 %*w/w*) (Figure 2-20b), while molecules with a high PEO content (> 43 %*w/w*) had little tendency to associate (Figure 2-20c). The rigidity of the molecules also governed the type of topology formed at the air-water interface to some extent: High branching density copolymers had a lower association level as compared to low branching density copolymers. Most copolymers incorporating very compact cores, in particular, remained as isolated micelles at the air-water interface.[65]

The formation of superstructures under the influence of compression and temperature variations was also investigated.[66] The formation of larger structures was enhanced by compression (Figure 2-21) and increased at higher temperatures (Figure 2-22). Both effects were attributed to increased van der Waals attractive forces between the PS cores. The formation of these superstructures was also determined to be reversible, at least in some cases, when the external stimuli were removed. It was further confirmed using DLS

measurements that the formation of superstructures occurred upon spreading of the polymeric solution at the air-water interface rather than in solution.

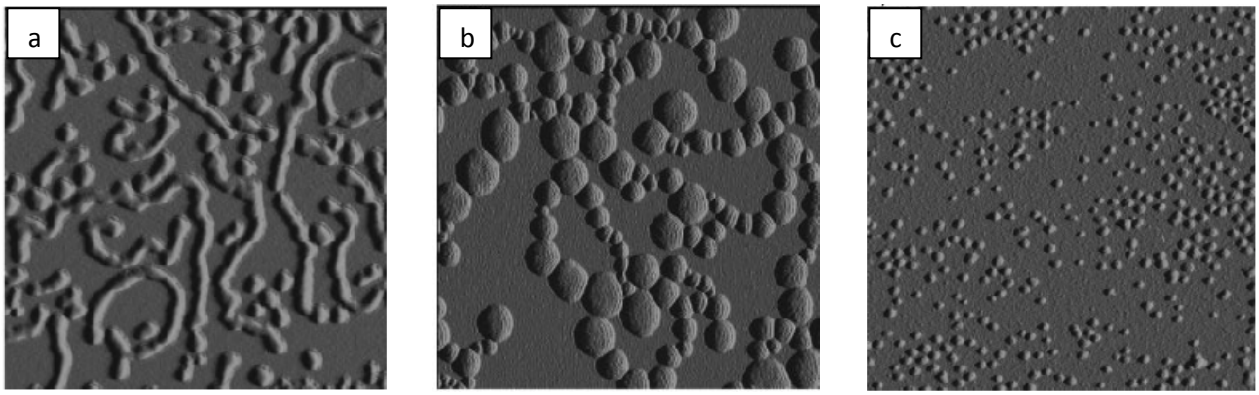

Figure 2-20: AMF images for (a) G1-30PS-LB-31 (ribbon-like structure), (b) G1-30PS-LB-15 (island-like structure), and (c) G1-5PS-HB-74 (non-associated molecules).
Image size 1.5 x 1.5 μm^2. Adapted from Njikang et al.[65]

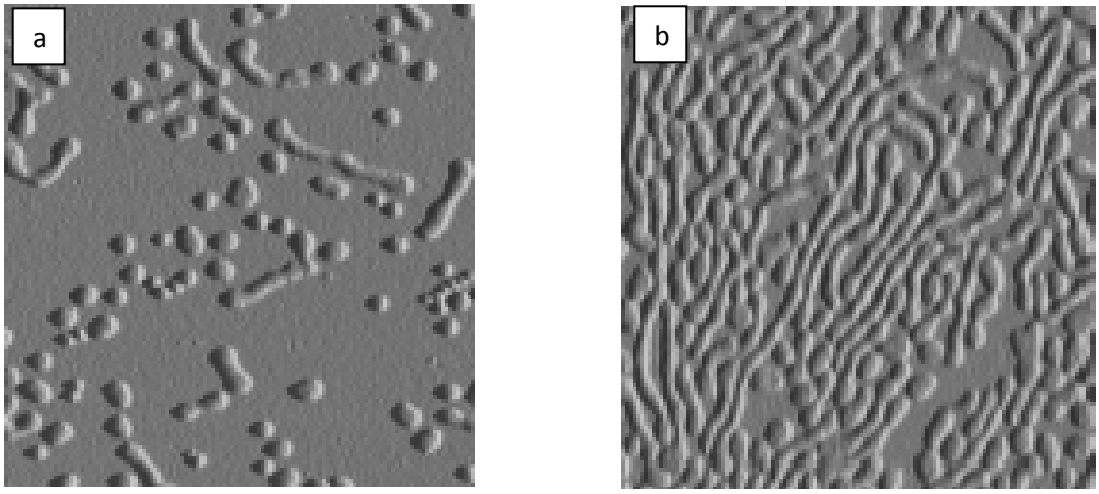

Figure 2-21: AFM images for G1-30PS-LB-22 at (a) 0 mN/m and (b) 8 mN/m.
Image size 1.5 x 1.5 μm^2. Adapted from Njikang et al.[66]

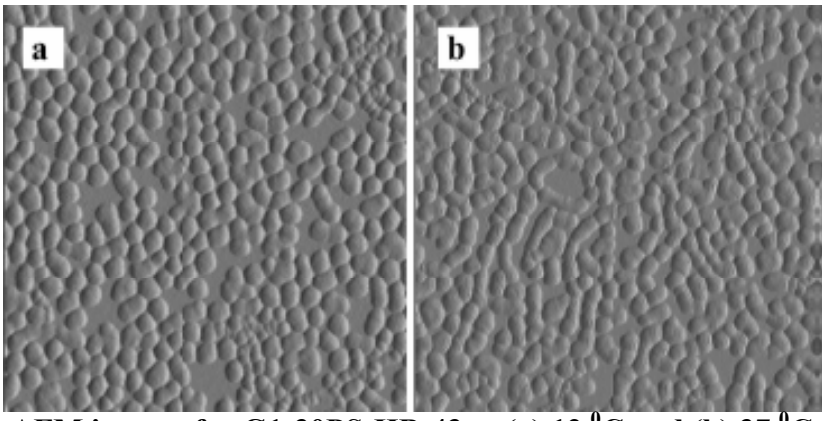

Figure 2-22: AFM images for G1-30PS-HB-43 at (a) 12 ^{0}C and (b) 37 ^{0}C. Image size 1.5 x 1.5 μm^2. From Njikang et al.[66]

2.4 Dendritic polymers as polymer processing additives

The application of dendritic polymers as rheology modifiers was first proposed by Kim et al.[67] who showed that blending hyperbranched polyphenylene with PS in a 5 %*w/w* ratio yielded a 50 % decrease in melt viscosity at 180 ^{0}C. Other studies were conducted by Hong et al.[3] for the extrusion of LLDPE blended with a hyperbranched polymer (Boltorn® H30, a hydroxyl-functionalized dendritic polyester). A reduction in the severity of SS defects was observed at 0.05-0.1 %*w/w*, and at higher concentrations (0.5-1.0 %*w/w*) SS formation was eliminated completely. Studies of the same blends in film blowing operations yielded comparable results.[4]

Very little research effort has been devoted to developing applications for AP. Since Hong et al. successfully demonstrated the application of a hyperbranched polymer as a PPA, it is conceivable that AP could perform similarly or even better due to their specific characteristics. For example, the rigid sphere behavior and high molecular weight of AP may be beneficial when they are used as additives, as these should favor phase separation from the host polymer. Khadir also suggested that AP molecules tend to migrate to the surface of

polymer melts.[68] This is interesting, since during polymer processing the additive should ideally migrate to the surface of the polymer melt for optimal performance. Teertstra investigated the potential of AP as PPA for LLDPE at a concentration of 0.1 %*w/w* for fluorinated arborescent PIP homopolymers, and to a lesser extent for the arborescent polystyrene-*graft*-polyisoprene copolymers used in the current investigation.[25] Arborescent PIP homopolymers with a fluorination level >30 mol% decreased melt defect formation and yielded small (ca. 10 %) load decreases in capillary rheometry experiments. The formation of mild CMF and stranding on the surface of the extrudate was also observed at shear rates below the critical level for CMF formation in virgin LLDPE. These mild defects were attributed to instability of the PPA coating on the surface of the extruding die and to partial coating of the die. Significant improvement in performance was demonstrated when combining the fluorinated arborescent PIP homopolymers with a coadditive (PEG), and led to the elimination of melt fracture at shear rates up to 1000 s^{-1}. The enhanced performance under these conditions was attributed to the action of the coadditive as a partitioning agent between the PPA and the host polymer, preventing the breakup of the PPA droplets during extrusion. A few fluorinated polystyrene-*graft*-polyisoprene copolymers were investigated and yielded only marginal processability improvements. The influence of the generation number, the side chain length, and the fluorination level of the copolymers was not studied, for example. One of the major objectives of the work described in this Thesis was to examine in detail the influence of these parameters on the performance of fluorinated polystyrene-*graft*-polyisoprene copolymers as PPA.

Chapter 3 – Objectives

The main objective of this project was to expand the investigation on the effectiveness of polystyrene-*graft*-polyisoprene copolymers functionalized with a perfluorinated hydrosilane (PHS, tridecafluoro-1,1,2,2-tetrahydrooctyl)dimethylhydrosilane) molecules as PPA for LLDPE. The copolymers used were synthesized from linear and G0 acetylated PS substrates with substitution levels of 30 and 33 mol%, respectively, and a chloromethylated G1PS substrate with a substitution level of 24 mol%. The linear PS and G0PS substrates were grafted with $\overline{M_w}$ ≈ 5,000 and $\overline{M_w}$ ≈ 30,000 PIP side chains; G0PS grafted with $\overline{M_w}$ ≈ 15,000 and $\overline{M_w}$ ≈ 45,000 PIP side chains were also investigated. The G1PS substrate was only investigated with $\overline{M_w}$ ≈ 30,000 PIP side chains. For comparison, linear PIP samples with $\overline{M_w}$ ≈ 5,000, $\overline{M_w}$ ≈ 30,000 and $\overline{M_w}$ ≈ 115,000 were also investigated. Fluorinated substituents were introduced on 17 to 50 % of the isoprene units by hydrosilylation with the PHS.

The copolymers were characterized by GPC analysis and ^{1}H NMR spectroscopy to obtain information on the molecular weight, the polydispersity, and the composition of the copolymers. The PPA were blended at concentrations of 0.1 and 0.5 %*w/w* with a commercial LLDPE resin (LL1001.32, Exxon Mobil Chemical), and in some cases with PEG4K as a coadditive. The performance of the PPA was evaluated by melt extrusion on a capillary rheometer, in terms of the elimination of melt defects and the load required on the extrusion plunger to maintain a constant deformation (shear) rate. The blends were also characterized by light microscopy to determine the size of the PPA droplets within the LLDPE matrix.

The systematic approach selected aimed to establish structure-property correlations for the novel additives and to optimize their performance as PPA.

Chapter 4 – Experimental Procedures

4.1 General procedures

Most of the chemical reactions used in the synthetic portion of the project were water-sensitive. Consequently, all the glassware used was either oven-dried at 110 ^{0}C for 12 h or flamed under high vacuum to remove moisture adsorbed on its surface. The monomers and other reagents utilized in the anionic polymerization and grafting reactions were purified on a high-vacuum line connected to a nitrogen (N_2) purification system and glass ampoules equipped with high-vacuum poly(tetrafluoroethylene) (PTFE) stopcocks and ground glass joints for direct mounting on the polymerization reactor.

4.2 Solvent and reagent purification

Tetrahydrofuran (THF; EMD OmniSolv) was purified by distillation over sodium benzophenone ketyl under N_2. Cyclohexane (Fisher, ACS reagent) was purified over oligostyryllithium under N_2. The solvents were transferred directly from the distillation stills to the polymerization reactor and other high-vacuum manifolds through PTFE tubing. Nitrobenzene (Aldrich, 99%) was purified by distillation over $CaCl_2$ under reduced pressure and stored under N_2. Isoprene (Aldrich, 99%) was purified immediately before polymerization with *n*-butyllithium (*n*-BuLi; Aldrich, 1.6 M in hexane, 2 mL for 30 mL of isoprene), degassed with three freezing-evacuation-thawing cycles, and recondensed into an ampoule which was then filled with N_2 and sealed. *sec*-Butyllithium (*sec*-BuLi; Aldrich, 1.4 M in hexane) was titrated by the method of Burchat et al.[69] *n*-BuLi (Aldrich, 1.6 M in hexane), anhydrous aluminum chloride ($AlCl_3$; Acros, 98.5 %, powder), lithium chloride (LiCl; Aldrich, ≥ 98 %), acetyl chloride (Aldrich, ≥ 98 %), 1H,1H,2H-perfluoro-1-octene (Matrix Scientific, 98 %), chlorodimethylsilane (Alfa Aesar, 97 %), platinum-

divinyltetramethyldisiloxane (Karstedt catalyst; United Chemical Technologies, 2 wt% in xylene), and chlorotris(triphenylphosphine)rhodium(I) (Wilkinson's catalyst; Strem Chemicals, 99 %) were all used as received from the suppliers.

4.3 Acetylation of PS substrates

The PS substrates used for the preparation of the copolymers were previously synthesized by Teertstra[25] and characterized by GPC analysis on an instrument consisting in a Waters 501 pump, a Waters R401 differential refractometer, and a MiniDawn MALLS detector. Please refer to Section 4.7 for more details on the characterization procedures.

Linear and G0 PS substrates were randomly functionalized with acetyl coupling sites according to the method of Li and Gauthier.[38] The functionalization of a G0PS substrate, with side chains having a weight-average molecular weight ($\overline{M_w}$) = 15,000, is described as an example. The polymer (5.13 g, 49.3 mmol styrene units) contained in a 250 mL round bottom flask was dried under vacuum for 12 h and dissolved in 150 mL of nitrobenzene with stirring after sealing the flask with a rubber septum. The flask was maintained in a water bath at room temperature and purged with nitrogen while stirring. A solution prepared from 10 mL of nitrobenzene, 1.26 mL (17.8 mmol) of acetyl chloride, and 2.44 g (18.3 mmol) of $AlCl_3$ was prepared and injected into the round bottom flask with stirring. The reaction was allowed to proceed for two hours at room temperature (23 ^{0}C) and terminated with 5 mL of 10 %*v/v* methanol/water solution. The acetylated polymer was precipitated into 1 L of methanol acidified with 10 %*v/v* of concentrated HCl. The polymer was further purified three times by dissolution in THF and precipitation in acidified methanol. The solid was finally rinsed five times with 30 mL of methanol, collected by filtration and dried under vacuum for

12 h. The acetylation level was determined by ^{1}H NMR spectroscopy analysis. The acetylation level of the polymer was 35 % and the recovery yield was 96 % (5.63 g).

4.4 Synthesis of arborescent polystyrene-*graft*-polyisoprene

Three PS substrates were used in the synthesis of the copolymers: a linear PS with $\overline{M_w}$ ≈ 5,000, a G0PS substrate with $\overline{M_w}$ ≈ 5,000 side chains (backbone $\overline{M_w}$ ≈ 5,000, $\overline{M_w}$ (LS) = 104,000, f_w = 17), and a G1PS substrate with $\overline{M_w}$ ≈ 5,000 side chains (derived from the G0 substrate, $\overline{M_w}$ (LS) = 730,000, f_w = 145). The linear PS and G0PS substrates were acetylated to substitution levels of 30 and 33 mol%, respectively. The G1PS substrate was chloromethylated to a substitution level of 24 %. The acetyl sites were coupled with mixed microstructure "living" PIP chains to generate the copolymers as described previously.[70] PIP side chains with $\overline{M_w}$ ≈ 5,000 and 30,000 were grafted onto the linear and G0PS substrates. The G0 substrate was also reacted with PIP side chains having $\overline{M_w}$ ≈ 15,000 and 45,000. Another copolymer sample was obtained by grafting PIP side chains with $\overline{M_w}$ ≈ 30,000 onto the chloromethylated G1PS substrate. A complete list of the samples synthesized provided in Table 4-1.

The following procedure describes the purification of an acetylated G0PS substrate by azeotropic distillation using the high-vacuum manifold shown in Figure 4-1. An ampoule (A) was connected to the manifold which was evacuated and flamed under vacuum. After cooling, the manifold was purged with nitrogen. The stopcock of ampoule (A) was removed and the substrate (5 g; 11 meq acetyl groups) dissolved in 50 mL of THF was filtered with a 0.45 μm PTFE filter directly into the ampoule through the stopcock opening. The ampoule was then sealed under nitrogen, the system was evacuated, and the stopcock of the ampoule

was opened slightly until the solution started boiling to degas it. After isolating the manifold from the vacuum line, flask (D) was cooled in liquid nitrogen and the stopcock of the ampoule was opened to remove all the solvent. The transfer rate of THF was increased by immersing the ampoule in a warm water bath. After all the THF was removed, flask (D) was isolated by closing stopcock (B), the ampoule was cooled with liquid nitrogen, and ca. 30 mL of dry THF was added to flask (C) (immersed in a water bath) from the still. The solvent quickly transferred to the ampoule when the stopcock was opened. The THF in the ampoule was then thawed and stirred to fully dissolve the acetylated PS substrate before removal by condensation to flask D as before. The azeotropic purification cycle was repeated two more times. After the last cycle, 30 mL of THF was used to dissolve the acetylated PS substrate and the ampoule was sealed under nitrogen.

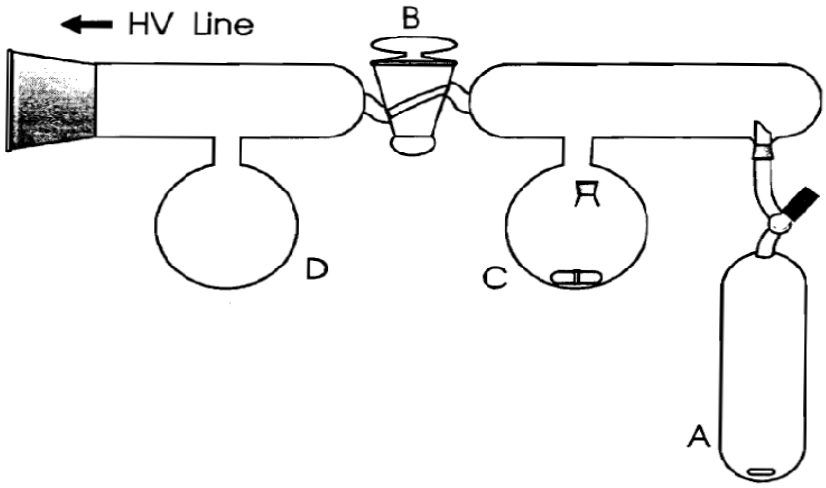

Figure 4-1: Manifold for azeotropic purification of grafting substrate.
From Cao.[71]

The following procedure describes the synthesis of a copolymer derived from the G0PS acetylated substrate (f_w = 17, $\overline{M_w}$ = 104,000, acetylation level = 33 mol%) and $\overline{M_n}$ ≈ 15,000 PIP side chains. The isoprene monomer was dried through three freezing-evacuation-thawing cycles as described below on the high-vacuum manifold shown in Figure 4-2. An

ampoule (A) was connected to the manifold which was evacuated and flamed. After cooling, the ampoule was sealed and the manifold was purged with nitrogen. Isoprene monomer (17.6 g, 258 mmol) was then added to flask (B) with 2 mL (3.2 mmol) of *n*-BuLi solution through the opening on top of the manifold. The manifold was sealed and the solution was stirred for 5 min. Partial vacuum was applied to degas the monomer until the isoprene started boiling, the solution was frozen in liquid nitrogen, and the system was fully evacuated for 10 min. The manifold was isolated from the vacuum line and the solution was thawed by immersing flask (B) in a water bath at room temperature while stirring. Two additional cycles of freezing, evacuation, and thawing were used to purify the monomer. After the last cycle, the isoprene was recondensed to ampoule (A) by cooling in liquid nitrogen. The opening of the PTFE stopcock was adjusted to recondense the purified monomer in ca. 45 min. The ampoule was then filled with nitrogen, sealed, and stored at 5 ^{0}C until it was used.

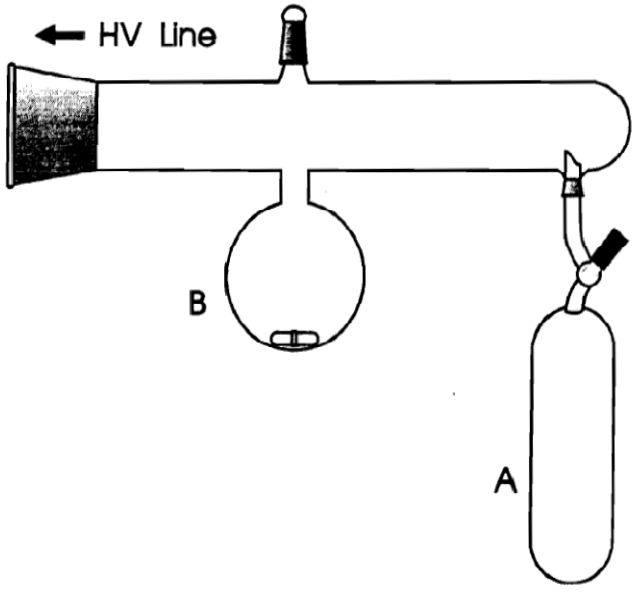

Figure 4-2: Manifold for monomer purification.
From Cao.[71]

Table 4-1: List of copolymer samples synthesized

Sample	PS substrate[a,c]	PIP target $\overline{M_n}$
PS-PIP6	PS	5×10^3
PS-PIP30[2]	PS	30×10^3
G0PS-PIP6	G0PS	5×10^3
G0PS-PIP13	G0PS	15×10^3
G0PS-PIP24	G0PS	20×10^3
G0PS-PIP45	G0PS	45×10^3
G1PS-PIP30[b]	G1PS	30×10^3

[a] Polystyrene substrates synthesized by Teerstra.[25]

[b] Sample synthesized by Teerstra.[25]

[c] Linear PS substrate had an acetylation level of 30 mol% and $\overline{M_w}$ = 6,500. G0PS had an acetylation level of 33 mol% and $\overline{M_w}$ = 104,000. G1PS had a chloromethylation level of 24 mol% and $\overline{M_w}$ = 104,000.

The anionic polymerization and grafting reactions were carried out in a 500 mL five-neck round bottom flask (Figure 4-3). A magnetic stirring bar and LiCl (0.294 g, 6.93 mmol) were first placed in the reactor which was mounted on the vacuum line. The dry THF line, a rubber septum, and the ampoules containing the isoprene monomer (17.6 g, 258 mmol) and the acetylated G0PS substrate were then mounted on the reactor which was evacuated, flamed to remove adsorbed water, and filled with N_2. THF (200 mL) was charged in the reactor before cooling to -20 ^{0}C with a methanol/water/dry ice slurry. Isoprene (10 drops) was added to the reactor and titrated with *sec*-BuLi (ca. 18 drops) using a syringe through the rubber septum, to obtain a light yellow color. *sec*-BuLi (1.07 mL, 1.17 mmol, for a calculated $\overline{M_n}$ = 15,000) was then added followed by all the isoprene. The polymerization reaction was allowed to proceed at -20 ^{0}C for 30 min, then at 0 ^{0}C for 30 min, and finally at room temperature for 30 min. A 10 mL sample of the PIP side chains was withdrawn through the

septum with a syringe and terminated with 1 mL of degassed methanol acidified with 1-2 drops of concentrated HCl, recovered by precipitation in methanol, dried under vacuum, and analyzed by GPC and ^{1}H NMR spectroscopy. The reactor was cooled to 0 ^{0}C and the living PIP solution was titrated with the acetylated PS substrate dropwise over ca. 15 min until the color of the solution faded. The grafting reaction was allowed to proceed further for 20 min and terminated with 10 mL of degassed acidified methanol. The graft copolymer was precipitated in methanol and purified by precipitation fractionation from a hexane solution (polymer concentration ca. 50 mg/mL) using 2-propanol as a non-solvent. The crude and the fractionated products were analyzed by GPC.

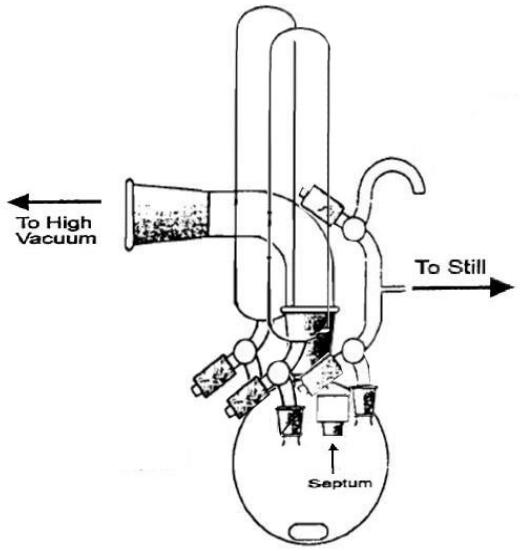

Figure 4-3: Reactor for the polymerization and grafting reactions.

Adapted from Cao.[71]

The copolymers derived from linear PS and G1PS substrates grafted with $\overline{M_n}$ ≈ 30,000 PIP side chains, also used in the investigation, were previously synthesized by Teertstra.[25]

For comparison, three linear PIP samples with $\overline{M_w}$ = 6,000, 29,000, and 115,000 were also synthesized by the same method described for the preparation of the PIP side chains, to obtain a similar mixed chain microstructure.

4.5 Synthesis of PHS

The procedure used was a combination of methods described by Hwang et al. and Ojima et al.[72,73] 1H, 1H, 2H-Perfluoro-1-octene (130.0 g, 0.376 mol) and 0.296 g (0.320 mmol) of Wilkinson's catalyst were placed into a ChemGlass 125 mL high pressure flask equipped with a magnetic stir bar. Chlorodimethylsilane (50 g, 0.528 mol) and THF (25 mL) were added to the flask which was sealed with the threaded PTFE stopper, and the flask was heated to 120 ^{o}C in an oil bath for 48 h while stirring. Complete conversion of the octene to the perfluorinated chlorosilane was confirmed by ^{1}H NMR spectroscopy analysis. The sample was distilled under reduced pressure (20 mm Hg) at 60 ^{0}C (yield 150.3 g, 91 %). The full amount of perfluorinated chlorosilane recovered was then reduced with $LiAlH_4$ (30.4 g, 0.803 mol) in 500 mL of THF with stirring for 24 h. Complete reduction of the perfluorinated chlorosilane to (tridecafluoro-1,1,2,2-tetrahydrooctyl)dimethylhydrosilane was confirmed by ^{1}H NMR analysis. The PHS was distilled under reduced pressure (20 mmHg) at 60 ^{0}C (yield 98.4 g, 71 %). The reagent was finally purified by stirring over CaH_2 for 48 h and distillation under reduced pressure (yield 90.6 g, 92 %). The purity of the PHS was confirmed by ^{1}H NMR spectroscopy [0.45 ppm (doublet), 1.15 ppm (multiplet), 2.19 ppm (septet), 3.95 ppm (septet)].

4.6 Hydrosilylation

The pendent double bonds of PIP were functionalized with PHS through hydrosilylation. The procedure used was derived from the method reported by Hempenius et al. for the hydrosilylation of polybutadiene.[47] The reaction provided as an example uses sample G0PS-PIP45 (f_w = 177, $\overline{M_w}$ = 7,919,000, PDI = 1.10) as a substrate. The copolymer (1.6 g, 23.5 meq isoprene units) was placed in a 250 mL round bottom flask with a magnetic stirring bar, dried under vacuum for 48 h, and dissolved in 100 mL of dry cyclohexane under nitrogen after sealing the flask with a rubber septum. After dissolution of the copolymer, PHS (4.353 g, 10.49 mmol) and 0.3 mL of Karstedt catalyst were added to the flask with stirring. The reaction was terminated either when the desired hydrosilylation level was attained (as determined by ^{1}H NMR analysis), when there was no further increase in the substitution level, or when the copolymer precipitated out of solution. The reaction was terminated by adding 2 mL of degassed methanol and stirring for 10 min. The sample was precipitated in a solution of 10 %*v/v* acetone in methanol. It was further purified by three cycles of redissolution in THF and precipitation in methanol. The functionalized polymer was finally dried under vacuum and the hydrosilylation level was determined by ^{1}H NMR analysis.

4.7 Characterization

The PS grafting substrates, the PIP side chains, the crude (non-fractionated) graft copolymers, and the fractionated graft copolymers were characterized by GPC analysis. The instrument used for routine characterization incorporated a Waters 501 HPLC pump, a guard column, a Jordi gel DVB mixed bed column (500 x 10 mm^2, linear PS molecular weight

range 500 – 8.0 x 10^6), and a Waters 410 Differential Refractometer (DRI) detector. THF served as eluent at a flow rate of 1.0 mL/min and the instrument was calibrated with linear PS standards having a molecular weight range between 1.25 x 10^3 and 2.75 x 10^6. This method only provided apparent molecular weights for the arborescent copolymers and the PIP samples.

The absolute molecular weight of the copolymers, the PIP side chains, and the linear PIP samples was determined on a Viscotek TDA 302 GPC instrument equipped with a light scattering detector. The system included a Waters AF inline degasser, a Waters 515 HPLC pump, a 717plus auto sampler, one 50 x 7.5 mm Polymer Laboratories gel 10 µm guard column, and three PLgel 10 µm mixed-B columns (300 x 7.5 mm^2) covering a molecular weight range between 500 and 10 x 10^6. The system utilized a Viscotek TDA 302 Triple detector incorporating right-angle (RALS) and low-angle light scattering (LALS) detectors operating at 670 nm, as well as DRI and viscometer detectors. A UV detector (model 2501) was also incorporated as an add-on. The molecular weight distribution of the samples was calculated with the OmniSEC v3.0 software package from Viscotek.

Refractive index increment (d*n*/d*c*) measurements for the arborescent copolymers and the linear PIP samples were conducted on a Brice-Phoenix differential refractometer equipped with a 632 nm band-pass interference filter. Calibration of the refractometer was accomplished using NaCl at five concentrations between 2 and 10 g/L.

The microstructure of the PIP samples and the composition of the copolymers were determined by ^{1}H NMR spectroscopy analysis on a Bruker AC-300 nuclear magnetic resonance spectrometer in $CDCl_3$ at a concentration of ca. 10 mg/mL. The method used to analyze the microstructure of the PIP side chains was described by Essel and Pham.[74]

4.8 Blending of fluorinated polystyrene-*graft*-polyisoprene and PEG4K with LLDPE

A commercial LLDPE resin (LL1001.32, Exxon Mobil Chemical, supplied by Imperial Oil Ltd.) containing 2 %*w/w* of butene as comonomer and stabilized with 0.03 %*w/w* of octadecyl-3-(3,5-di-*tert*-butyl-4-hydroxyphenyl)propionate, having a melt flow index of 1.0 g/10 min (ASTM D1238), was used in the investigations. A PEG4K sample (Baker, $\overline{M_n}$ = 3,600) was also investigated as coadditive in some cases. The fluorinated and PEG4K additives were dried under vacuum for 48 h prior to blending. Using PIP5-F31 as an example, the following procedure describes the mixing of a master batch to a 1.0 %*w/w* concentration of PPA, and the dilution of the PIP5-F31 master batch with LLDPE to a concentration of 0.5 %*w/w*. The PIP5-F31 master batch was obtained by compounding the LLDPE resin (198.0 g) with 2.0 g of PIP5-F31, to obtain a 1.0 %*w/w* PPA concentration, using a Haake Torque Rheometer equipped with a 3000 mixing chamber at 190 ^{0}C (5 min at 50 rpm). The master batch was then diluted to 0.5 %*w/w* PPA by further compounding with virgin LLDPE, corresponding to 100 g of the 1 %*w/w* PPA master batch and 100 g of virgin LLDPE resin at 190 ^{0}C (5 min at 50 rpm).

Three of the PPA samples (G0PS-PIP5-F17, PS-PIP5-F25, and PIP5-F31), selected on the basis of their performance at 0.5 %*w/w*, were also evaluated in combination with the PEG4K coadditive. In this case, a PEG4K master batch was prepared as described above from 2.0 g of PEG4K and 198.0 g of virgin resin at 190 ^{0}C (5 min at 50 rpm). Using PIP5-F31 as an example, the PIP5-F31 (40 g) and PEG4K (60 g) master batches were combined in a 2 : 3 weight ratio and further diluted with virgin LLDPE (100 g) to obtain a final

concentration of 0.5 %*w/w* additives (0.2% PPA and 0.3% PEG4K) using the Haake torque rheometer at 190 ^{0}C (5 min at 50 rpm) in one step.

Three samples (G0PS-PIP5-F17, PS-PIP5-F25, PIP5-F31) were also investigated at a lower concentration (0.1 %*w/w*), corresponding to 40 g of the 0.5 %*w/w* PPA master batch combined with 160 g of LLDPE at 190 ^{0}C (5 min at 50 rpm). Furthermore, the PPA-coadditive blends were tested at 0.1 %*w/w* (0.06 % PEG4K + 0.04 % additive) by combining 16 g of 0.5 %*w/w* PPA master batch, 24 g of 0.5 %*w/w* PEG4K master batch, and 160 g of LLDPE at 190 ^{0}C (5 min at 50 rpm). This again corresponds to a 3 : 2 PEG4K to PPA ratio.

In addition to the blends described above, a mixed PPA blend was prepared by combining the G0PS-PIP5-F17, PS-PIP5-F25, and PIP5-F31 additives into a single LLDPE blend, to shed light on the influence of sample polydispersity on PPA performance. The mixed blend at 0.5 %*w/w* was obtained by combining 33.3 g of the G0PS-PIP5-F17 master batch, 33.3 g of the PS-PIP5-F25 master batch, 33.3 g of the PIP5-F31 master batch, and 100.0 g of virgin LLDPE resin at 190 ^{0}C (5 min at 50 rpm). Another mixed blend at 0.5 %*w/w* incorporating PEG4K (0.3 % PEG4K + 0.2 % PPA) was also prepared from 13.3 g of the G0PS-PIP5-F17 master batch, 13.3 g of the PS-PIP5-F25 master batch, 13.3 g of the PIP5-F31 master batch, 60.0 g of the PEG4K master batch, and 100.0 g of virgin LLDPE resin at 190 ^{0}C (5 min at 50 rpm). The mixed PPA blends (without and with PEG4K) were also investigated at a lower concentration (0.1 %*w/w*). In the first case, 13.3 g of the G0PS-PIP5-F17 0.5 %*w/w* blend, 13.3 g of the PS-PIP5-F25 0.5 %*w/w* blend, 13.3 g of the PIP5-F31 0.5 %*w/w* blend, and 160.0 g of virgin LLDPE resin were combined at 190 ^{0}C (5 min at 50 rpm). The 0.1 %*w/w* mixed blend with PEG4K (0.06 % PEG4K + 0.04 % additive) was obtained by combining 160.0 g of virgin LLDPE with 5.3 g of the G0PS-PIP5-F17 0.5 %*w/w*

blend, 5.3 g of the PS-PIP5-F25 0.5 %*w/w* blend, 5.3 g of the PIP5-F31 0.5 %*w/w* blend, and 24.0 g of the PEG4K 0.5 %*w/w* blend.

All the diluted blend samples were mechanically ground into ca. 2-3 mm flakes for extrusion testing and PPA droplet size analysis.

4.9 Extrusion testing

Extrusion testing of the polymer blends was conducted on a Galaxy V capillary rheometer (Model 8052) equipped with a stainless steel die. The die had a length of 1.00 inch, a length/diameter (L/D) ratio of 50, and an entrance angle of 90^0. The polymer blends (20 g) were loaded into the extrusion barrel and heated to 190 ^{0}C for 5 min before extrusion of the polymer while applying a load of 150 lb. Before testing the samples and in-between runs, residual PPA was removed from the die wall by extruding 20 g of LLDPE containing 50 %*w/w* of $CaCO_3$ and then 20 g of virgin LLDPE. The LLDPE containing 50 %*w/w* of $CaCO_3$ was prepared by blending 100 g of $CaCO_3$ (Baker, 99.9 %) with 100 g of LLDPE using the Haake Torque Rheometer equipped with a 3000 mixing chamber at 190 ^{0}C (5 min at 50 rpm). The pure LLDPE extrusion provided baseline control, together with visual examination of the extrudate, to ensure that the extrusion was not affected by the additives used in the previous test (i.e. no glossiness remaining at a shear rate of 300 s^{-1}). The blend was extruded at a shear rate of 300 s^{-1} until a constant load (constant load) was achieved. Reloading of the barrel with 20 g of the blend was necessary when the blend in the barrel had all been extruded. To achieve a constant initial load, 3 to 5 fillings of the barrel with polymer blend were necessary in some cases, to ensure uniform coating of the die wall with the additive. When a constant load was attained, the barrel was refilled with 20 g of polymer blend and the extrusion test was initiated. The blends were extruded at shear rates between

50 and 1600 s^{-1}, until a constant load was achieved at each shear rate, and the test was stopped when CMF was observed.

4.10 Optical microscope study of droplet size

The droplet size study was adapted from a procedure developed for the analysis of the Dynamar additive (FX9613) dispersed in polyolefins.[75] Four to six flakes of the ground sample were placed between two 2.5 × 7.5 cm^2 microscope glass slides. The slides were heated on a hot plate at ca. 150 ^{0}C for 5 min and a 10-lb weight was put on the glass slides to create a thin film (ca. 200 μm). The slides were examined on a Radical RXL-4B optical microscope at room temperature, at a magnification of 100x. The microscope was equipped with an AmScope 640x480 digital camera and calibrated using a 1.0 mm ABBOTA stage micrometer slide with 10 μm divisions.

Images of the samples at 100x magnification were recorded with the digital camera. The size (diameter) of the additive droplets was measured using the software (AmScope 3.0) provided with the instrument and the measured values were exported to Excel for averaging and standard deviation calculations. A minimum of 11 droplet diameter measurements was used in each analysis.

Chapter 5 – Results and Discussion

5.1 Introduction

Arborescent polystyrene-*graft*-polyisoprene samples were synthesized and functionalized with PHS according to Scheme 5-1. This was achieved by grafting living PIP side chains onto polystyrene substrates randomly functionalized with acetyl coupling sites. After purification, the isoprene homo- and copolymers were functionalized with PHS through hydrosilylation.

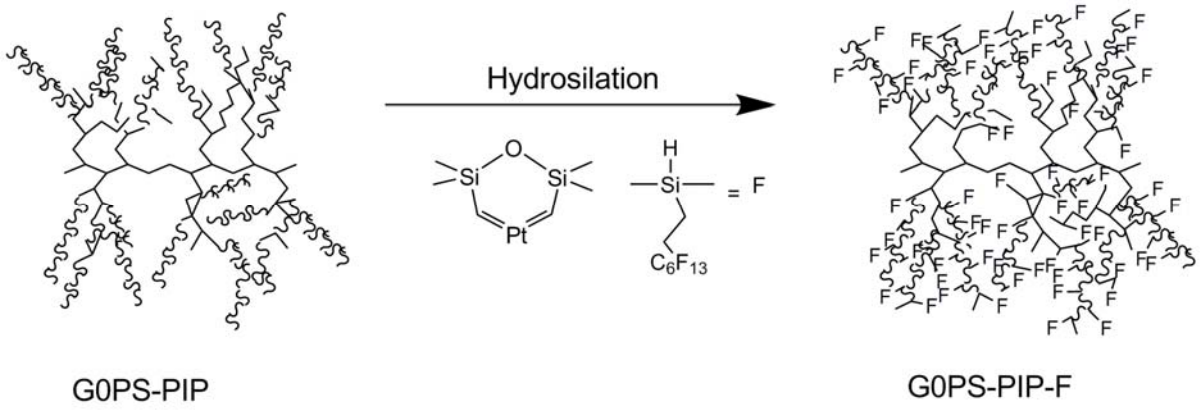

Scheme 5-1: Synthetic scheme for PHS-functionalized polystyrene-*graft*-polyisoprene copolymer.

5.2 Acetylation of polystyrene substrates

The PS substrates used in the current investigation were synthesized by Teertstra[25] and were characterized by GPC analysis using a combination of DRI and RALS/LALS detectors (Table 5-1). The branching density of the substrates was held relatively constant by using a side chain $\overline{M_w} \approx 5{,}000$ and a comparable acetylation level of 24-33 mol% in all cases. The branching functionality, f_w, defined as the number of side chains added in the last grafting reaction, was calculated from Equation 5-1, where $\overline{M_w}(G), \overline{M_w}(G-1)$, and $\overline{M_w^{sc}}$

represent the absolute weight-average molecular weight of the graft polymer of generation G, of the preceding generation, and of the side chains, respectively.[25] The number of coupling sites on each polymer substrate was calculated from its absolute molecular weight and functionalization level. As expected, f_w and the number of coupling sites both increase roughly geometrically for successive generations.

Table 5-1: Linear and arborescent PS substrates characterization data

Polymer	$\overline{M_w}^{sc\ a}$ (x 10^3)	$\overline{M_w}/\overline{M_n}^{sc\ a}$	$\overline{M_w}^{AP\ b}$ (x 10^3)	f_w	$COCH_3$/ CH_2Cl (mol %)[c]	Grafting Sites
PS (linear)[d]	6.5	1.08	—	—	30	19
G0PS[d]	5.8	1.07	104	17	33	329
G1PS[e]	4.6	1.09	727	145	24	1,700

[a] Absolute $\overline{M_w}$ of side chains from GPC analysis calibrated with linear PS standards.
[b] Absolute $\overline{M_w}$ of arborescent polymer from GPC analysis with RALS/LALS detectors.
[c] Acetylation/chloromethylation level determined by ^{1}H NMR analysis.
[d] Acetylated PS substrates.
[e] Chloromethylated PS substrate synthesized by Teertstra.[25]

$$f_w = \frac{\overline{M_w}(G) - \overline{M_w}(G-1)}{\overline{M_w^{sc}}} \qquad \textbf{Equation 5-1}$$

With the exception of sample G1PS, grafting sites were introduced on the PS substrates by acetylation. Similar acetylation levels were achieved for both the linear and the G0PS substrates through careful control of the reaction conditions, time, and stoichiometry, as determined by ^{1}H NMR spectroscopy analysis (Figure 5-1). After the acetylation reaction (Figure 5-1B), two new peaks appear at 7.5 and 2.5 ppm, corresponding to the two aromatic protons (b) α to the acetyl group and to the acyl protons (a), respectively. The substitution

level *x* was determined from the ratio of the integrated peak intensities at 2.5 ppm (A_{Ac}) and 6.2-7.2 ppm (A_{Ar}) as shown on Figure 5-1B using the equation $A_{Ac} / A_{Ar} = 3x / 5\text{-}3x$.

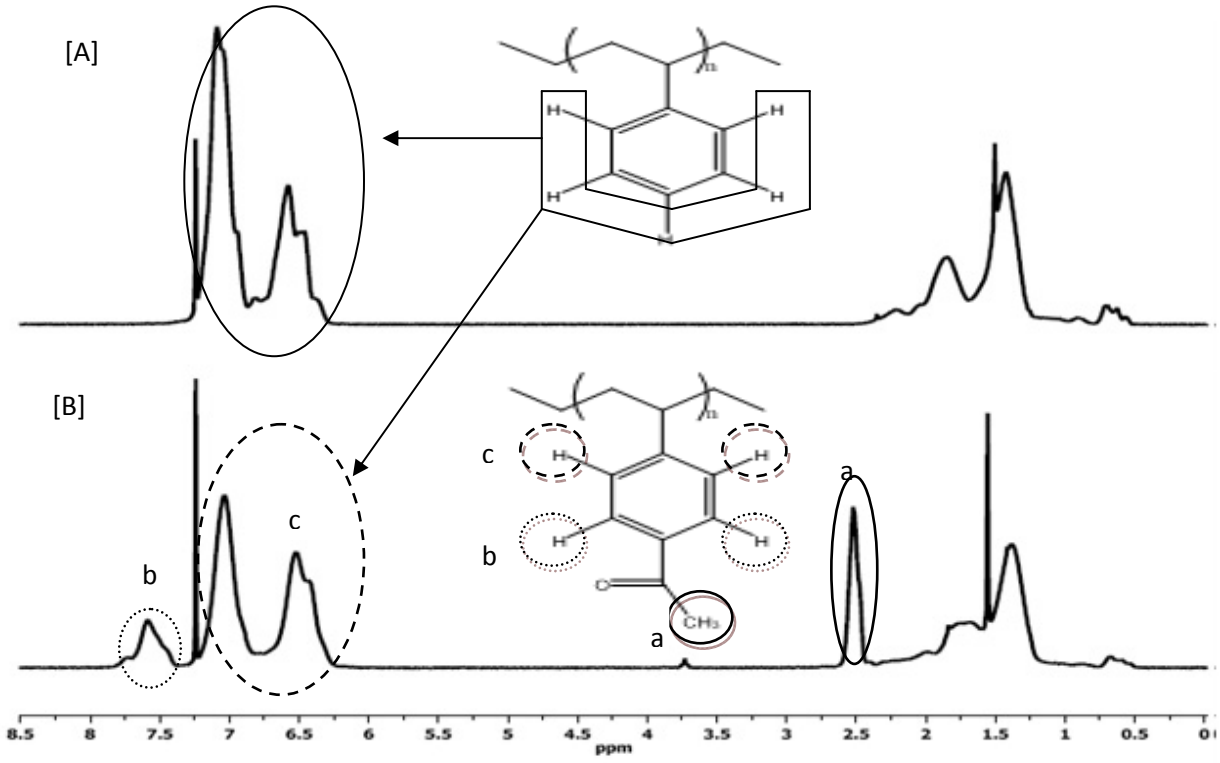

Figure 5-1: ^{1}H NMR spectrum for linear PS (A) and acetylated linear PS (B).
The peak at ca. 7.25 ppm is due to residual $CHCl_3$.

The low polydispersity index of the acetylated substrates ($\overline{M_w}/\overline{M_n} \leq 1.09$) indicates that no cross-linking occurred during the functionalization reactions used to introduce the coupling sites.

5.3 Arborescent polystyrene-*graft*-polyisoprene copolymers

sec-BuLi was used to initiate the polymerization of isoprene in THF at -20 ^{0}C, to obtain PIP side chains with a narrow MWD. The absolute weight-average molecular weight and PDI determined by GPC analysis with the RALS/LALS detectors for PIP samples

removed before the grafting reactions and for the arborescent copolymer samples are reported in Table 5-2. The refractive index increment (*dn/dc*) values of each polymer, determined using a differential refractometer with a 632 nm bandpass interference filter, are also reported in Table 5-2. The nomenclature used for the copolymers identifies the generation number of the substrate and the molecular weight of the grafted PIP side chains. For example, G0PS-PIP45 corresponds to a copolymer obtained by grafting a G0PS substrate with a PIP side chain having a $\overline{M_w} \approx 45{,}000$.

The PDI of all the linear PIP, PIP side chain, and graft copolymer samples synthesized is low (1.01-1.10; see e.g. Figure 5-2). These low PDI values indicate that all the arborescent polystyrene-*graft*-polyisoprene copolymer molecules have a comparable number of side chains of uniform length.

For increasing PIP side chain lengths, the branching functionality (f_w) attained decreases as a result of enhanced steric hindrance. Also, as the generation number of the substrate increases, the number of potential grafting sites increases geometrically over successive generations. The coupling efficiency (C_e), defined as the percent fraction of coupling sites consumed in the grafting reaction, was calculated as the ratio of f_w to the total number of coupling sites on the substrate.

Table 5-2: Molecular weight characterization of linear PIP and arborescent polystyrene-*graft*-polyisoprene copolymers

Polymer	Polyisoprenes Side Chain		Linear PIP/Arborescent copolymers				
	$\overline{M_w}$[b] (x 10^3)	PDI ($\overline{M_w}/\overline{M_n}$)	$\overline{M_w}$[b]	PDI ($\overline{M_w}/\overline{M_n}$)	f_w	C_e (%)[c]	*dn/dc*
PIP6	--	--	6.1 x 10^3	1.02	--	--	0.109
PIP29	--	--	2.86 x 10^4	1.02	--	--	0.118
PIP115	--	--	1.14 x 10^5	1.05	--	--	0.118
PS-PIP6	6.5	1.01	1.39 x 10^5	1.01	19	100	0.116
PS-PIP30[a]	28.0	1.09	3.96 x 10^5	1.10	14	73	--
G0PS-PIP6	6.0	1.01	1.83 x 10^6	1.01	283	86	0.111
G0PS-PIP13	13.0	1.01	3.40 x 10^6	1.05	248	75	0.115
G0PS-PIP24	24.1	1.02	5.06 x 10^6	1.02	206	62	0.111
G0PS-PIP45	44.6	1.10	7.92 x 10^6	1.10	177	54	0.113
G1PS-PIP30[a]	30.0	1.09	14.3 x 10^6 [d]	--	450	26	--

[a] Copolymer prepared by Teertstra.[25]
[b] Absolute weight-average molecular weight from GPC analysis with RALS/LALS detector.
[c] Coupling efficiency.
[d] Absolute molecular weight from batchwise static light scattering measurements.[25]

The coupling efficiency is maximized for lower generation substrates (linear PS versus G0PS) and short PIP side chains ($\overline{M_w}$ ≈ 5,000 versus 30,000). Decreased coupling efficiencies, also reported by Li and Gauthier,[38] were attributed to steric congestion of the acetylated polystyrene substrates as more chains are added: Coupling sites deeper within the substrate become shielded and unable to react with the living chains in the reaction mixture.

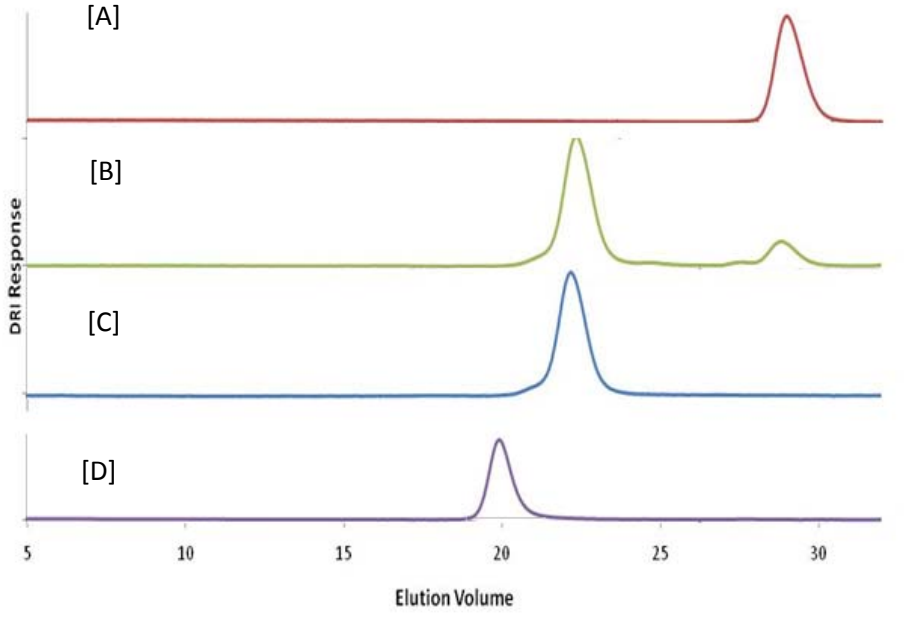

Figure 5-2: GPC traces for grafting linear PIP ($\overline{M_w}$ ≈ 6,000) onto the G0PS substrate.
[A] Linear PIP, [B] crude G0PS-PIP6, [C] purified product; [D] Purified G0PS-PIP24 shown for comparison.

The PIP content of the copolymer samples was determined from their ^{1}H NMR spectra (Figure 5-3B). After grafting PIP onto an acetylated PS substrate, the PS aromatic proton signal (A_{Ar}) is attenuated as compared to the PIP olefinic proton signal (A_{PIP}). This is attributed to the large number of PIP side chains grafted onto the PS substrate overwhelming the signals from the aromatic protons. The PIP content was calculated using the equation $A_{PIP} / A_{Ar} = 2x / (5-5x)$ where A_{PIP} represents the integrated intensity of the olefinic protons

resonance in the isoprene units (4.2-6.1 ppm) and A_{Ar} is for the aromatic protons from styrene (6.2-7.2 ppm).

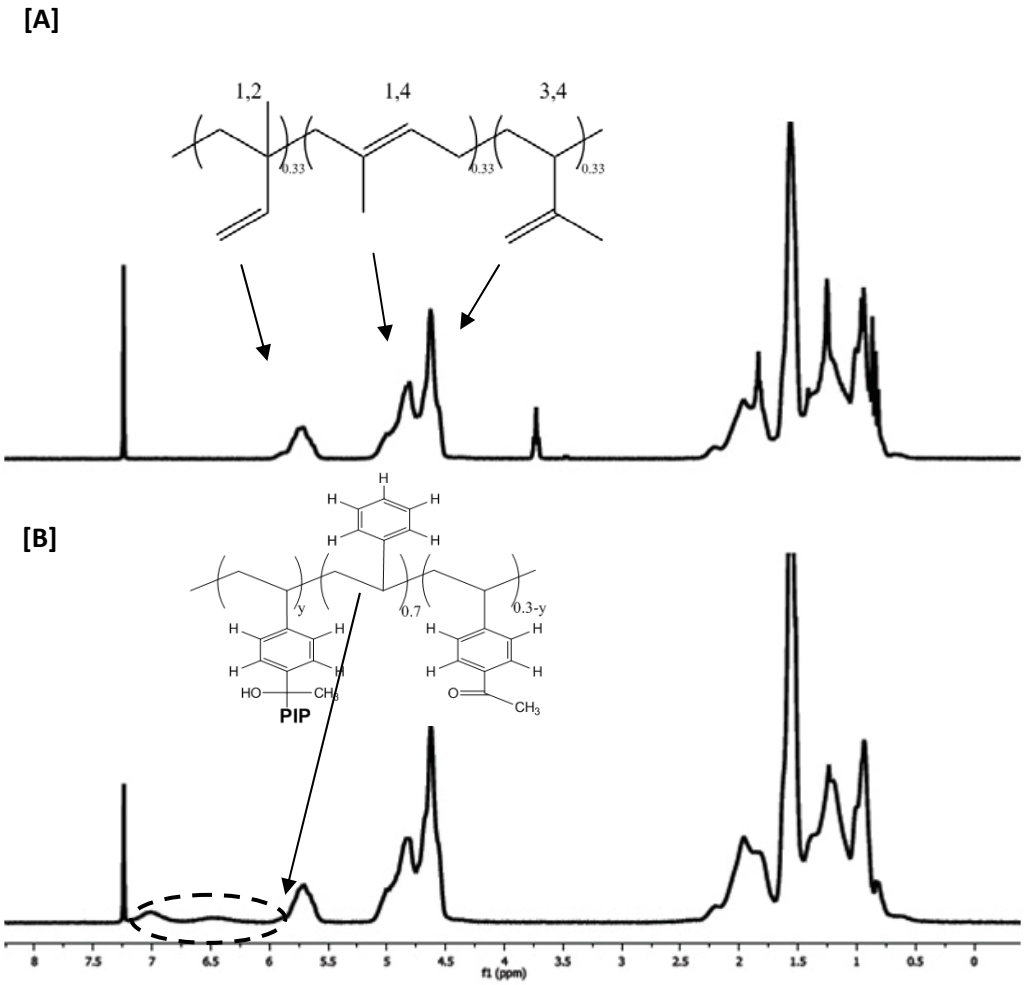

Figure 5-3: ^{1}H NMR spectra for PIP6K (A) and PS-PIP6K (B).

The signal at 7.25 is due to residual $CHCl_3$.

For example, the PIP content was determined to be 97 %*w/w* for PS-PIP6 by that method (Figure 5-3B and Table 5-3). The polystyrene component was essentially undetectable in all the other copolymer samples. These are noted as having > 98 %*w/w* PIP content in Table 5-3. The difference in weight-average molecular weight between the copolymer and the substrate can also be used to estimate the PIP content of the copolymers,

and ranges from 95-99 %*w/w* (third column in Table 5-3). ^{1}H NMR analysis clearly provided an overestimated value for the PIP content of copolymer G0PS-PIP6 as compared to the composition calculated from the difference in molecular weight. This is attributed to differences in relaxation characteristics between the PS substrate and the PIP side chains affecting the relative intensity of the peaks.[25] This problem is also obvious for some of the copolymers derived from upper generation substrates (e.g. G0PS-PIP6, G1PS-PIP30), where the restricted mobility of the PS chains within the crowded core led to no detectable signal in spite of their significant PS content.

Table 5-3: PIP content and microstructure analysis results

Polymer	PIP (%*w/w*)		Composition (mol %)[c]		
	^{1}H NMR	$\overline{M_w}$[b]	% 1,2-	% 1,4-	% 3,4-
PIP6	--	--	31	38	31
PIP29	--	--	35	32	33
PIP115	--	--	33	34	33
PS-PIP6	97	95	28	35	37
PS-PIP30[a]	>98	99	31	33	36
G0PS-PIP6	>98	94	31	37	32
G0PS-PIP13	>98	97	33	34	33
G0PS-PIP24	>98	98	34	36	30
G0PS-PIP45	>98	99	31	40	29
G1PS-PIP30[a]	>98	95	35	30	35

[a] Data from Teertstra.[25]

[b] Calculated from the absolute $\overline{M_w}$ of the graft copolymers and the substrates.

[c] From ^{1}H NMR analysis.

The microstructure of the linear PIP and side chain samples was analyzed by ^{1}H NMR spectroscopy (Figure 5-3A). The detailed analysis indicates that the PIP microstructure is comparable for all the samples, with roughly equal proportions of 1,2- (28-35 mol%), 1,4-

(30-40 mol%), and 3,4- (29-37 mol%) isoprene unit additions, typical for polymerization in a polar solvent such as THF (Table 5-3).

5.4 Synthesis of PHS

The procedure developed for the synthesis of the PHS was adapted from methods described by Hwang et al. and Ojima et al.[72,73] The modification was necessary due to the precipitation of Wilkinson's catalyst out of solution over the first few hours of the reaction, leading to decreased conversion into the perfluorochlorosilane. A small amount of THF (15 %*v/v*) added to the reaction increased the solubility of the catalyst, leading to complete conversion of the octene substrate within 48 hours. The use of a pressure flask also helped to improve catalyst solubilization, which only tended to precipitate out of solution near the end of the reaction.

The reaction yielded essentially pure PHS after distillation, as confirmed by ^{1}H NMR analysis (Figure 5-4B). The coupling reaction of 1H,1H,2H-perfluoro-1-octene (Figure 5-4A) with dimethylchlorosilane led to an upfield shift of the two peaks corresponding to protons "a" and "b" on the figure. The relative position of the two peaks is also inverted as a result of the increased shielding effect experienced by the "b" protons, as seen when comparing Figures 5-4A and B. The two methyl groups directly attached to the Si atom produce a singlet at 0.45 ppm (peak "c").

The extent of shielding of the three proton types increased after the reduction of the chlorosilane to the corresponding silane (PHS) (Figure 5-4C). A new peak "d" also appeared between 3.8 - 4.0 ppm for the silane proton, which is coupled with the "c" protons and splits the peak into doublets.

The two peaks present in all three ^{1}H NMR spectra at 1.5 and 7.25 ppm correspond to water and chloroform, respectively. The large water peak could not originate from the product, which was dried over calcium hydride. The water peak was due to contamination of the deuterated chloroform, as confirmed by ^{1}H NMR analysis of the pure solvent.

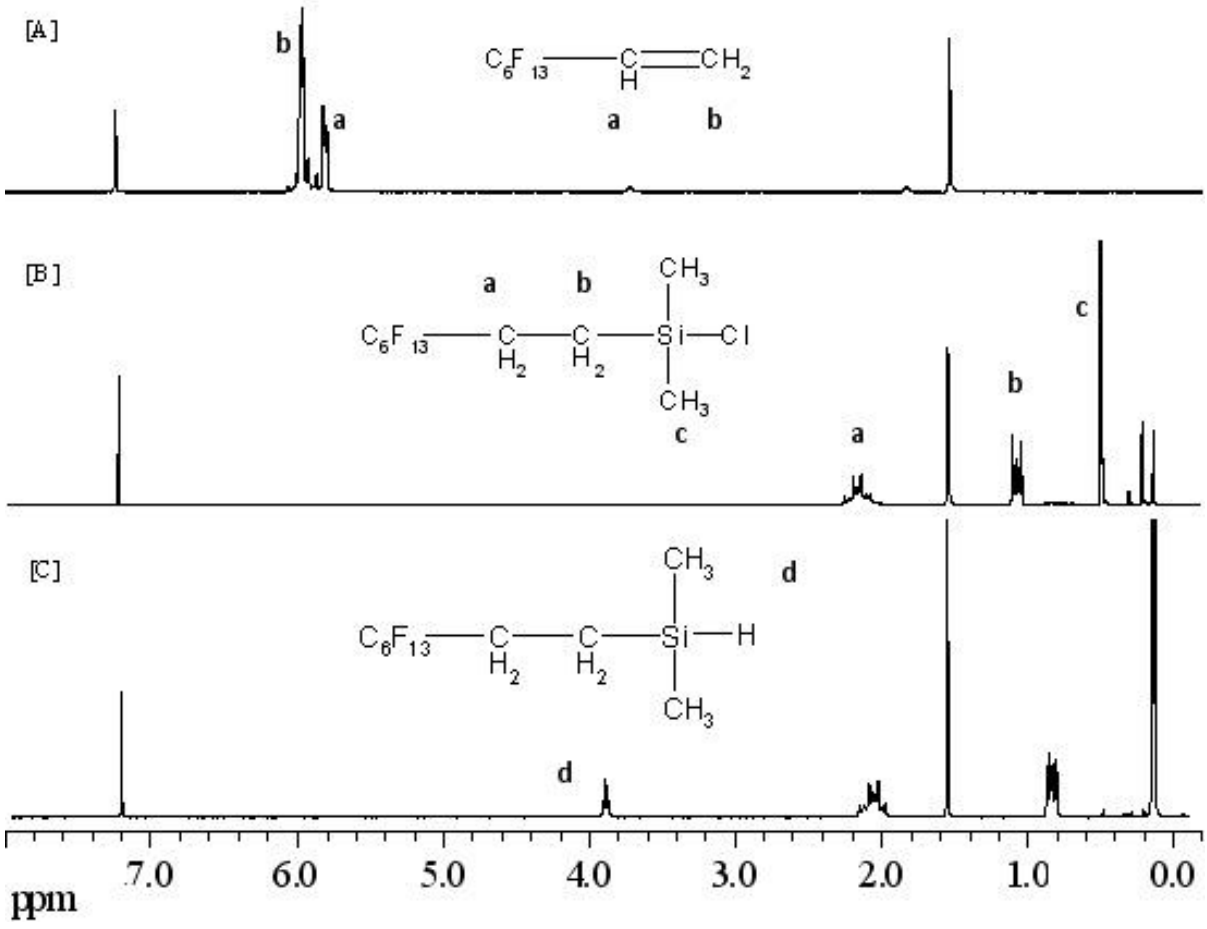

Figure 5-4: Evolution of the ^{1}H NMR spectrum from 1H,1H,2H-perfluoro-1-octene to (tridecafluoro-1,1,2,2-tetrahydrooctyl)dimethylsilane.
(A) (tridecafluoro-1,1,2,2-tetrahydrooctyl)dimethylhydrosilane, (B) (tridecafluoro-1,1,2,2-tetra-hydrooctyl)dimethylchlorosilane, and (C) 1H,1H,2H-perfluoro-1-octene.

5.5 Hydrosilylation of PIP

The linear PIP homopolymers and the arborescent copolymers were chemically modified with the PHS through hydrosilylation. The reaction was conducted in distilled cyclohexane under nitrogen atmosphere. The substitution level of the polymers was controlled by varying the stoichiometry of the reaction. For example, 1.5 times as much PHS was used for the synthesis of G0PS-PIP13-F41 as for G0PS-PIP13-F31. Approximately 93 % and 97 % of the PHS added reacted with the G0PS-PIP13 copolymer in each reaction, respectively. In general, over 85 % of the PHS added reacted with the polymer substrate. As the reaction proceeds, changes in polarity cause the polymer to precipitate from the solution. This sets an upper limit of ca. 39 mol% to the substitution level attainable under these conditions. The reactions were immediately terminated when precipitation of the polymer was observed, to ensure composition homogeneity of the product. The characteristics of the PHS-substituted polymers obtained are summarized in Table 5-4. The nomenclature used for the PHS-modified copolymers indentifies the generation number of the copolymer, the molecular weight of the grafted PIP side chains, and the fluorination level attained. For example, G0PS-PIP45-F39 corresponds to a copolymer of overall generation G1, derived from a G0PS substrate, with $\overline{M_w}$ ≈ 45,000 PIP side chains and with PHS substituted on 39% of the isoprene units.

The substitution level of the polymers was monitored by ^{1}H NMR analysis, and also estimated from the mass of polymer recovered for comparison. ^{1}H NMR spectra are compared in Figure 5-5 for the PHS, a copolymer with $\overline{M_w}$ ≈ 6,000 PIP side chains (PS-PIP6), and a fluorinated copolymer (PS-PIP6-F41). The peaks for the silylmethyl (A_{Si}) groups at ca. 0 ppm (6 protons) and the olefinic protons (A_{PIP}) from 4.5-6 ppm (6 protons)

can be used to determine the substitution level according to the equation $A_{PIP} / A_{Si} = 2x / (6\text{-}6x)$. The substitution levels thus determined ranged from 17 to 44 mol%. The substitution level estimated from mass recovery was significantly lower, which is attributed to the loss of product during polymer purification. For consistency, the substitution level determined by ^{1}H NMR analysis was adopted for sample labeling.

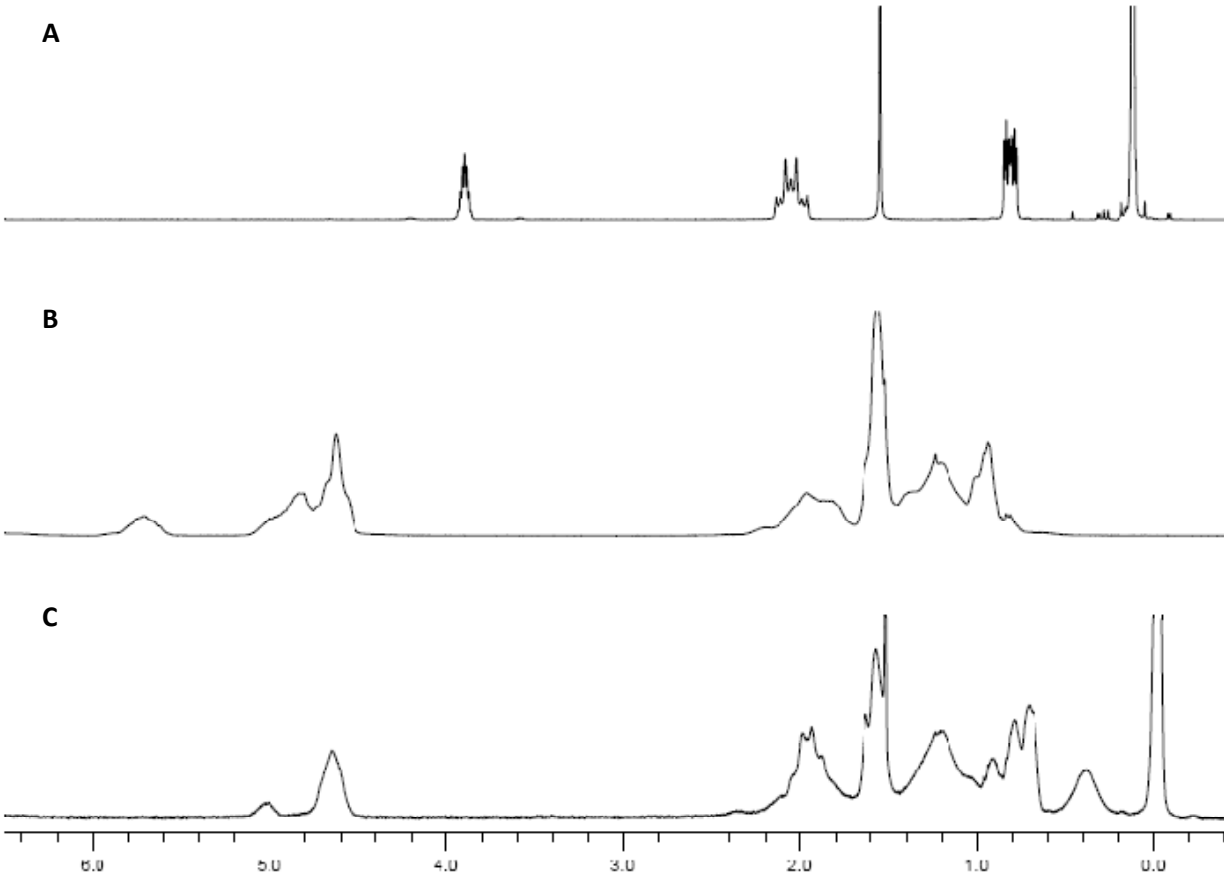

Figure 5-5: ^{1}H NMR spectra for the hydrosilylation of PIP with the PHS.
(A) PHS, (B) PS-PIP6, and (C) PS-PIP6-F41.

The influence of PHS substitution on the GPC elution behavior of the polymers is relatively small, as can be seen in Figure 5-6 when comparing GPC traces for PS-PIP6 and PS-PIP6-F25, as well as for G0PS-PIP6 and G0PS-PIP6-F17. A slight shift of the peak to

higher apparent molecular weights is observed for the fluorinated polymers. A small shoulder is also apparent on the left of the peak in both fluorinated samples, possibly indicating a small amount of cross-linking occurring during the hydrosilylation reaction with the PHS.

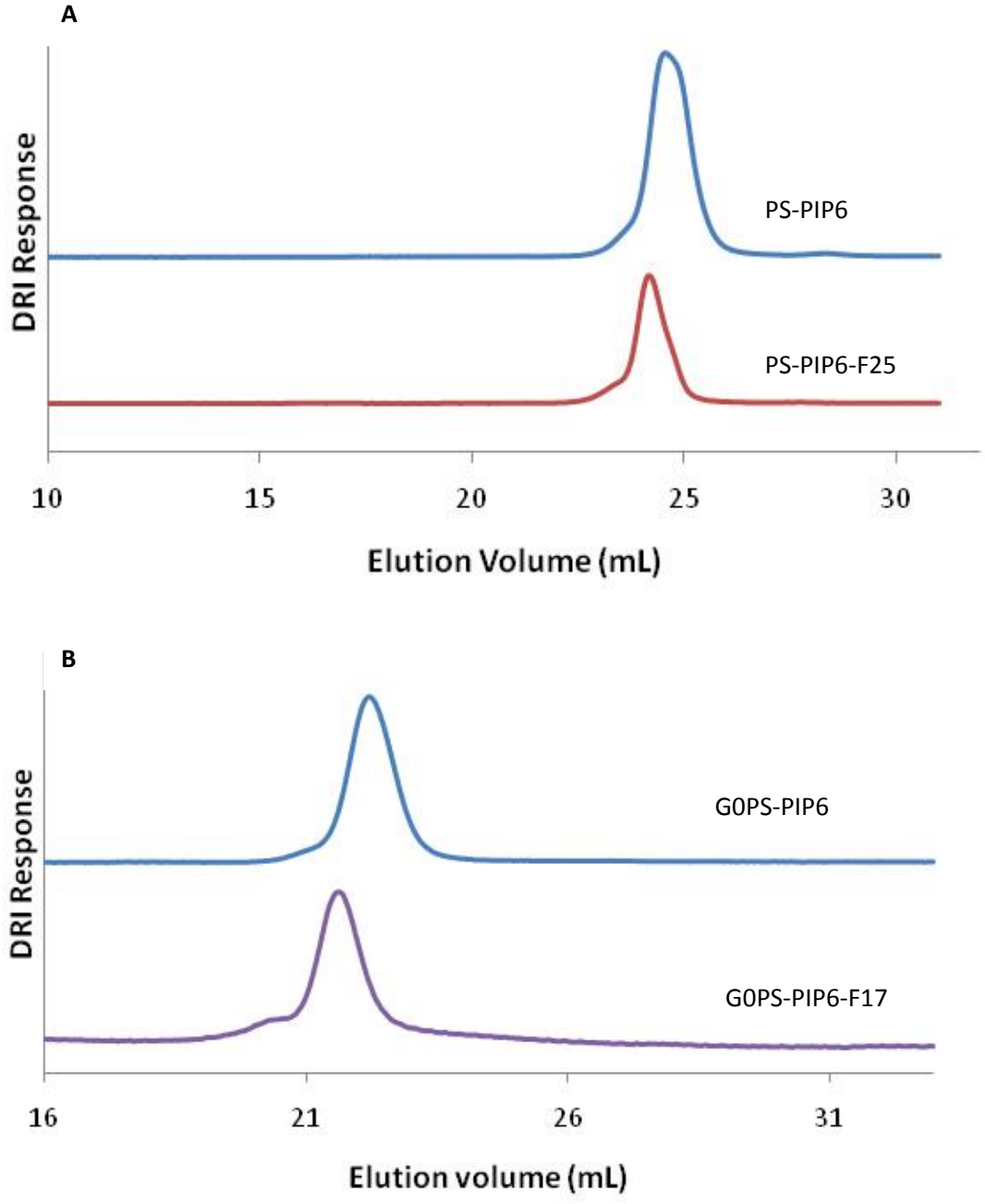

Figure 5-6: GPC elution curves for the conversion of (A) PS-PIP6 to PS-PIP6-F25 and (B) G0PS-PIP6 to G0-PIP6-F17.

Table 5-4: PHS modification of linear PIP and arborescent copolymers

Polymer	PHS (mol %)		$\overline{M_w}^{app\ c}$ (x 10^3)	$\overline{M_w}/\overline{M_n}^{app\ c}$	$\overline{M_w}^{abs}$ [d]
	^{1}H NMR[a]	MR[b]			
PIP6-F21	21	16	5.5	1.08	1.37 x 10^4
PIP6-F31	31	14	5.8	1.08	1.74 x 10^4
PIP6-F39	39	28	6.3	1.10	2.03 x 10^4
PIP29-F21	21	18	28.1	1.14	6.44 x 10^4
PIP29-F25	25	12	27.7	1.09	7.12 x 10^4
PIP29-F35	35	27	28.9	1.09	8.83 x 10^4
PIP29-F37	37	24	28.3	1.08	9.17 x 10^4
PIP115-F26	26	9	116	1.18	2.92 x 10^5
PIP115-F42[e]	42	25	Insol	Insol	4.02 x 10^5
PS-PIP6-F25	25	16	58.3	1.08	3.23 x 10^5
PS-PIP6-F41[e]	41	23	Insol	Insol	4.41 x 10^5
PS-PIP6-F50[e]	50	12	Insol	Insol	5.07 x 10^5
PS-PIP30-F44[f]	44	--	160	1.06	1.42 x 10^6
G0PS-PIP6-F17	17	14	233	1.13	3.55 x 10^6
G0PS-PIP6-F22	22	18	170	1.08	4.06 x 10^6
G0PS-PIP6-F27	27	23	269	1.14	4.56 x 10^6
G0PS-PIP6-F42[e]	42	30	Insol	Insol	6.08 x 10^6
G0PS-PIP6-F52[e]	52	44	Insol	Insol	7.09 x 10^6
G0PS-PIP13-F31	31	18	109	1.08	9.35 x 10^6
G0PS-PIP13-F41	42	31	Insol	Insol	1.13 x 10^7
G0PS-PIP24-F25	25	21	536	1.19	1.25 x 10^7
G0PS-PIP24-F39	39	27	Insol	Insol	1.66 x 10^7
G0PS-PIP45-F19	19	16	549	1.33	1.69 x 10^7
G0PS-PIP45-F28	28	25	556	1.54	2.11 x 10^7
G0PS-PIP45-F39[e]	39	29	Insol	Insol	2.63 x 10^7
G1PS-PIP30-F31[f]	31	27	Insol	Insol	1.68 x 10^8

[a] From ^{1}H NMR analysis.

[b] From mass recovery.

[c] Apparent molecular weight from GPC analysis with a linear PS standards calibration curve.

[d] Absolute weight-average molecular weight determined from fluorine content (^{1}H NMR) and absolute weight-average molecular of copolymer substrate.

[e] Sample insoluble in THF.

[f] Sample synthesized by Teertstra.[25]

The apparent molecular weight and PDI values obtained by GPC analysis of the fluorinated copolymers are also reported in Table 5-4. High molecular weight samples with a fluorination level above 39 mol% were insoluble in THF, so they could not be analyzed by GPC. In spite of the presence of a small shoulder pointed out above, the PDI of the samples remained low after hydrosilylation (<1.2 for most samples). However samples G0PS-PIP45-F19 and G0PS-PIP45-F28 yielded PDI values of 1.33 and 1.54, respectively. The increased PDI of these samples could be due to side reactions, as the samples dissolved in THF were difficult to filter prior to GPC analysis. An alternate explanation for the increased PDI could also be limited solubility of the higher generation polymers, however. Furthermore, these polymers could have reached the exclusion limit of the GPC column due to their large size.

The molar substitution levels determined by NMR analysis were converted to weight percent (%*w/w*) fluorine contents using Equation 5-2; these are also reported in Table 5-5. The %*w/w* fluorine content increases rapidly with the molar substitution level of the polymers, but slows down at substitution levels above ca. 20 mol%. This leads to %*w/w* fluorine contents falling within a relatively narrow range (31-46 %*w/w*), even though the molar substitution level varied between 17 and 52 mol%, as shown in Figure 5-7.

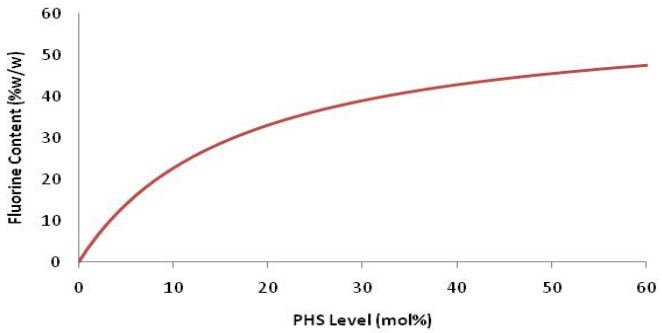

Figure 5-7: Fluorine content (*%w/w*) variation with the molar PHS substitution level.

$$Fluorine\ content\ (wt\%) =$$

$$100\left(\frac{(Atomic\ wt\ of\ F)(number\ of\ F\ atoms\ in\ PHS)(mol\%\ of\ PHS\ substitution)}{(MW\ of\ IP)(mol\%\ of\ unreacted\ IP\ units)+(MW\ of\ PHS\text{-}substituted\ IP)(mol\ \%\ of\ PHS\ substitution)}\right)$$

$$Fluorine\ content\ (wt\%) = 100\left(\frac{(18.99)(13)(mol\%\ of\ PHS\ substitution)}{(68.11)(1-mol\%\ of\ PHS\ sub.)+(68.11+406)(mol\ \%\ of\ PHS\ sub.)}\right)$$

$$Fluorine\ content\ (wt\%) = 100\left(\frac{246.87(mol\%\ of\ PHS\ substitution)}{68.11+68.11(mol\%\ of\ PHS\ sub.)+474.11(mol\ \%\ of\ PHS\ sub.)}\right)$$

$$Fluorine\ content\ (wt\%) = 100\left(\frac{246.87(mol\%\ of\ PHS\ substitution)}{68.11+406(mol\ \%\ of\ PHS\ substitution)}\right) \qquad \textbf{Equation 5-2}$$

The microstructure of the residual isoprene units in the PHS-substituted polymers was determined by ^{1}H NMR analysis (Table 5-5). The results obtained show that 1,2-isoprene units are more reactive towards hydrosilylation than the 1,4- and 3,4-units. A significant fraction of 1,4-units reacted under the conditions used, while 3,4-units apparently did not react. Overlapping of the NMR signals for the *cis*- and *trans*- isoprene units prevents the resolution of the two isomers. These results are in agreement with the findings of a previous investigation by Teertstra.[25] Interestingly, three of the samples synthesized (PIP29-F21, PS-PIP6-F25, and G0PS-PIP6-F17) behaved differently from the other polymers: The reactivity of 1,2- and 1,4-units in these samples was apparently similar, with no selectivity for the 1,2- over the 1,4-units. This peculiar but interesting effect could be due to impurities present in the reaction, but the exact origin of these deviations still needs to be determined. A common feature of these three samples is that they have a low substitution level.

Table 5-5: Composition and residual isoprene units microstructure of PHS-substituted PIP

Polymer	F content (%*w*/*w*)	Residual Isoprene Units Microstructure (%)		
		1,2	1,4	3,4
PIP6-F21	34	21	33	46
PIP6-F31	40	9	44	47
PIP6-F39	43	8	30	62
PIP29-F21	34	29	27	42
PIP29-F25	36	17	31	52
PIP29-F35	41	14	24	62
PIP29-F37	42	13	22	65
PIP115-F26	37	11	33	56
PIP115-F42	44	0	30	70
PS-PIP6-F25	36	25	20	55
PS-PIP6-F41	43	0	44	56
PS-PIP6-F50	46	0	42	58
PS-PIP30-F44[a]	44	0	31	69
G0PS-PIP6-F17	31	31	32	37
G0PS-PIP6-F22	35	19	34	47
G0PS-PIP6-F27	38	22	32	46
G0PS-PIP6-F42	44	0	41	59
G0PS-PIP6-F52	46	0	34	66
G0PS-PIP13-F31	40	21	28	51
G0PS-PIP13-F41	43	0	42	58
G0PS-PIP24-F25	36	18	31	51
G0PS-PIP24-F39	43	6	17	77
G0PS-PIP45-F19	32	25	34	41
G0PS-PIP45-F28	38	14	37	49
G0PS-PIP45-F39	43	4	32	64
G1PS-PIP30-F31[a]	40	11	32	57

[a] Synthesized by Teertstra.[25]

5.6 Extrusion testing

The performance of the fluorinated polymer samples as polymer processing additives (PPA) was investigated by blending them at two different concentrations (0.5 and 0.1 %*w*/*w*,

identified as the high and low PPA concentrations, respectively) with a commercial LLDPE resin. The influence of the additives on the processability of the resin was assessed by capillary rheometry, on the basis of 1) their ability to eliminate melt defects, and 2) the reduction in extrusion load on the instrument relatively to the pure LLDPE resin. The die used had a length of 1.00 inch, an L/D ratio of 50, and an entrance angle of 90^0. The tests were performed at 190 ^{0}C at shear rates between 50 and 1600 s^{-1}. The virgin LLDPE resin yielded SS at a shear rate of 200 s^{-1} and CMF at 400 s^{-1}.

5.6.1 High PPA concentration

Preliminary studies conducted by Teertstra[25] on the use of arborescent polystyrene-*graft*-polyisoprene as PPA at 0.1 %*w/w* yielded marginal effects. In the current investigation, the work of Teertstra was extended to a higher concentration and a wider range of samples. The higher PPA concentration is not typical of commercial additives, but it is comparable with that used by Hong et al.[3,4] for other types of dendritic PPA. The results obtained for the extrusion of blends of LLDPE with 0.5 %*w/w* PPA are summarized in Table 5-6. Two samples (PIP6-F31 and PIP29-F25) led to *stranding* on the surface of the extrudate (Figure 5-8), defined as glossy stripes appearing alongside SS defects. Stranding typically indicates partial coating of the additives on the surface of the die, without the creation of a layer sufficiently stable to suppress SS formation.[76]

Several of the PPA samples (PIP6-21, PIP6-F39, PIP29-F35, PS-PIP6-F25, PS-PIP6-F50, G0PS-PIP6-F27, and G0PS-PIP13-31) also led to a mild form of CMF, characterized by alternating glossy and dull surfaces on the extrudate (Figure 5-9). The dull surface is clearly rougher than the glossy surface, but not nearly as serious as in the case of SS formation.

Furthermore, it is interesting to note that mild CMF occurred at very low shear rates (100 s^{-1}) and was immediately followed by normal CMF as the shear rate was increased.

Table 5-6: Extrusion results for LLDPE at 0.5 %*w/w* PPA concentration

Sample	Load reduction (%)[a,b]				Extrudate Appearance[c]
	50 s^{-1}	100 s^{-1}	200 s^{-1}	300 s^{-1}	
FX9613	64.8	69.2	65.9	60.3	Glossy@50-1000 s^{-1}
PIP6-F21	6.3	--	--	--	Mild CMF@100 s^{-1}; Glossy@400 s^{-1}
PIP6-F31	18.0	24.8	--	45.4	Stranding@50-100 s^{-1}; Glossy@300-1000 s^{-1}
PIP6-F39	7.6	--	--	--	Mild CMF@100 s^{-1}
PIP29-F21	8.2	7.9	--	--	CMF@≥200 s^{-1}
PIP29-F25	11.1	11.6	14.0	18.0	Stranding@50-200 s^{-1}; Glossy@300-400 s^{-1}
PIP29-F35	3.1	--	--	24.0	Mild CMF@100 s^{-1}; Glossy@300-600 s^{-1}
PIP29-F37	10.7	10.2	--	--	CMF@≥200 s^{-1}
PIP115-F26	7.5	5.9	4.0	3.4	CMF@≥400 s^{-1}
PIP115-F42	9.4	8.4	6.6	--	CMF@≥300 s^{-1}
PS-PIP6-F25	11.8	--	--	28.7	Mild CMF@100 s^{-1}; Glossy@300-400 s^{-1}
PS-PIP6-F41	8.6	--	--	--	CMF@≥100 s^{-1}
PS-PIP6-F50	7.3	--	--	--	Mild CMF@100 s^{-1}
PS-PIP30-F44[d]	1.7	3.0	--	--	CMF@≥200 s^{-1}
G0PS-PIP6-F17	9.2	6.4	--	20.3	Glossy @300-400 s^{-1}
G0PS-PIP6-F22	3.1	3.6	3.12	3.0	SS@200-400 s^{-1}
G0PS-PIP6-F27	9.0	--	--	--	Mild CMF@100 s^{-1}
G0PS-PIP6-F42	12.0	10.4	--	--	CMF@≥200 s^{-1}
G0PS-PIP6-F52	5.4	7.2	--	--	Glossy@400-600 s^{-1}
G0PS-PIP13-F31	8.0	--	--	--	Mild CMF@100 s^{-1}
G0PS-PIP13-F41	11.8	9.2	--	--	CMF@≥200 s^{-1}
G0PS-PIP24-F25	8.22	7.6	--	--	CMF@≥200 s^{-1}
G0PS-PIP24-F39	7.46	7.5	--	--	CMF@≥200 s^{-1}
G0PS-PIP45-F19	4.4	3.4	--	9.2	Glossy@300-400 s^{-1}
G0PS-PIP45-F28	4.4	6.0	4.5	--	CMF@≥300 s^{-1}
G0PS-PIP45-F39	7.5	7.2	5.8	--	SS@200 s^{-1}
G1PS-PIP30-F31[d]	6.1	5.1	4.1	4.1	SS@200-300 s^{-1}

[a] Percent reduction in comparison to virgin LLDPE resin.
[b] '--' indicates that CMF occurred, so the load is not reported.
[c] Virgin LLDPE resin displays SS at 200-300 s^{-1} and normal CMF at 400 s^{-1}.
[d] Sample synthesized by Teertstra.[25]

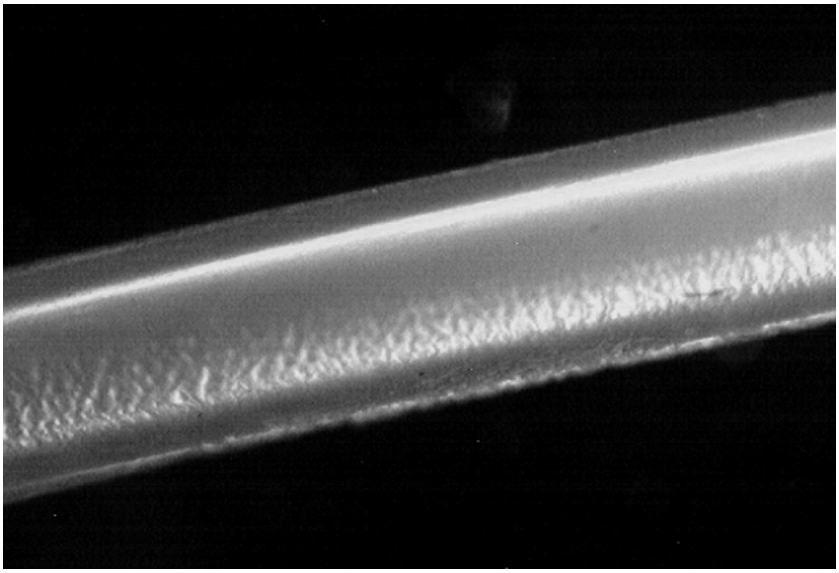

Figure 5-8: Surface stranding for a 0.5 %*w/w* blend of PIP30-F25 in LLDPE.
Stranding is seen as bands of glossy surface (top and bottom of filament) surrounded by mild SS (closest side). The diameter of the filament is 0.061 cm.

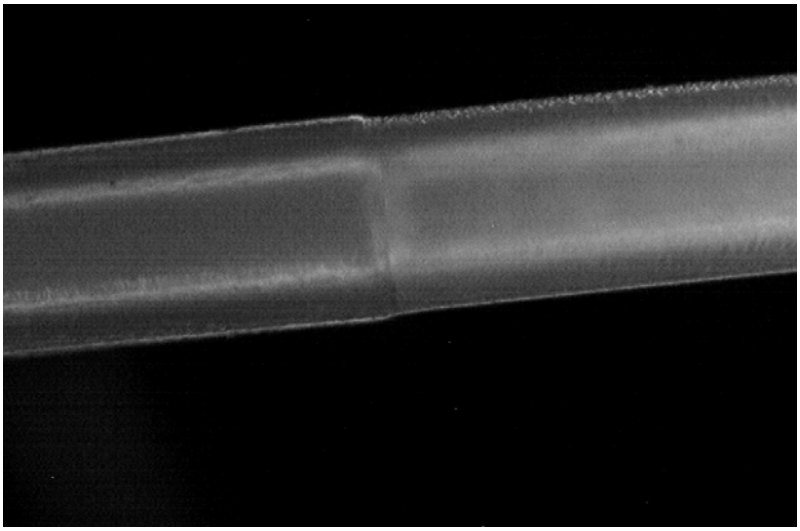

Figure 5-9: Mild CMF for a 0.5 %*w/w* blend of PIP6-F39 in LLDPE.
Mild CMF appears as alternating segments of glossy (left) and dull (right) surfaces. Observed at a shear rate of 100 s^{-1}; the diameter of the filament is 0.058 cm.

No load reductions are reported in Table 5-6 when CMF occurred, as the load oscillated between two values that were usually several hundred pounds apart under these conditions. In some cases (PIP6-F31, PIP6-F21, PIP29-F35, PS-PIP6-F25, G0PS-PIP6-F17,

G0PS-PIP6-F52, G0PS-PIP45-F19), the onset of CMF was observed at low shear rates but it was eliminated afterwards, which suggests that these samples require a minimum shear rate to coat the die. CMF formation eventually returned as the shear rate was increased due to the gradual load buildup.

A series of fluorinated linear PIP samples was synthesized for comparison with the branched copolymers, to provide insight into the influence of branching on PPA performance. When comparing linear PPA samples derived from the same linear PIP substrate but with different fluorination (substitution) levels, it appears that samples with substitution levels between 25 and 35 mol% perform best. Furthermore, when comparing samples of different molecular weights but having similar substitution levels, the lower molecular weight samples have a superior performance. For example, PIP115-F26 and PIP29-F25 have similar compositions but the lower molecular weight sample (PIP29-F25) yielded larger load reductions and a glossy extrudate up to 400 s^{-1}, while CMF started at 400 s^{-1} for PIP115-F26. On the basis of the results reported by Teertstra[25] for PIP5-F36 blended at 0.1 %*w/w* with LLDPE, it was expected that PIP6-F31, when blended at a higher concentration (0.5 %*w/w*), would lead to further performance improvement: At 0.1 % *w/w*, that additive delayed the onset of CMF to 800 s^{-1} and reduced the load by 8.2 % at 200 s^{-1}. PIP6-F31 was indeed able to eliminate SS and to delay the onset of CMF up to shear rates of 1000 s^{-1} when used at a higher concentration. This enhanced effect is attributed to the fact that PIP6-F31 is a low molecular weight additive, which allows it to migrate easily from the LLDPE matrix to the die wall during extrusion. A higher PPA concentration should facilitate the migration of the additive to the die wall, thus promoting die coating.

When comparing the linear polymers to the arborescent copolymers, it appears that the more compact samples are more efficient at delaying the onset of melt fracture. For example, PIP116-F26 ($\overline{M_w}^{app}$=116 x 10^3, $\overline{M_w}^{abs}$=2.92 x 10^5) and PS-PIP6-F25 ($\overline{M_w}^{app}$=58.3 x 10^3, $\overline{M_w}^{abs}$=3.23 x 10^5) have comparable absolute molecular weights and chemical composition but PS-PIP6-F25 has a much lower apparent molecular weight than PIP116-F26 when measured by GPC. The lower apparent molecular weight of PS-PIP6-F25 indicates that the sample is more compact than PIP116-F26.

The trends among the fluorinated polystyrene-*graft*-polyisoprene copolymer samples, and particularly the arborescent (G1 and G2) additives, are not very clear. This is partly due to the difficulty in selecting the parameters serving as a basis for comparison (comparable molecular weight, branching functionality, substitution level, etc.). Generally speaking no major processability improvements were observed for these samples but as the generation number of the copolymers increased, the performance of the additives usually decreased. For example, PS-PIP6-F25 yielded a significant (12 %) load reduction at 100 s^{-1} and the extrudate remained glossy up to 400 s^{-1}, but for G0PS-PIP6-F27 mild CMF started at 100 s^{-1} and normal CMF was observed immediately afterwards. Similar effects were also observed as the molecular weight of the grafted PIP chains was increased (e.g. G0PS-PIP6-F17 versus G0PS-PIP45-F19). All the PPA samples led to some load reduction at the different shear rates investigated, but in many cases the reduction remained within the experimental error limits (estimated at ca. 5 % in these types of measurements).[25]

Samples PS-PIP6-F25 ($\overline{M_w}^{app}$ = 58,000, $\overline{M_w}^{abs}$ = 3.23 x 10^5) and PS-PIP30-F44 ($\overline{M_w}^{app}$ = 160,000, $\overline{M_w}^{abs}$ = 1.42 x 10^6) have apparent molecular weights respectively lower and higher than one of the linear PPA samples PIP115-F26 tested ($\overline{M_w}^{app}$ = 116,000, $\overline{M_w}^{abs}$ =

2.92 x 10^5). PS-PIP6-F25 has a branched structure and short side chains leading to a much lower apparent molecular weight (smaller hydrodynamic volume in THF) than PIP115-F26 and PS-PIP30-F44, however. When the performance of these additives was compared at 0.5 %*w/w*, PS-PIP6-F25 performed far better than PIP115-F25 and PS-PIP30-F44: The load reduction was much larger and the appearance of the extrudate remained glossy between 300 and 400 s^{-1}, albeit a minimum shear rate was required for the formation of a stagnant coating. This suggests that the performance of additives with a lower apparent molecular weight (i.e. more compact molecules) is superior.

A commercial PPA sample, FX9613, was also tested at a concentration of 0.5 %*w/w* in LLDPE (Table 5-6). The commercial additive reduced the load by 60-69% and completely eliminated SS. The onset of CMF was delayed to shear rates of 1100 s^{-1}. The load reduction is compared for FX9613 and for PIP6-F31 as a function of shear rate in Figure 5-10. The load reduction is much more pronounced at low shear rates for the commercial additive but at shear rates above 800 s^{-1}, PIP6-F31 actually led to larger load reductions.

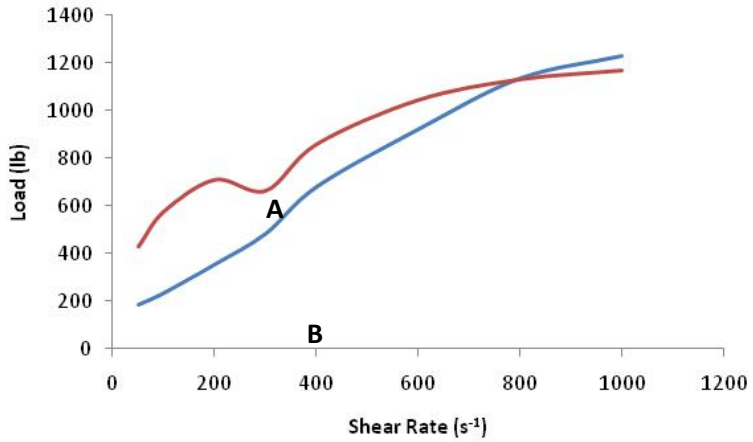

Figure 5-10: Load variation with the shear rate for (A) PIP6-F31 and (B) FX9613.
The sudden drop in load seen in curve A is attributed to efficient coating of the die beyond 300 s^{-1}.

The sudden drop in load for PIP6-F31 observed at a shear rate around 300 s^{-1}, coinciding with the appearance of a glossy surface on the extrudate, has been linked to the formation of a stable PPA coating in previous studies.[15,21] It therefore seems likely that the transition from mild CMF to a glossy surface observed for some of the additives has the same origin. Following the load drop the additive not only eliminated SS, but also delayed the onset of CMF.

5.6.2 Low PPA concentration

Three samples were selected on the basis of their good performance at 0.5 %*w/w* to be evaluated at a lower concentration (0.1 %*w/w*), more typical of commercial PPA applications. The samples selected were PIP6-F31, PS-PIP6-F25, and G0PS-PIP6-F17. The commercial additive FX9613 was also tested at 0.1 %*w/w*. The results obtained for all the samples are reported in Table 5-7. As expected, the performance of all PPA was diminished when their concentration was reduced. For example, PS-PIP6-F25 eliminated SS formation and delayed CMF at shear rates of up to 400 s^{-1} when it was used at 0.5 %*w/w*, but it yielded no processability improvement at 0.1 %*w/w*. The same trend was observed for the linear additive: PIP6-F31 yielded glossy extrudates from 300-1000 s^{-1} at 0.5 %*w/w* concentration, but only SS and CMF defects were observed at 0.1 %*w/w*. Relatively speaking, smaller molecules like PIP6-F31 performed better than larger polymers at the lower concentration: While all samples suffered from melt defects, the reduction in load still decreased in the order PIP6-F31 > PS-PIP6-F25 > G0PS-PIP6-F17 at shear rates between 50 and 200 s^{-1}. This again reinforces the hypothesis that smaller molecules migrate more efficiently to the die wall during extrusion, which leads to their enhanced performance. The performance of FX9613 at 0.1 %*w/w* is excellent in comparison to the PPA synthesized: This additive still

eliminated SS, delayed the onset of CMF, and yielded a large reduction in load at all shear rates. In comparison to the results obtained for FX 9613 at 0.5 %*w/w*, however, the magnitude of the load reduction was decreased and the onset of CMF was only delayed to 1000 s^{-1} (versus 1100 s^{-1} for the commercial additive at 0.5 %*w/w*).

Table 5-7: Extrusion performance for LLDPE at 0.1 %*w/w* concentration of selected PPA

Sample	Load Reduction[a,b] (%)				Extrudate Appearance[c]
	50 s^{-1}	100 s^{-1}	200 s^{-1}	300 s^{-1}	
FX9613	43.8	56.4	57.3	53.7	Glossy@50-800 s^{-1}; CMF@≥ 1000 s^{-1}
PIP6-F31	10.1	10.0	9.4	--	SS@200 s^{-1}; CMF@≥300 s^{-1}
PS-PIP6-F25	9.2	7.4	--	--	CMF@≥200 s^{-1}
G0PS-PIP6-F17	3.1	2.4	1.6	--	SS@200 s^{-1}, CMF@≥300 s^{-1}

[a] Percent reduction as compared to virgin LLDPE.
[b] Experimental error limit on load reduction is ca. 5 %.
[c] Pure LLDPE displayed SS at 200-300 s^{-1} and normal CMF at 400 s^{-1}.

5.6.3 Mixed PPA samples

The same PPA samples selected for performance evaluation at 0.1 %*w/w* (PIP6-F31, PS-PIP6-F25, and G0PS-PIP6-F17) were also blended in a 1:1:1 ratio at overall PPA concentrations of 0.5 and 0.1 %*w/w*, to determine whether any synergistic effects could result from a broad PPA molecular weight distribution. The results obtained in performance testing are summarized in Table 5-8. The mixed PPA blends at 0.5 %*w/w* concentration yielded more significant load reductions than at the lower concentration (0.1 %*w/w*), but no significant processability improvement was observed at either concentration: CMF actually started at lower shear rates (200 s^{-1}) under these conditions. No significant improvements

were observed in terms of surface appearance and load reduction when the mixed blends were compared with the individual additives either (Tables 5-6 and 5-7). For example, PS-PIP6-F25 at 0.5 %*w/w* yielded a load reduction of ca. 28 % at 300 s^{-1}, but CMF already occurred for the mixed blend at same shear rate. Similar results were obtained for the two other samples.

Table 5-8: Extrusion performance for LLDPE with mixed PPA blends at 0.1 %*w/w* and 0.5 %*w/w*

	Load Reduction[a,b] (%)				
Concentration[c]	50 s^{-1}	100 s^{-1}	200 s^{-1}	300 s^{-1}	Extrudate Appearance[d]
0.1 %*w/w*	5.9	5.6	--	--	CMF@≥200 s^{-1}
0.5 %*w/w*	12.0	8.5	--	--	Mild CMF@50-100 s^{-1}; CMF@≥200 s^{-1}

[a] Percent reduction as compared to virgin LLDPE.
[b] Experimental error limit for load reduction is ca. 5 %.
[c] PIP6-F31, PS-PIP6-F25 and G0PS-PIP6-F17 blended in 1:1:1 ratio, and diluted with LLDPE.
[d] Pure LLDPE displays SS at 200-300 s^{-1} and normal CMF at 400 s^{-1}.

5.6.4 Coadditive effects

Coadditives are commonly used in polymer processing to enhance the performance of fluoroelastomer PPA. They are low molecular weight compounds such as PEG[27-29] and poly(ε-caprolactone).[26] The purpose of coadditives is to encapsulate the PPA droplets and promote their migration to the die wall. During extrusion, the PPA droplets experience large shear stresses that may lead to their breakup. The low molecular weight of the coadditives allows a reduction in the shear stresses experienced by the droplets.[26,28] Two PEG samples (PEG4K and PEG10K) were previously investigated by Teertstra as coadditives for fluorinated comb-branched PIP homopolymers, and PEG4K was shown to be most efficient

at enhancing the performance of the PPA.[25] Consequently, PEG4K was investigated to determine whether it could enhance the performances of the fluorinated PPA used in the current study. The mixed PPA sample and the three samples selected for testing at low concentration (PIP6-F31, PS-PIP6-F25, and G0PS-PIP6-F17) were further studied to determine whether they could benefit from the coadditive as reported previously. In a patent by Duchesne and Johnson,[28] it was suggested that the ratio of additive to coadditive used should be between 1:1 and 1:10. It was also pointed out in their examples that ratios of 1:1 and 2:1 were not as effective as ratios of 1:4, 1:2, and 3:5.[28] In a contradictory patent by Woods,[29] it was suggested that the ratio of additive to coadditive used should be between 1:1 to 1:0.005. Also, Teertstra have shown that a ratio of 2:3 were useful at eliminating the onset of melt fracture.[25] Consequently, a ratio of 2:3, which falls within the limit of 1:1 and 1:10, was selected to evaluate the effectiveness of the selected samples with PEG4K. The influence of PEG4K on the PPA performance was monitored at both 0.5 and 0.1 %*w/w* concentrations. For comparison, the commercial PPA (FX9613) was also tested with PEG4K at both concentrations. Blends of pure PEG4K with virgin LLDPE at 0.5 and 0.1 %*w/w* were also extruded for comparison. The results obtained for overall PPA-coadditive concentrations of 0.5 and 0.1 %*w/w* are summarized in Tables 5-9 and 5-10, respectively.

When comparing Table 5-9 for the coadditive blends with the results reported for the pure (Table 5-6) and mixed (Table 5-8) PPA at a concentration of 0.5 %*w/w*, the addition of PEG4K appears to have reduced the load slightly. An important incremental load reduction was observed for G0PS-PIP6-F17 in the presence of PEG4K, the load reduction approaching 30 % as compared to 9 % without PEG4K at 50 s^{-1}. It should also be noted that all three PPA

(PIP6-F31, PS-PIP6-F25, and G0PS-PIP6-F17) displayed a minimum shear rate for enhanced effectiveness.

However, the minimum shear rate required for optimal performance was shifted to higher values as compared to the same additives extruded without coadditive. For example, PIP6-F31 at a concentration of 0.5 %*w/w* without PEG4K required a minimum shear rate of 300 s^{-1} for the elimination of surface defects, but in the presence of PEG4K a minimum shear rate of 600 s^{-1} was required to achieve the same result. For both G0PS-PIP6-F17 and PS-PIP6-F27 the minimum shear rate shifted from 300 to 400 s^{-1}. The appearance of the extrudate remained glossy for both additives at shear rates up to 600 s^{-1}. While all additives were similarly efficient at eliminating surface defects with or without PEG4K, the presence of PEG4K was nonetheless beneficial in terms of enhanced load reductions at low shear rates. The mixed PPA blend did not benefit from the addition of PEG4K, however: The coadditive did not delay the onset of melt fracture nor increased the load reduction.

For comparison, for FX9613 with PEG4K the onset of CMF was delayed to even higher shear rates and a larger reduction in load was observed. These results are in agreement with those reported by Chapman, who attributed the enhanced PPA performance to the coadditive acting as an interfacial agent for the PPA.[26] The extrusion of the blend of pure PEG4K with LLDPE at a concentration of 0.5 %*w/w* yielded surprising results: It delayed the onset of CMF to 1000 s^{-1} after passing through a threshold shear rate of 300 s^{-1}. The effect of pure PEG4K on the LLDPE resin at this relatively high concentration (0.5 %*w/w*) suggests that PEG4K, being a small molecule, also migrates readily to the die wall and provides sufficient lubrication to eliminate SS and delay the onset of CMF.

Table 5-9: Extrusion performance for LLDPE with selected PPA and PEG4K coadditive at an overall concentration of 0.5 %*w/w*

Sample[c]	Extrusion Load, Percent Reduction and Surface Appearance (%)[a,b]							
	50 s^{-1}	100 s^{-1}	200 s^{-1}	300 s^{-1}	400 s^{-1}	600 s^{-1}	800 s^{-1}	1000 s^{-1}
PEG4K	452(14) Glossy	655(14) Glossy	-- CMF	-- CMF	812 Glossy	915 Glossy	1000 Glossy	1060 Glossy
FX9613	150(65) Glossy	221(69) Glossy	341(66) Glossy	448(56) Glossy	594 Glossy	777 Glossy	926 Glossy	1041 Glossy
Mixed Blend	464(11) Glossy	693(9) Glossy	-- CMF	-- CMF	-- CMF	-- CMF	-- CMF	-- CMF
PIP6-F31	425(19) Glossy	-- CMF	-- CMF	-- CMF	-- CMF	1032 Glossy	1084 Glossy	-- CMF
PS-PIP6-F25	450(14) Glossy	651(14) Glossy	-- CMF	-- CMF	992 Glossy	1110 Glossy	-- CMF	-- CMF
G0PS-PIP6-F17	368(30) Stranding	646(15) Stranding	-- CMF	-- CMF	1037 Glossy	1140 Glossy	-- CMF	-- CMF

[a] Percent reduction as compared to virgin LLDPE resin.

[b] Experimental error limit for load reduction is ca. 5 %.

[c] PEG4K blended with additives in a 3 : 2 ratio and diluted to 0.5 %*w/w* with LLDPE.

When comparing Table 5-10 for the coadditive blends with the results reported for the pure (Table 5-6) and mixed (Table 5-8) PPA at a concentration of 0.1 %*w/w*, it can be seen that there is no significant improvement in both load reduction and surface defect mitigation in the presence of coadditive at the lower concentration. The load reductions for the mixed blend, PIP6-F31, PS-PIP6-F25, and G0PS-PIP6-F17 are all unchanged within experimental error limits, and the overall appearance of the extrudate resembles that of the virgin LLDPE. Consequently, the additives have no significant influence on the extrusion process at a low (0.1 %*w/w*) concentration.

The commercial PPA FX9613 with PEG4K still performed remarkably well in the presence of coadditive even at a concentration of 0.1 %*w/w*. The load reduction remained large (>42 %), but the addition of PEG4K did not lead to further decrease in load (in contrast to the incremental decrease observed at the higher concentration). Furthermore, the onset of CMF was only delayed to 800 s^{-1} as compared to 1000 s^{-1} for pure FX9613 at 0.1 %*w/w*. One should consider that the FX9613 concentration in the blend is effectively decreased to 0.04 %*w/w* in the presence of PEG4K, since it is the overall concentration of PPA and coadditive that is 0.1 %*w/w*. Again, the extrusion with pure PEG4K at 0.1 %*w/w* yielded surprising results as it delayed the onset of CMF to 800 s^{-1} (as compared with 1000 s^{-1} for a PEG4K concentration of 0.5 %*w/w*).

Table 5-10: Extrusion performance for LLDPE with selected PPA and PEG4K coadditive at an overall concentration of 0.1 %*w/w*

	Extrusion Load, Percent Reduction and Surface Appearance (%)[a b]							
Sample[c]	50 s^{-1}	100 s^{-1}	200 s^{-1}	300 s^{-1}	400 s^{-1}	600 s^{-1}	800 s^{-1}	1000 s^{-1}
PEG4K	502(4) Glossy	731(4) Glossy	912(12) Stranding	996(18) Stranding	1086 Glossy	1172 Glossy	1231 Glossy	-- CMF
FX9613	305(42) Glossy	341(55) Glossy	462(56) Glossy	599(42) Glossy	786 Glossy	1007 Glossy	1174 Glossy	-- CMF
Mixed Blend	491(6) Glossy	723(5) Glossy	998(4) SS	-- CMF	-- CMF	-- CMF	-- CMF	-- CMF
PIP6-F31	484(8) Glossy	717(6) Glossy	991(5) SS	-- CMF	-- CMF	-- CMF	-- CMF	-- CMF
PS-PIP6-F25	474(9) Glossy	704(8) Glossy	978(6) SS	-- CMF	-- CMF	-- CMF	-- CMF	-- CMF
G0PS-PIP6-F17	487(7) Glossy	715(6) Glossy	-- CMF	-- CMF	-- CMF	-- CMF	-- CMF	-- CMF

[a] Percent reduction as compared to virgin LLDPE resin.

[b] Experimental error limit for load reduction is ca. 5 %.

[c] PEG4K blended with additives in a 3 : 2 ratio and diluted to 0.5 %*w/w* with LLDPE.

5.7 Droplet size analysis

It has been suggested that the optimal average PPA droplet size allowing the formation of a stable coating on the surface of the die is around 2 μm.[76] Other researchers also suggested that the optimal droplet size is between 2-5 μm.[10,26,77]

The size of the PPA droplets was determined for selected LLDPE blends (FX9613, mixed blend, PIP6-F31, PS-PIP6-F25, and G0PS-PIP6-F17) alone and in the presence of PEG4K at concentrations of 0.1 and 0.5 %*w/w* by optical microscopy. The average droplet size and the standard deviation determined for each sample are reported in Table 5-11. Considering the magnitude of the standard deviations on the measurements, there are no significant size differences among all the samples tested. The average size of PPA droplets varies between 1.38 ± 0.29 μm to 2.08 ± 0.47 μm and 1.03 ± 0.25 μm to 1.49 ± 0.33 μm for samples blended with and without PEG4K, respectively. A typical image recorded for a sample is shown in Figure 5-11. When comparing the droplet size for FX9613 with the other samples, the values found are also similar. Keeping in mind that the large variations in droplet size make the trends less statistically significant, smaller PPA average droplet sizes are nonetheless observed in the absence of coadditives. For example, PIP6-F31 with PEG4K at 0.5 %*w/w* concentration yielded an average droplet size of 1.47 ± 0.37 μm, while without PEG4K an average value of 1.20 ± 0.26 μm was found. This result reinforces the generally accepted view that encapsulation of the PPA droplets by the coadditive prevents their breakup under the influence of high shear forces during processing. However, there is obviously no clear link between improved polymer processability and the measured PPA droplet size in the current investigation.

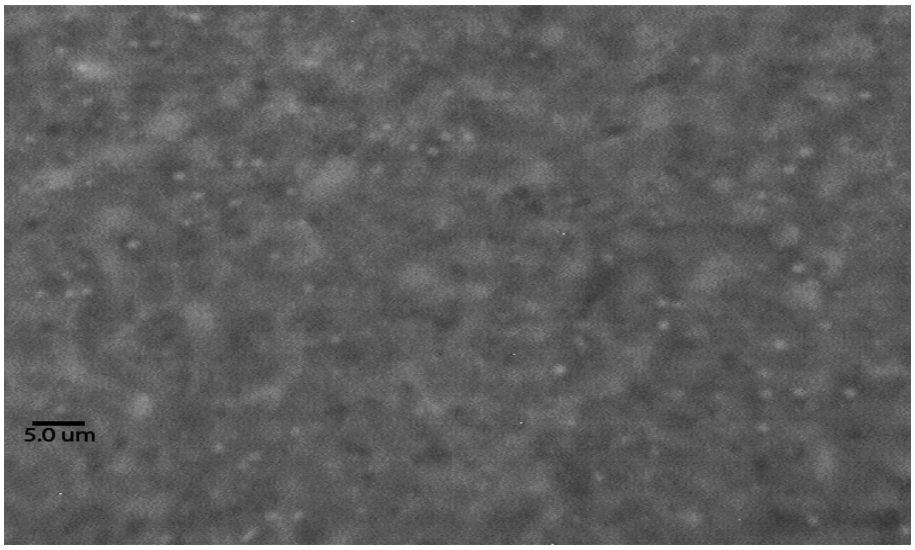

Figure 5-11: Micrograph at 100× for PIP6-F31 blend with LLDPE at 0.5 %*w/w*.
The additive droplets (average diameter 1.20 ± 0.26 μm) are visible as small bright spots.

Table 5-11: Average droplet size for LLDPE blends with selected PPA at 0.5 %*w/w* and 0.1 %*w/w* concentrations with and without PEG4K coadditive

Sample	Concentration (%*w/w*)	With PEG4K (±)[a] (μm)	Without PEG4K (±)[a] (μm)
FX9613	0.5	1.38(0.29)	1.03(0.25)
	0.1	1.38(0.34)	1.39(0.30)
Mixed PPA	0.5	1.58(0.30)	1.36(0.30)
	0.1	1.47(0.34)	1.37(0.31)
PIP6-F31	0.5	1.47(0.37)	1.20(0.26)
	0.1	1.73(0.46)	1.49(0.33)
PS-PIP6-F25	0.5	1.58(0.42)	1.26(0.29)
	0.1	2.08(0.47)	1.20(0.35)
G0PS-PIP6-F17	0.5	1.40(0.37)	1.41(0.28)
	0.1	1.50(0.31)	1.41(0.29)

[a] Standard deviation calculated for 11 – 84 diameter measurements

Chapter 6 – Conclusions and Suggestions for Future Work

A series of arborescent polystyrene-*graft*-polyisoprene copolymers and linear PIP samples was synthesized and subsequently functionalized to different levels by hydrosilylation with a perfluorohydrosilane. The arborescent polystyrene-*graft*-polyisoprene copolymers were synthesized by a "grafting onto" method, by coupling PIP side chains with acetylated PS substrates of different architectures. The PIP side chains and the linear PIP samples were synthesized in THF to obtain a mixed microstructure with roughly equal proportions of 1,2-, 1,4- and 3,4-units. The hydrosilylation reaction was generally selective for the 1,2-isoprene units, but 1,4-units also reacted to a lesser extent. The fluorinated PIP arborescent copolymers and linear homopolymers were investigated for their potential use as PPA in the processing of LLDPE, mainly at a concentration of 0.5 %*w/w*. Three samples (PIP6-F31, PS-PIP6-F25, and G0PS-PIP6-F17) were selected on the basis of their superior performance to be evaluated at 0.1 %*w/w* and in the presence of PEG4K as a coadditive. A mixed PPA blend of PIP6-F31, PS-PIP6-F25, and G0PS-PIP6-F17 was also evaluated at 0.1 and 0.5 %*w/w* to examine potential synergistic effects. For comparison, a commercial additive (FX9613) and the PEG4K coadditive were evaluated under the same conditions.

The arborescent copolymers, when blended with LLDPE at a concentration of 0.5 %*w/w*, all reduced the load measured during extrusion processing, even though the magnitude of the reduction remained within the (5%) experimental error limits in some cases. Many of the samples required a minimum (critical) shear rate for good performance, suggesting that coating of the die was non-optimal below the critical shear rate. Thus PS-PIP6-F25 and G0PS-PIP6-F17 at 0.5 %*w/w* yielded glossy surface between shear rates of 300 s^{-1} and 400 s^{-1}. Furthermore, the load reduction reached 20 – 30 % as compared to virgin LLDPE for a shear rate of 300 s^{-1}. Linear PIP samples such as PIP29-F25 and PIP29-F35

also yielded glossy extrudates beyond 300 s^{-1} and reduced the load by up to 24 % as compared to virgin LLDPE. Good performance improvements were achieved with PIP6-F31 at 0.5 %*w/w*, which eliminated SS formation and delayed the onset of CMF to 1100 s^{-1}. This additive actually outperformed the commercial benchmark additive at shear rates above 800 s^{-1}. In general, most linear and arborescent PIP copolymers reduced the load, and some of the samples were able to eliminate SS formation and to delay the onset of CMF. No significant processability improvements were observed for the *mixed* blends with or without coadditive at 0.5 %*w/w*, however, with only a slight load reduction and no improvement in the surface appearance of the extrudate. The performance of three of the PPA samples was significantly improved at 0.5 %*w/w* with the addition of a coadditive, but these were still outperformed by the commercial additive with PEG4K.

The PPA samples, when evaluated at 0.1 %*w/w* concentration, all displayed decreased performance. The addition of a coadditive nevertheless decreased the load slightly in some cases as compared with the same PPA samples blended at 0.1 %*w/w* without coadditive, but without significant improvements in the appearance of the extrudate. The commercial additive blended with and without coadditive at 0.1 %*w/w* again outperformed all the PPA under these conditions.

The size of the PPA droplets dispersed within the LLDPE matrix was investigated. The average size of the droplets fell within a relatively narrow range between 1.03–2.08 μm. While the standard deviation on the measurements was large, the PPA blended with the coadditive at both concentrations yielded larger average diameters as compared with the same samples without coadditive. This result is consistent with earlier suggestions that

encapsulation of the PPA droplets by PEG reduces the magnitude of shear forces experienced by the additive during extrusion.

On the basis of the results obtained, arborescent polystyrene-*graft*-polyisoprene copolymers appear to have little potential to compete with commercial PPA such as FX9613. Nonetheless, fluorinated linear PIP (e.g. PIP6-F31) and very compact branched polymer structures (e.g. PS-PIP6-F25) appear quite promising. Linear PIP-F31 eliminated SS and delayed the onset of CMF to shear rates above 1000 s^{-1} at 0.5 %*w/w*. PS-PIP6-F25 eliminated melt defects between 300 and 400 s^{-1} and reduced the load by up to 28 %. The addition of PEG4K to the additive at an overall concentration of 0.1 %*w/w* had no influence on PPA performance, but at 0.5 %*w/w* it apparently enhanced the performance of larger PPA molecules. For G0PS-PIP6-F17, for example, the load at 50 s^{-1} was reduced by 9.2 % without PEG4K and by 30 % with PEG4K.

Surprising results were obtained for PEG4K blended by itself with LLDPE at both 0.1 and 0.5 %*w/w*: Significant improvements in surface appearance were observed, albeit the load reduction was only marginal. This nonetheless suggests that PEG4K may have good potential as a PPA, in spite of potential product contamination problems. At both concentrations, CMF was delayed to higher shear rates and SS was eliminated. However, a minimum shear rate was required before optimum performance was achieved.

In future investigations, the structure and composition of both linear and arborescent PIP copolymers could be further optimized to enhance their performance. In the current study, linear PIP with fluorination levels between 25 and 35 mol% performed best. Since the lower molecular weight linear PIP samples were most efficient, polymers with even lower molecular weights (e.g. with $\overline{M_w}$, = 1000 – 2000) should be examined as PPA. The most

compact arborescent copolymer structures likewise performed best among the branched PPA, so further copolymer syntheses incorporating even shorted PIP segments and more compact PS substrates (i.e. with shorter side chains) are also worthwhile examining. Other coadditives such as polycaprolactone, and different ratios of PPA to coadditive could be investigated, as suggested by Duchesne.[28] This includes ratios ranging from 1:1 to 1:10, but ratios outside of this range (e.g. 2 parts PPA to 1 part coadditive) may also be of interest. Finally, the influence of the molecular weight of the coadditive performance would be worthwhile exploring.

References

(1) Odian, G. *Principles of Polymerization, 4th ;* Wiley:Hoboken , 2004; pp 174-180.

(2) Gauthier, M. In *Ionic Polymerizations and Related Processes;* Puskas, J. E., Michel, A. and Barghi, S., Eds.; Kluwer Academic: Dordrecht, 1999; pp 239-257.

(3) Hong, Y.; Cooper-White, J. J.; Mackay, M. E.; Hawker, C. J.; Malmström, E.; Rehnberg, N. *J. Rheol.* **1999**, *43*, 781-793.

(4) Hong, Y.; Coombs, S. J.; Cooper-White, J. J.; Mackay, M. E.; Hawker, C. J.; Malmström, E.; Rehnberg, N. *Polymer* **2000**, *41*, 7705-7713.

(5) Rubin, I. I. In *Injection Molding – Theory and Practice;* Wiley Interscience:New York, 1972; pp 210-211.

(6) Friedrich, CHR.; Eckstein A.; Striker, F.; Mulhaupt R. In *Metallocene-Based Polyolefins – Preparation, Properties and Technology, Vol. 2;* Scheirs, J.; Kaminsky, W., Eds.;Wiley Interscience:Chichester, 2000; pp 402.

(7) Ramamurthy, A. V. *Adv. Poly. Technol.* **1986**, *6*, 489-499.

(8) Ramamurthy, A. V. *J. Rheol.* **1986**, *30*, 337-357.

(9) Achilleos, E. C.; Georgiou, G.; Hatzikiriakos, S. G. *J. Vinyl Additive Technol.* **2002**, *8*, 7-24.

(10) Bigio, D.; Meillon, M. G.; Kharchenko, S. B.; Morgan, D.; Zhou, H.; Oriani, S. R.; Macosko, C. W.; Meigler, K. B. *J. Non-Newtonian Fluid Mech.* **2005**, *131*, 22-31.

(11) Ghanta, V. G.; Riise, B. L.; Denn, M. M. *J. Rheol.* **1999**, *43*, 435-442.

(12) Lenk, R. S. *Plastics Rheology-Mechanical Behaviour of Solid and Liquid Polymers;* Wiley Interscience: New York, 1968; pp 94-108.

(13) Cogswell, F. N. *J. Non-Newtonian Fluid Mech.* **1977**, *2*, 37-47.

(14) Brydson, J. A. *Flow Properties of Polymer Melts;* Van Nostrand Reinhold: New York, 1970; pp 78-81.

(15) Migler, K. B.; Lavallée, C.; Dillon, M. P.; Woods, S. S.; Gettinger, C. L. *J. Rheol.* **2001**, *45*, 565-581.

(16) Migler, K. B.; Son, Y.; Qiao, F.; Flynn, K. *J. Rheol.* **2002**, *46*, 383-400.

(17) Rosenbaum, E. E.; Randa, S. K.; Hatzikiriakos, S. G.; Stewart, C. W.; Henry, D. L.; Buckmaster, M. *Polym. Eng. Sci.* **2000**, *40*, 179-190.

(18) Hatzikiriakos, S. G.; Kazatchkov, I. B.; Vlassopoulos, D. *J. Rheol.* **1997**, *41*, 1299-1316.

(19) Ryan, K. J.; Lupton, K. E.; Pape, P. G.; John, V. B. *J. Vinyl Additive Tech.* **2000**, *6*, 7-19.

(20) Hauenstein, D. E.; Cimbalik, D. J.; Pape, P. G. *J. Vinyl Additive Tech.* **1997**, *3*, 242-248.

(21) Liu, X.; Li, H. *J. Appl. Polym. Sci.* **2004**, *93*, 1546-1552.

(22) Mackley, M. R.; Rutgers, R. P. G.; Gilbert, D. G. *J. Non-Newtonian Fluid Mech.* **1998**, *76*, 281-297.

(23) Woods, S. S.; Pocius, A. V. *J. Plastic Film Sheeting* **2001**, *17*, 62-87.

(24) Markarian, J. S. *J. Plastic Film Sheeting* **2001**, *17*, 333-337.

(25) Teertstra, S. J. *Ph.D. Thesis*, University of Waterloo, Waterloo, ON, 2006.

(26) Chapman Jr., G. R.; Oriani, S. R. US Patent 6,642,310, 2003.

(27) Duchesne, D.; Blacklock, J. E.; Johnson, B. V.; Blong, T. J. *ANTEC* **1989**, 1343-1347.

(28) Duchesne, D.; Johnson, B. V. US Patent 4,855,360, 1989.

(29) Woods, S. S. US Patent 6,734,252, 2004.

(30) Buhleier, E.; Wehner, W.; Vögtle, F. *Synthesis* **1978**, 155-158.

(31) Teertstra, S. J.; Gauthier, M. *Prog. Polym. Sci.* **2004**, *29*, 277-327.

(32) Tomalia, D. A.; Hedstrand, D. M.; Ferritto, M. S. *Macromolecules* **1991**, *24*, 1435-1438.

(33) Yin, R.; Swanson, D. R.; Tomalia, D. A. *Polym. Mater. Sci. Eng.* **1995**, *73*, 277-278.

(34) Yin, R.; Qin, D.; Tomalia, D. A.; Kukowska-Latallo, J.; Baker, Jr., J.R. *Polym. Mater. Sci. Eng.* **1997**, *77*, 206-207.

(35) Hawker, C. J.; Fréchet, J. M. J. In *Step-Growth Polymers for High-Performance Materials;* Hedrick, J. L., Labadie, J. W., Eds.; ACS Symp. Ser. 624; American Chemical Society: Washington, 1996; pp 132-144.

(36) Seiler, M. *Chem. Eng. Technol.* **2002**, *25*, 237-253.

(37) Gauthier, M.; Möller, M. *Macromolecules* **1991**, *24*, 4548-4553.

(38) Li, J.; Gauthier, M. *Macromolecules* **2001**, *34*, 8918-8924.

(39) Gauthier, M.; Li, W.; Tichagwa, L. *Polymer* **1997**, *38*, 6363-6370.

(40) Munam, A.; Gauthier, M. *J. Polym. Sci. , Part A:Polym. Chem.* **2008**, *46*, 5742-5751.

(41) Gauthier, M.; Möller, M.; Burchard, W. *Macromol. Symp.* **1994**, *77*, 43-49.

(42) Choi, S.; Briber, R. M.; Bauer, B. J.; Topp, A.; Gauthier, M.; Tichagwa, L. *Macromolecules* **1999**, *32*, 7879-7886.

(43) Yun, S.I.; Lai, K.C.; Briber, R.M.; Teertstra, S. J.; Gauthier, M.; Bauer, B. J. *Macromolecules* **2008**, *41*, 175-183.

(44) Frank, R. S.; Merkle, G.; Gauthier, M. *Macromolecules* **1997**, *30*, 5397-5402.

(45) Hempenius, M. A.; Zoetelief, W. F.; Gauthier, M.; Möller, M. *Macromolecules* **1998**, *31*, 2299-2304.

(46) Sheiko, S. S.; Gauthier, M.; Möller, M. *Macromolecules* **1997**, *30*, 2343-2349.

(47) Hempenius, M. A.; Michelberger, W.; Möller, M. *Macromolecules* **1997**, *30*, 5602-5605.

(48) Kee, R. A.; Gauthier, M. *Macromolecules* **1999**, *32*, 6478-6484.

(49) Teertstra, S. J.; Gauthier, M. *Macromolecules* **2007**, *40*, 1657-1666.

(50) Cowie, J. M. G. *Eur. Polym. J.* **1975**, *11*, 297-300.

(51) Fetters, L. J.; Lohse, D. J.; Richter, D.; Witten, T. A.; Zirkel, A. *Macromolecules* **1994**, *27*, 4639-4647.

(52) Roovers, J. *J. Non-Cryst. Solids* **1991**, *131-133*, 793-798.

(53) Robertson, C. G.; Roland, C. M.; Paulo, C.; Puskas, J. E. *J. Rheol.* **2001**, *45*, 759-772.

(54) Kee, R. A.; Gauthier, M. *Macromolecules* **2002**, *35*, 6526-6532.

(55) Gauthier, M.; Li, J.; Dockendorff, J. *Macromolecules* **2003**, *36*, 2642-2648.

(56) Yun, S. I.; Gadd, G. E.; Lo, V.; Gauthier, M.; Munam, A. *Macromolecules* **2008**, *41*, 7166-7172.

(57) Dockendorff, J.; Gauthier, M.; Mourran, A.; Möller, M. *Macromolecules* **2008**, *41*, 6621-6623.

(58) Kee, R. A.; Gauthier, M. *J. Polym. Sci., Part A:Polym. Chem.* **2008**, *46*, 2335-2346.

(59) Six, J.L.; Gnanou, Y. *Macromol. Symp.* **1995**, *95*, 137-150.

(60) Taton, D.; Cloutet, E.; Gnanou, Y. *Macromol. Chem. Phys.* **1998**, *199*, 2501-2510.

(61) Angot, S.; Taton, D.; Gnanou, Y. *Macromolecules* **2000**, *33*, 5418-5426.

(62) Walach, W.; Kowalczuk, A.; Trzebicka, B.; Dworak, A. *Macromol. Rapid Commun.* **2001**, *22*, 1272-1277.

(63) Grubbs, R. B.; Hawker, C. J.; Dao, J.; Fréchet, J. M. J. *Angew Chem. Int. Ed. Engl.* **1997**, *36*, 270-272.

(64) Gauthier, M.; Tichagwa, L.; Downey, J. S.; Gao, S. *Macromolecules* **1996**, *29*, 519-527.

(65) Njikang, G. N.; Cao, L.; Gauthier, M. *Macromol. Chem. Phys.* **2008**, *209*, 907-918.

(66) Njikang, G. N.; Cao, L.; Gauthier, M. *Langmuir* **2008**, *24*, 12919-12927.

(67) Kim, Y. H.; Webster, O. W. *Macromolecules* **1992**, *25*, 5561-5572.

(68) Khadir, A.; Gauthier, M. *Polym. Mater. Sci. Eng.* **1997**, *77*, 174-175.

(69) Burchat, A. F.; Chong, J. M.; Nielsen, N. *J. Organomet. Chem.* **1997**, *542*, 281-283.

(70) Li, J.; Gauthier, M.; Teertstra, S. J.; Xu, H.; Sheiko, S. S. *Macromolecules* **2004**, *37*, 795-802.

(71) Cao, L. *M.Sc. Thesis*, University of Waterloo, Waterloo, 1997.

(72) Hwang, S. S.; Ober, C. K.; Perutz, S.; Iyengar, D. R.; Schneggenburger, L. A.; Kramer, E. J. *Polymer* **1995**, *36*, 1321-1325.

(73) Ojima, I.; Fuchikami, T.; Yatabe, M. *J. Organomet. Chem.* **1984**, *260*, 335-346.

(74) Essel, A.; Pham, Q. T. *J. Polym. Sci., Part A-1* **1972**, *10*, 2793-2801.

(75) Anon. Dyneon (3M company) *Dynamar Polymer Processing Additives - Optical Microscopy Method for Dispersion Analysis in Polyolefins*. *http://multimedia.3m.com/mws/mediawebserver?66666UuZjcFSLXTtlx&EMXMcEVuQEcuZgVs6EVs6E666666--* (accessed March/3, 2009).

(76) Amos, S. E.; Giacoletto, G. M.; Horns, J. H.; Lavallée, C.; Woods, S. S. In *Plastics Additives Handbook;* Zweifel, H., Ed.; Hanser Gardner: Cincinnati, 2001; pp 553-584.

(77) Oriani, S. R. *J. Plastic Film Sheeting* **2005**, *21*, 179-198.